PLOIDY AND SIZE IN THE ARABIDOPSIS SEPAL

A Dissertation

Presented to the Faculty of the Graduate School

of Cornell University

In Partial Fulfillment of the Requirements for the Degree of

Doctor of Philosophy

By

Dana Olivia Robinson

May 2018

Ploidy and Size in the *Arabidopsis* Sepal

Abstract

Dana Olivia Robinson, Ph.D.

Cornell University 2018

Ploidy and size phenomena have been correlated across several biological scales, from subcellular to organismal. Whole-genome multiplication increases ploidy in whole plants and is broadly associated with increases in cell and organism size. Endoreduplication, which increases ploidy in individual cells, is strongly correlated with increased cell size and nuclear volume. We use the *Arabidopsis* sepal as a model to study these phenomena.

In my first study, I investigated scaling relationships between ploidy and size by simultaneously quantifying nuclear size, cell size, and organ size in sepals in an isogenic series of diploid, tetraploid, and octoploid plants. We found that pavement cell size increases linearly with ploidy across this series, but organ area increases more modestly due to a compensatory decrease in cell number. Cellular growth rates are similar at all ploidy levels. Likewise, transcriptome size increases with ploidy, and while most genes retain their proportional expression pattern, expression of cell wall-associated genes increases disproportionately with ploidy. We observed that cell size and nuclear size are maintained at a constant ratio; the value of this constant is similar in diploid and tetraploid plants, and slightly lower in octoploid plants. However, cell size is maintained when nuclear size is reduced in the *crwn1* mutant, indicating that cell size scales to ploidy rather than nuclear size. These results shed light on how size is regulated in plants and how cells and organisms of differing sizes are generated by ploidy change.

In my second study, I imaged promoter and protein expression for the SIAMESE-like CDK inhibitor LGO, which controls the entry into endocycles in sepal pavement cells. I found that LGO is

broadly transcribed, but that post-transcriptional regulation limits *LGO* protein to a small number of cells. This expression pattern is consistent with the scattered pattern of endopolyploid cells observed in mature sepals.

In my third study, I explored variation in sepal cell size patterning in a panel of Brassicaceae species. I found that some, but not all, species had an interspersed pattern of small and large cells on the sepal's abaxial surface; sepals with homogeneous cell size did not modulate curvature during anthesis.

BIOGRAPHICAL SKETCH

Dana Robinson was born in Downers Grove, Illinois in September 1990. She attended the Illinois Mathematics and Science Academy in Aurora, Illinois, and first developed an interest in plant biology during an internship at the University of Chicago. She majored in Biology and Environmental Science at Knox College in Galesburg, Illinois, where she participated in a summer research project on the reproductive ecology of a rare prairie wildflower and wrote an Honors thesis on the anatomy and phylogenetic distribution of subterranean flowering in the Leguminosae. A summer internship at the Boyce Thompson Institute first brought her to Cornell in 2011; she returned as a graduate student in 2013 and joined the lab of Dr. Adrienne Roeder in the spring of 2014. Since 2016, her research has focused on ploidy and size.

ACKNOWLEDGEMENTS

Thanks to Adrienne for her support, trust, and engagement throughout my graduate career.

Thanks to Mike Scanlon and Jeff Doyle, my committee members, for their guidance and support.

Thanks to past and present members of the Roeder lab, Lilan Hong, Xian Qu, Heather Meyer, Mingyuan Zhu, Joe Cammarata, and Lila Luna, for training, support, friendship, and advice. Thanks to Xinran Ma for valuable contributions and an uplifting attitude.

Thanks to the Weill Institute, the Weill Plant Growth Facility, and the Lammerding, Bretscher, and Scanlon labs for sharing equipment, reagents, and expertise.

Thank you to the scientists responsible for my undergraduate training: Ji-young Lee and Jean Greenberg at the University of Chicago, Katherine Chi and Brenda Molano-Flores at the University of Illinois at Urbana-Champaign, Sue Sherman-Broyles at Cornell University, and Linda Dybas at Knox College.

Thanks to my fellow graduate students, and especially to my cohort, for support and commiseration.

Thank you to my parents, Nancy Robinson-Bogan and Brad Robinson, my stepfather, Dave Bogan, my brother, Eric Robinson, and my grandparents, Jean-Ann and Alex Eggers for encouraging my curiosity.

Thank you to the McNair Program and the NSF for financial support.

TABLE OF CONTENTS

Reprinted with permission from Current Opinion in Genetics and Development. Original research paper: Robinson, D.O. & Roeder, A. H. K. (2015). Themes and variations in cell type patterning in the plant epidermis. *Current Opinion in Genetics and Development*, 32. https://doi.org/10.1016/j.gde.2015.01.008.

Available online at www.sciencedirect.com

ScienceDirect

Current Opinion in Genetics & Development

Themes and variations in cell type patterning in the plant epidermis

Dana Olivia Robinson and Adrienne HK Roeder

It has recently become evident that plant development, like animal development, has molecular patterning modules that are reused again and again to create different cell type patterns. Here we focus on three of these plant modules: (1) the MYB-bHLH-WD40 protein complex, (2) the transmembrane calpain protease DEFECTIVE KERNEL1 (DEK1), and (3) homeodomain leucine zipper (HD-ZIP) class IV transcription factors acting in concert with SIAMESE-related cyclin-dependent kinase inhibitors. These three modules initiate the patterning of multiple cell types in the plant epidermis: the regular spacing of trichomes (leaf hairs), the stripes of root hairs, diverse pigmentation patterns in petals, the scattering of giant cells, and the files of bulliform cells. Varied combinations of players and additional regulatory inputs partially account for the diversity of patterns that are generated by reusing the same molecular mechanisms.

Address
Weill Institute for Cell and Molecular Biology and School of Integrative Plant Science, Section of Plant Biology, Cornell University, Ithaca, NY 14853, USA

Corresponding author: Roeder, Adrienne HK (ahr75@cornell.edu)

Current Opinion in Genetics & Development 2015, **32**:55–65

This review comes from a themed issue on **Developmental mechanisms, patterning and organogenesis**

Edited by **Deborah J Andrew** and **Deborah Yelon**

For a complete overview see the Issue and the Editorial

Available online 27th February 2015

http://dx.doi.org/10.1016/j.gde.2015.01.008

Introduction

During both plant and animal development, specialized cell types are formed in complex spatial and temporal patterns. In animal systems, it is well established that molecular patterning mechanisms are reused many times to arrange multiple different cell types. For example, in *Drosophila*, Notch-Delta signaling first generates the regular spacing pattern of sensory bristle precursor cells and later breaks the symmetry between bristle precursors' progeny, leading to the specification of shaft, socket, glia, and neuron cells [1]. Plants evolved multicellularity independently from animals [2], and plant genomes lack homologs of most animal patterning genes, including Notch/Delta, Wingless/Wnt, Hedgehog, SMAD/TGF-β, and JAC/STAT [3,4]. Although plants' patterning modules evolved independently, it is becoming increasingly evident that both lineages have evolved multifunctional patterning modules that pattern multiple cell types [5].

In plant biology, patterns are discussed on two scales. The larger scale describes the arrangement of organs or of structures in a given organ: phyllotaxy (arrangement of leaves) and venation are patterns in this sense (for reviews see [6–8]). A second scale of pattern refers to the arrangement of cell types within a tissue [9]. The epidermis, the tissue covering the plant's outer surface, provides an ideal system in which to study this type of pattern. Land plants have a highly multifunctional epidermis, in which discrete cell types function in protection (trichomes), gas exchange (stomata, which have been covered extensively elsewhere and will not be discussed further here; [10,11]), uptake (root hairs), communication with pollinators (pigmentation), and curvature control (bulliform cells and giant cells). Each of these cell types occurs in a characteristic pattern; the mechanisms generating these patterns have been a subject of intensive study.

At least three modules are shared in the patterning of many plant epidermal cell types. The first module is a transcriptional activator complex consisting of a MYB family member, a bHLH family member, and a WD40 repeat protein (the MBW complex): MYB and bHLH proteins are transcriptional regulators, and the WD40 repeat protein is believed to facilitate protein–protein interactions within the complex [5]. Patterning occurs through the movement of components between cells, presumably through the plasmodesmata, channels connecting the cytoplasm of adjacent cells. Members of these three transcription factor families have been shown to function in the initiation of at least seven epidermal cell types in *Arabidopsis*, maize, *Antirrhinum*, and *Petunia* [5].

The transmembrane calpain protease DEFECTIVE KERNEL1 (DEK1) functions in the second patterning module. It is necessary for patterning multiple cell types in *Arabidopsis* and maize. DEK1 is thought to be activated by a signal received through the transmembrane and loop domains. The protease is then thought to cleave itself autocatalytically from the rest of DEK1 protein, and subsequently to cleave downstream targets [12••,13–19]. DEK1 functions with other components including CRINKLY4 (CR4); how these interact is still unclear, although feedback loops are likely to be involved [15–19].

A third module, acting downstream of either module 1 or 2, consists of a homeodomain leucine zipper (HD-ZIP) class IV transcription factor and a cyclin-dependent kinase inhibitor in the plant-specific SIAMESE-related (SMR) protein family (HD-ZIP IV endoreduplication module) [20,21]. Class IV HD-ZIP proteins have recently been shown to inhibit cell proliferation [22]. SMR proteins suppress normal mitotic cell divisions and trigger entry into endoreduplication. This module leads to the differentiation of the cell type, generally in concert with endoreduplication. In *Arabidopsis*, the HD-ZIP class IV family contains 16 genes and the SMR family contains six [20,21].

These modules' functions are well described in trichomes and root hairs, two of the first patterning systems studied. Studies are now revealing that they are also important in the patterning of other systems, and are also revealing the importance of diversity in the modules. Here, we will discuss the parallels and differences among these modules in established and emerging patterning systems, which include anthocyanin pigmentation, giant cells, and bulliform cells.

Canonical patterning systems

Trichomes

In the model species *Arabidopsis thaliana*, an evenly distributed pattern of single-celled hairs, called trichomes, forms on the leaf blade. Trichomes are initiated three cells apart, on average, and almost never directly neighbor one another [23]. This pattern is believed to be generated by a lateral inhibition mechanism, somewhat similar to a Turing-style reaction diffusion network, in which transcriptional activators and inhibitors diffuse from cell to cell [9,24–27•]. Trichome cell fate is initiated by a MYB-bHLH-WD40 complex in which the R2R3 MYB protein is GLABRA1 (GL1), the bHLH protein is GLABRA3 (GL3) or its redundant partner ENHANCER OF GL3 (EGL3), and the WD40 protein is TRANSPARENT TESTA GLABRA 1 (TTG1) (Figure 1, Table 1; [9,28,29]). The members of the GL1–GL3–TTG1 complex are initially expressed at low levels in all epidermal cells, but are thought to activate a positive feedback loop in a few initial cells in which random fluctuations above the average level occur [24–26,27•,30•]. The GL1–GL3–TTG1 complex also transcriptionally activates several R3 MYB-encoding genes: *TRIPTYCHON* (*TRY*), *CAPRICE* (*CPC*), *ENHANCER OF TRY AND CPC 1* (*ETC1*), and *TRICHOME-LESS* (*TCL*) [26,27•,29,31,32]. The R3 MYBs bind GL3–TTG1 in competition with GL1, but lack a transcriptional activation domain, creating an inactive version of the complex [26,27•,33,34]. TRY and CPC proteins move out of incipient trichome cells and into neighboring cells, presumably by diffusing through plasmodesmata, creating a zone of inhibition surrounding the localized peak of activation [25,26,29]. The WD40 protein TTG1 also moves between cells, but GL1 and GL3 are cell-autonomous in the leaf [29,35–37]. TTG1 is trapped in the trichome nucleus through interaction with GL3, leading to a depletion of TTG1 in the surrounding cells, which in turn inhibits surrounding cells from becoming trichomes [36,37]. New methods for the statistical analysis of the trichome distribution will allow more detailed analysis of trichome patterning in the future [38,39].

The active GL1–GL3–TTG1 complex initiates trichome differentiation by directly upregulating the HD-ZIP class IV gene *GLABRA2* (*GL2*) and the cell cycle gene *SIAMESE* (*SIM*) — *SIM* controls endoreduplication, a process essential for trichome development (Figure 1, Table 1; [21,31,32,40–44]). Endoreduplication is required for the maintenance of trichome identity: some *sim* mutant cells initiate trichome development, but then revert back to epidermal pavement cells [44].

Recent evidence suggests that subfunctionalization of HD-ZIP class IV genes has occurred in trichome differentiation. GL2 is required for trichome differentiation on the leaf blade, but GL2 and HD-ZIP IV transcription factor HOMEODOMAIN GLABROUS11 (HDG11) have redundant roles in trichome formation at the leaf margins in *Arabidopsis* [30•].

Root hair patterning

The molecular mechanisms of root hair patterning in *Arabidopsis* largely parallel those of trichome patterning, but generate a very different pattern: striped files of hair and non-hair cells (Figure 1, Table 1; [45]). Root hair patterning is initiated by a MBW complex that shares two members — GL3/EGL3 and TTG1 — with the trichome MBW complex, but includes the R2R3 MYB *WEREWOLF* (*WER*) instead of GL1 [45–48]. This complex directly and indirectly activates the same R3 MYB inhibitors (e.g. *TRY* and *CPC*) as in trichomes, and these move to neighboring cell files to form inactive complexes with GL3 and TTG1 [49–53,54•]. Root hair patterning differs from trichome patterning in two respects. First, root hairs are patterned based on positional information: hair cells occur only over a junction between two underlying cortex cells, and non-hair cells occur over single cortex cells [55]. The position-sensing mechanism is still not entirely clear, but is known to include the receptor-like kinase SCRAMBLED (SCM), expressed in the epidermis, and the transcription factor JACKDAW (JKD), expressed in the underlying cortex layer [27•,56,57]. SCM inhibits expression of *WER* in hair cells. Second, root hair differentiation occurs in cells expressing the inactive version of the MBW complex. The inactive R3 MYBs TRY and CPC accumulate in hair cells, whereas the active R2R3 MYB WER accumulates in non-hair cells [54•,58]. The active complex upregulates expression of the HDZIP IV transcription factor GL2 in non-hair

Figure 1

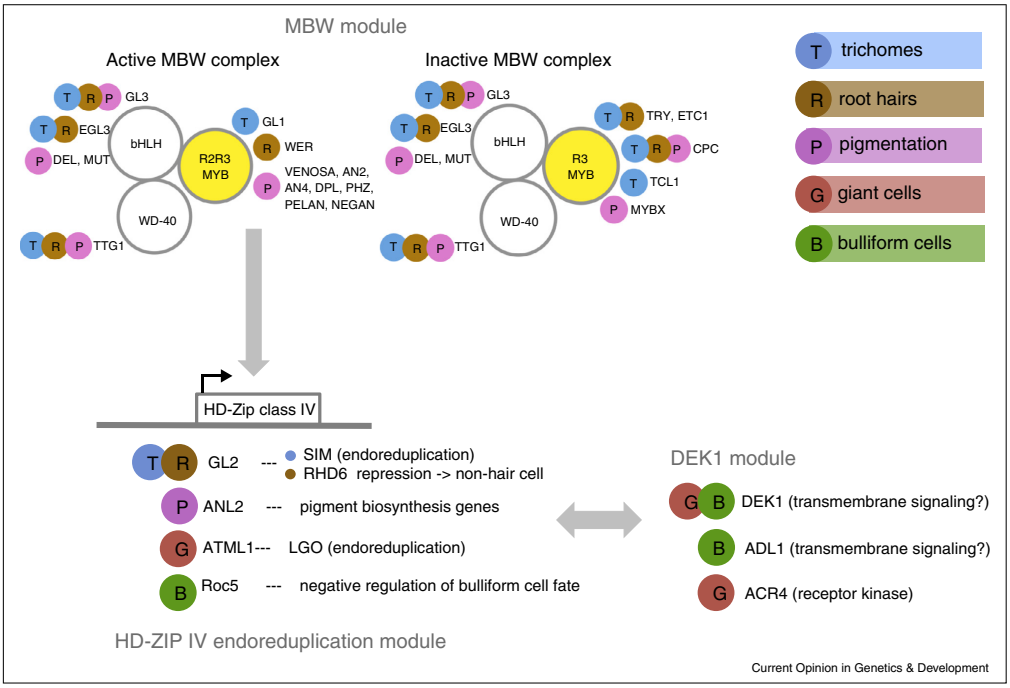

Schematic of plant epidermal patterning modules. The MBW complex is a transcriptional activator complex composed of a MYB family member (gold-filled circle), a bHLH family member, and a WD-40 repeat protein. Complexes containing an R2R3 MYB are able to initiate transcription; complexes with an R3 MYB are inactive. The active complex activates expression of R3 MYBs, which move to neighboring cells to create a zone of inhibition around cells with the active complex. The HD-ZIP IV endoreduplication module includes an HD-ZIP class IV transcription factor and a member of the SIAMESE related family (SMR), which lead to differentiation and endoreduplication. DEK1 has a less well-understood role in the patterning of multiple cell types; it is thought to be involved in transmembrane signaling. Colored circles indicate which specific gene family member has been implicated in the formation of each of five epidermal cell types.

cells. GL2 represses RHD6 expression and prevents hair cell differentiation [58–61]. No SMR protein is currently known to be involved in root hair patterning, but endoreduplication does occur in both root hair and non-hair cells [62,63]. Taken as a whole, the commonalities between trichome and root hair patterning suggest that the MYB-bHLH-WD40 complex has evolved to mediate the formation of multiple types of pattern.

Novel/emerging patterning systems

Pigmentation

Pigmentation is one of the most striking plant patterns — flowers' petals often display sectors, lines, and spots of color (Figure 2). These patterns serve to attract specific pollinators and to guide pollinator behavior at the flower [65••]. Many studies have investigated pigment biosynthesis (for recent reviews see [64,66]); however, the mechanisms by which individual cells choose to produce pigments have been explored only recently. These studies place the MBW complex as central to pattern establishment and reveal the importance of diversity in R2R3 MYBs in specifying location. They have also investigated the formation of complex, multi-cell patterns.

Anthocyanins, the dominant plant pigments, are responsible for most instances of blue, purple, orange, and red coloration. In most eudicots, anthocyanin biosynthesis is activated by a three-member MYB-bHLH-WD40 complex (Figure 1, Table 1; [5,65••,67]). In *Arabidopsis*, several players are held in common with the trichome/root hair-initiating complex. For instance, *GL3*, *TTG1*, *CPC*, *TRY*, and *ETC1* function in regulating anthocyanin biosynthesis [5,65••,68]. Pigmentation patterns are more diverse than the relatively invariant patterns of trichomes or root hairs, and the complex members are correspondingly more numerous.

Table 1

Patterning modules

Class	Gene	Process	Species	Gene number	Citation
MBW module					
bHLH	GL3 (GLABRA 3)	Involved in trichome and root hair differentiation, anthocyanin biosynthesis	*Arabidopsis*	AT5G41315	[5,28,47]
bHLH	EGL3 (ENHANCER OF GLABRA3)	Involved in trichome and root hair differentiation	*Arabidopsis*	AT1G63650	[26,47]
bHLH	DEL (DELILA)	Regulates anthocyanin pigmentation in corolla tube and petal lobe	*Antirrhinum*	M84913	[69**]
bHLH	MUT (MUTABILIS)	Regulates anthocyanin pigmentation in petal lobe	*Antirrhinum*		[69**]
WD-40	TTG1 (TRANSPARENT TESTA GLABRA 1)	Involved in trichome, root hair, pigmentation differentiation	*Arabidopsis*	AT5G24520	[28,46,65**]
R2R3 MYB	GL1 (GLABRA 1)	Involved in trichome initiation	*Arabidopsis*	AT3G27920	[9,28]
R2R3 MYB	WER (WEREWOLF)	Negatively regulates root hair cell fate	*Arabidopsis*	AT5G14750	[48]
R2R3 MYB	VENOSA	Regulates anthocyanin pattern 'venation'	*Antirrhinum*	DQ275531	[69**]
R2R3 MYB	AN2 (ANTHOCYANIN2)	Regulates anthocyanin pigmentation in petal limb	*Petunia*	AF146702	[70]
R2R3 MYB	AN4 (ANTHOCYANIN4)	Regulates anthocyanin pigmentation in petal tube and anthers	*Petunia*	HQ428104	[70]
R2R3 MYB	DPL (DEEP PURPLE)	Regulates anthocyanin pattern 'venation'	*Petunia*	HQ116169	[70]
R2R3 MYB	PHZ (PURPLE HAZE)	Regulates 'bud blush' anthocyanin pigment pattern	*Petunia*	HQ116170	[70]
R2R3 MYB	PELAN	Regulates anthocyanin pigmentation in petal lobe	*Mimulus*	KJ011144	[71**]
R2R3 MYB	NEGAN	Regulates anthocyanin pigmentation in nectar guide and spots	*Mimulus*	KJ011145	[71**]
R3 MYB	TRY (TRIPTYCHON)	Represses trichome fate, activates root hair cell fate	*Arabidopsis*	AT5G53200	[5,25]
R3 MYB	CPC (CAPRICE)	Represses trichome fate, activates root hair cell fate, involved in anthocyanin biosynthesis	*Arabidopsis*	AT2G46410	[5,25,73]
R3 MYB	ETC1 (ENHANCER OF TRY AND CPC 1)	Represses trichome fate, activates root hair cell fate	*Arabidopsis*	AT1G01380	[5,29]
R3 MYB	TCL1 (TRICHOMELESS1)	Represses trichome fate	*Arabidopsis*	AT2G30432	[27*]
R3 MYB	MYBX	Represses anthocyanin biosynthesis	*Petunia*	KF985022.1	[70]

Class	Gene	Function	Species	Gene number	Citation
DEK1 module					
Transmembrane calpain protease	DEK1 (DEFECTIVE KERNEL 1)	Promotes giant cell formation	*Arabidopsis*	AT1G55350	[78**]
Transmembrane calpain protease	DEK1 (DEFECTIVE KERNEL 1)	Negatively regulates bulliform cell fate	*Maize*	AY061805	[90]
Transmembrane calpain protease	ADL1 (ADAXIALIZED LEAF1)	Negatively regulates bulliform cell fate	Rice	OJ1311_H06.4	[91]
Receptor kinase	ACR4 (Arabidopsis CRINKLY4)	Promotes giant cell formation	*Arabidopsis*	AT3G59420	[78**]
HD-ZIP endoreduplication module					
HD-ZIP class IV	GL2 (GLABRA 2)	Activates trichome fate, suppresses root hair fate	*Arabidopsis*	AT1G79840	[42,43]
HD-ZIP class IV	HDG11 (HOMEODOMAIN GLABROUS 11)	Redundant with GL2 in trichome patterning, promotes giant cell formation	*Arabidopsis*	AT1G73360	[30*,78**]
HD-ZIP class IV	ANL2 (ANTHOCYANINLESS 2)	Involved in anthocyanin accumulation, root hair patterning	*Arabidopsis*	AT4G00730	[74,75]
HD-ZIP class IV	ATML1 (*Arabidopsis thaliana* MERISTEM LAYER 1)	Required for giant cell formation	*Arabidopsis*	AT4G21750	[78**]
HD-ZIP class IV	Roc5 (Rice outermost cell-specific gene5)	Negatively regulates bulliform cell fate	Rice	P0657H12.28	[89]
SMR protein	SIM (SIAMESE)	Promotes entry into endoreduplication	*Arabidopsis*	AT5G04470	[40,41]
SMR protein	LGO (LOSS OF GIANT CELLS FROM ORGANS)	Promotes entry into endoreduplication	*Arabidopsis*	AT3G10525	[77]

Figure 2

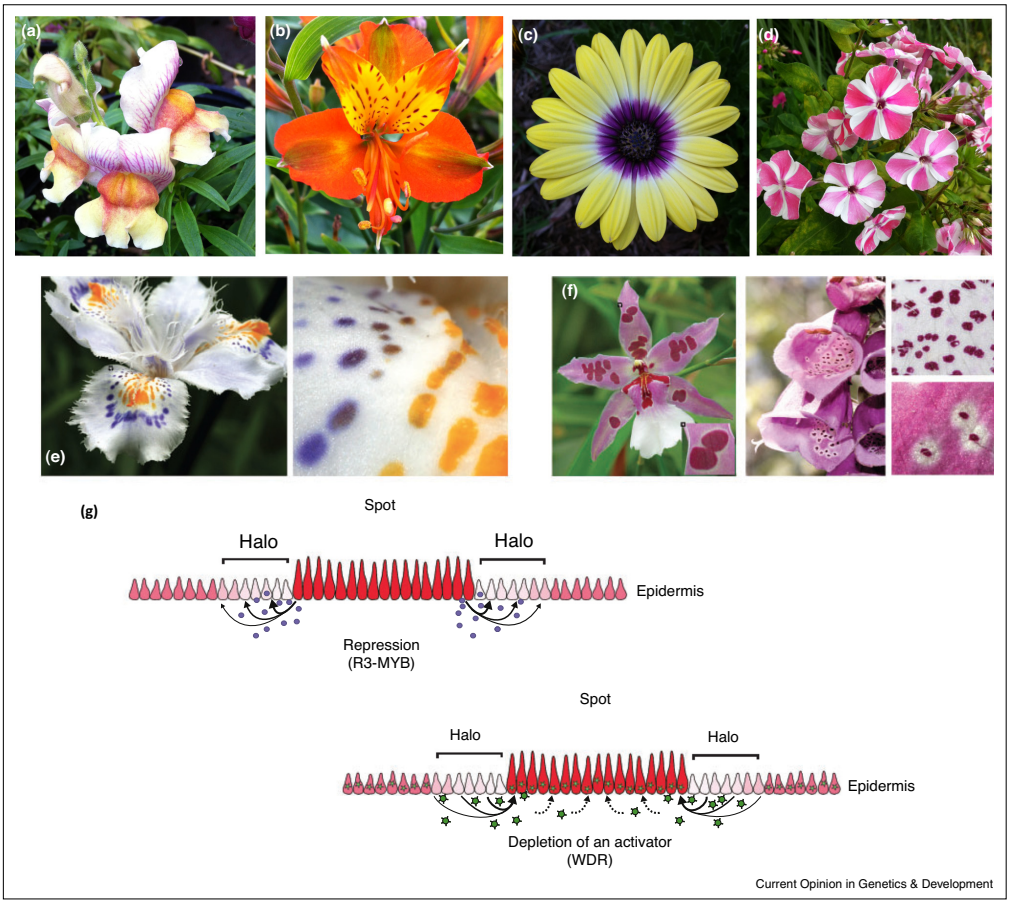

Pigmentation patterns in flowers. **(a)** Venation patterning in snapdragon (*Antirrhinum*). **(b)** Spots in Peruvian lily (*Alstroemeria*). **(c)** Bull's-eye in an aster. **(d)** Stripes in *Phlox*. **(e)** Non-haloed spots in *Iris japonica*. **(f)** Anthocyanin spots surrounded by pigment-depleted haloes in an orchid species (left) and in foxglove (*Digitalis purpurea*, right). **(g)** Two theoretical models for the formation of haloed spots: above, the expression of an R3 MYB inhibitor, and below, the depletion of an activator (WDR, the WD-repeat protein). (e)–(g) are reprinted with permission from [65] (http://www.publish.csiro.au/paper/FP12195.htm).

Recent studies suggest that most variation in pigment location and intensity is determined by specific R2R3 MYBs. For example, the R2R3 MYB protein *VENOSA* controls a pattern called 'venation' in *Antirrhinum majus* (the snapdragon): 'venation' describes stripes of pigment overlying veins in the adaxial petal epidermis (Figure 2a). *VENOSA* is expressed in a wedge of mesophyll and epidermal cells on the adaxial side of veins. The associated bHLH factors (DELILA and MUTABILIS) have broad epidermal expression, and venation pigmentation occurs where these domains overlap [69••]. Another R2R3 MYB gene, *DEEP PURPLE* (*DPL*), has been shown to control a similar pattern in *Petunia* [70]. Other associations between R2R3 MYBs and pigment patterns are also known in *Petunia*: *PURPLE HAZE* (*PHZ*) controls bud blush, and *AN2* and *AN4* control full petal and anther pigmentation [65••,70]. In *Mimulus* (monkeyflower), the R2R3 MYB gene *PELAN* controls anthocyanin

production in the petal lobe, and *NEGAN* controls nectar guides and spots [71••].

Other pigmentation patterns are less well understood, but are suggestive of intriguing patterning mechanisms. Multicellular spots of color occur in non-random, irregularly spaced distributions (Figure 2b, e, and f [65••]). Spot size and location are consistent among flowers of a given species. Theoretical models including the substrate depletion model and the reaction-diffusion model have been invoked to explain the activation of pigment biosynthesis in a small area of cells (Figure 2g; [24,65••,72]). Additionally, some spots are surrounded by haloes of cells lacking background pigment (Figure 2f). This may be explained by a lateral inhibition mechanism analogous to trichome fate inhibition by the *R3 MYB* genes (Figure 2g). Several R3 MYBs, including MYBX in petunia and CPC in *Arabidopsis*, are known to act as repressors of anthocyanin biosynthesis (Figure 1, Table 1; [65••,70,73]).

The HD-ZIP IV transcription factor ANTHOCYANINLESS2 (ANL2) promotes anthocyanin accumulation in subepidermal cells in *Arabidopsis* [74], a second parallel with trichome and root hair patterning systems (Figure 1, Table 1). At this point, it is not known how ANL2 relates to the MYB-bHLH-WD40 complex in regulating anthocyanin biosynthesis. Intriguingly, ANL2 also plays a role in root hair patterning. In *anl2* mutants, root epidermal cells divide abnormally to produce intervening cells, which distort the pattern of hair and non-hair cells [74,75], suggesting another link between HD-ZIP class IV proteins and inhibition of the mitotic cell cycle.

Giant cells

Giant cells are a subtype of pavement cells. Pavement cells make up the majority of the epidermis, and vary in size and ploidy: giant cells are the largest and most highly endoreduplicated of these cells [76,77]. Giant cells are most conspicuous in the *Arabidopsis* sepal, in which they are elongated (about 1/5 the length of the sepal) and bulge out of the plane of the epidermis (Figure 3a, b, and d). Whereas their number is fairly consistent (about 14 per sepal), giant cells show no obvious spatial distribution — they often occur next to one another, ruling out a traditional lateral inhibition mechanism like that of trichomes,

Figure 3

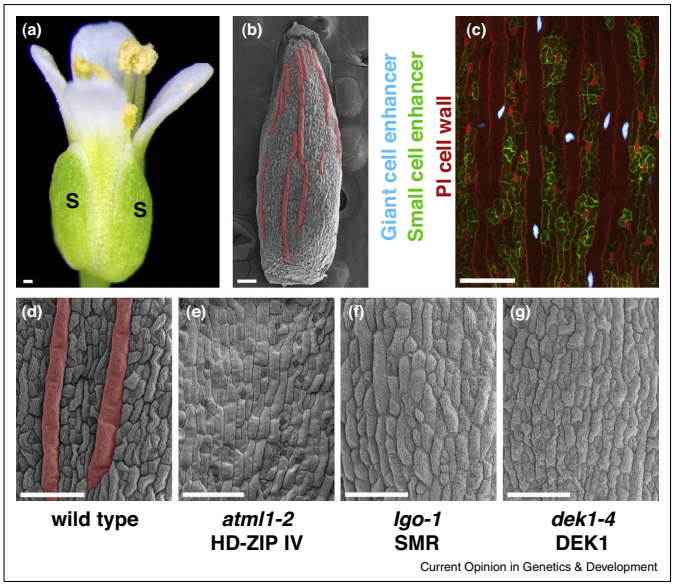

Giant cells in *Arabidopsis thaliana*. **(a)** Position of sepals (s) in an *Arabidopsis* flower. **(b)** Scanning electron micrograph of a sepal with giant cells false-colored in red. **(c)** Confocal image of an *Arabidopsis* sepal expressing fluorescent markers. The giant cell enhancer reporter (light blue) marks giant cell nuclei, which are large and elongated. The small cell marker (green) is ER-localized. The cell wall is stained with propidium iodide (PI; red). **(d–g)** Scanning electron micrographs of wild-type and mutant sepals illustrating loss of giant cells in *atml1-2*, *lgo-1*, and *dek1-4*. Scale bars represent 100 μm.

and they show no obvious correlation with sub-epidermal morphology as root hairs do [77,78••]. Giant cells' status as a distinct cell type is supported by the existence of unique molecular markers for giant and non-giant cells (Figure 3c; [78••]).

Although giant cells do not have a regular spatial pattern, they do share the HDZIP IV-endoreduplication module with other patterning systems. Giant cell formation requires *Arabidopsis thaliana* MERISTEM LAYER1 (ATML1), a HD-Zip Class IV protein, and LOSS OF GIANT CELLS FROM ORGANS (LGO), a SIAMESE family CDK inhibitor (Figure 3d–f; [77,78••]. Like SIM, LGO promotes entry into endoreduplication [77]. The decision to become giant could be stochastic — possibly due to noise in the molecular mechanism specifying endoreduplication [77,79]. Such a mechanism is consistent with the random distribution of giant cells in the sepal. This implies that a predictable pattern of cell size distribution could arise due to stochastic cell fate decisions.

Many patterning mechanisms, including trichomes, are thought to be initiated by stochastic fluctuations in regulators; feedback loops, including the MBW complex and intercellular signaling networks, amplify and modify these differences to create the pattern [24,79,80]. Although there is no evidence for the involvement of an MBW complex, there is evidence that intercellular signaling is required for giant cell formation. Both the transmembrane calpain protease DEK1 and the receptor kinase Arabidopsis CRINKLY4 (ACR4) promote giant cell formation (Figure 3g; [78••]). ATML1, DEK1, and ACR4 all promote epidermal identity specification before having a specific role in the formation of giant cells within the epidermis [15,18,81–84]. There is also recent evidence for an inhibitor of giant cell formation, which might be trafficked through the endomembrane system. The *sec24a-2* mutant produces ectopic giant cells on sepals and leaves in *Arabidopsis* [85•]. *SEC24A* encodes a COPII coat protein involved in loading cargo into vesicles for trafficking from the ER to Golgi. The giant cell system demonstrates that patterning mechanisms can play an important role even in generating irregular patterns.

Bulliform cells

Monocots (which include rice and maize), a major class of flowering plant, are morphologically and developmentally distinct from the eudicots (which include *Arabidopsis*, *Petunia*, and *Antirrhinum*). The two lineages' epidermal patterning differs greatly. Monocot pavement cells occur in orderly files, in contrast to the jigsaw arrangement of dicot pavement cells. Specialized cells, like stomata, occur at regular intervals within single cell files [86]. Monocots also have additional epidermal cell types, including bulliform cells and phytoliths (amorphous silica deposits) (Figure 4).

Figure 4

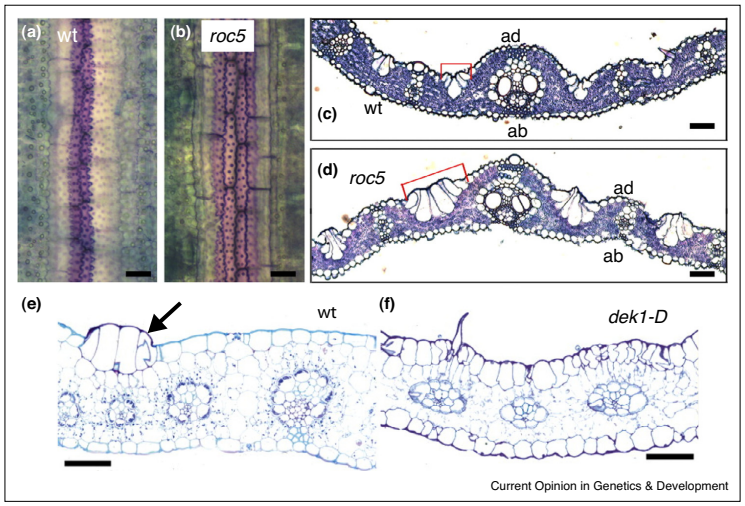

Bulliform cells. **(a, b)** Adaxial epidermal peels of *Oryza sativa* leaves. (a) is wild-type; (b) is a *roc5* mutant. Bulliform cells are stained purple. **(c, d)** Leaf cross-sections showing an increase in the number of bulliform cells (red brackets) in *Roc5* (d) as compared to wild-type (c). Figures a–d are reproduced with permission from [89, ©American Society of Plant Biologists]. **(e)** Cross-section of a maize leaf showing wild-type bulliform cells (arrow). **(f)** Gain of partial bulliform identity in all epidermal cells of a *dek1-D* mutant. Figures (e) and (f) are adapted with permission from [90] (http://dev.biologists.org/content/129/22/5217.long).

Bulliform cells are large, bubble-like cells that occur in files on the adaxial (upper) leaf surface (Figure 4a, c and e). They deflate under water stress, allowing the leaf to roll up and minimize further water loss [87–89]. They occur between and parallel to adaxial veins, usually in 3–5 parallel files [89]. There is currently no evidence that an MBW complex is involved in bulliform cell patterning. However, Zou *et al.* found that a HD-ZIP class IV encoding gene, *Roc5*, negatively regulates bulliform cell fate in rice (Figure 4a–d; [89]). Additionally, in both maize and rice, DEK1 and its rice ortholog Adaxialized leaf 1 (ADL1) regulate bulliform cell fate (Figure 4e,f; [90,91]). In contrast to giant cell patterning, in the monocot epidermis, the Roc5 and DEK1 repress bulliform cell formation. However, like giant cells, bulliform cells are endoreduplicated [78••,92]. In several plant species, DEK1 has an important role in coordinating patterning with cell division regulation [13,78••,93,94].

Conclusion

Plant epidermal patterning is complex. Three interrelated patterning modules control multiple cell type patterns (MBW: trichomes, root hairs, anthocyanin production; DEK1: giant cells and bulliform cells; HD-ZIP IV-endoreduplication: all of the above), and can produce multiple patterns of a single cell type (e.g. pigmented cells). To some extent, the patterning mechanisms are distinguished by the use of different individual members of the same gene family. However, many specific members are reused in multiple patterns, which raises the question of how specificity is achieved. Future studies might also explore the coordination of all these patterns in a tissue — how do patterns interact? Pigmentation, for example, is often correlated with trichomes and other cell types with surface morphology [65••]. Live imaging will be essential in establishing the coordination of patterning factors with the position and timing of cell differentiation [95].

Acknowledgements

We apologize to all those whose work we could not cite due to space constraints. We thank Lilan Hong, Heather Meyer, Erich Schwarz, and Mingyuan Zhu for comments and discussion of the manuscript. Our research on giant cell patterning is funded by the National Science Foundation Plant, Fungal, and Microbial Developmental Mechanisms IOS-1256733.

References and recommended reading

Papers of particular interest, published within the period of review, have been highlighted as:

- • of special interest
- •• of outstanding interest

1. Bray SJ: **Notch signalling: a simple pathway becomes complex**. *Nat Rev Mol Cell Biol* 2006, **7**:678-689.

2. He D, Fiz-Palacios O, Fu C-J, Fehling J, Tsai C-C, Baldauf SL: **An alternative root for the eukaryote tree of life**. *Curr Biol* 2014, **24**:465-470.

3. Goff SA: **A draft sequence of the rice genome (*Oryza sativa* L. ssp. *japonica*)**. *Science* 2005, **309**:879-879.

4. Arabidopsis Genome Initiative: **Analysis of the genome sequence of the flowering plant *Arabidopsis thaliana***. *Nature* 2000, **408**:796.

5. Ramsay NA, Glover BJ: **MYB–bHLH–WD40 protein complex and the evolution of cellular diversity**. *Trends Plant Sci* 2005, **10**:63-70.

6. Bennett T, Hines G, Leyser O: **Canalization: what the flux?** *Trends Genet* 2014, **30**:41-48.

7. Furuta KM, Hellmann E, Helariutta Y: **Molecular control of cell specification and cell differentiation during procambial development**. *Annu Rev Plant Biol* 2014, **65**:607-638.

8. Lee B-H, Yu S-I, Jackson D: **Control of plant architecture: the role of phyllotaxy and plastochron**. *J Plant Biol* 2009, **52**:277-282.

9. Larkin JC, Brown ML, Schiefelbein J: **How do cells know what they want to be when they grow up? Lessons from epidermal patterning in Arabidopsis**. *Annu Rev Plant Biol* 2003, **54**:403-430.

10. Lau OS, Bergmann DC: **Stomatal development: a plant's perspective on cell polarity, cell fate transitions and intercellular communication**. *Development* 2012, **139**:3683-3692.

11. Richardson LGL, Torii KU: **Take a deep breath: peptide signalling in stomatal patterning and differentiation**. *J Exp Bot* 2013, **64**:5243-5251.

12. •• Demko V, Perroud P-F, Johansen W, Delwiche CF, Cooper ED, Remme P, Ako AE, Kugler KG, Mayer KFX, Quatrano R *et al.*: **Genetic analysis of DEFECTIVE KERNEL1 loop function in three-dimensional body patterning in Physcomitrella patens**. *Plant Phys* 2014, **166**:903-919.
The authors demonstrate that the DEK1 loop domain is required for normal mitotic divisions in the moss *Physcomitrella patens*. The transmembrane domains are shown to be similar to the Major Facilitator Superfamily (MFS) domain of secondary transporters, a large and diverse group of membrane transport proteins.

13. Johnson KL, Faulkner C, Jeffree CE, Ingram GC: **The phytocalpain defective kernel 1 is a novel Arabidopsis growth regulator whose activity is regulated by proteolytic processing**. *Plant Cell* 2008, **20**:2619-2630.

14. Takada S, Iida H: **Specification of epidermal cell fate in plant shoots**. *Front Plant Sci* 2014:5.

15. Ingram GC: **Signalling during epidermal development**. *Biochem Soc Trans* 2007, **35**:156-160.

16. Tian Q, Olsen L, Sun B, Lid SE, Brown RC, Lemmon BE, Fosnes K, Gruis DF, Opsahl-Sorteberg H-G, Otegui MS *et al.*: **Subcellular localization and functional domain studies of DEFECTIVE KERNEL1 in maize and Arabidopsis suggest a model for aleurone cell fate specification involving CRINKLY4 and SUPERNUMERARY ALEURONE LAYER1**. *Plant Cell* 2007, **19**:3127-3145.

17. San-Bento R, Farcot E, Galletti R, Creff A, Ingram G: **Epidermal identity is maintained by cell–cell communication via a universally active feedback loop in *Arabidopsis thaliana***. *Plant J* 2014, **77**:46-58.

18. Johnson KL, Degnan KA, Ross Walker J, Ingram GC: **AtDEK1 is essential for specification of embryonic epidermal cell fate**. *Plant J* 2005, **44**:114-127.

19. Javelle M, Vernoud V, Rogowsky PM, Ingram GC: **Epidermis: the formation and functions of a fundamental plant tissue**. *New Phytol* 2011, **189**:17-39.

20. Nakamura M, Katsumata H, Abe M, Yabe N, Komeda Y, Yamamoto KT, Takahashi T: **Characterization of the class IV homeodomain-Leucine Zipper gene family in Arabidopsis**. *Plant Phys* 2006, **141**:1363-1375.

21. Peres A, Churchman ML, Hariharan S, Himanen K, Verkest A, Vandepoele K, Magyar Z, Hatzfeld Y, Van Der Schueren E, Beemster GTS *et al.*: **Novel plant-specific cyclin-dependent kinase inhibitors induced by biotic and abiotic stresses**. *J Biol Chem* 2007, **282**:25588-25596.

22. Horstman A, Fukuoka H, Muiño JM, Nitsch L, Guo C, Passarinho P, Sanchez-Perez G, Immink R, Angenent G, Boutilier K: **AIL and HDG proteins act antagonistically to control cell proliferation**. *Development* 2015, **142**:454-464.

23. Larkin JC, Young N, Prigge M, Marks MD: **The control of trichome spacing and number in Arabidopsis**. *Development* 1996, **122**:997-1005.

24. Meinhard H, Gierer A: **Applications of a theory of biological pattern formation based on lateral inhibition**. *J Cell Sci* 1974, **15**:321-346.

25. Schellmann S, Schnittger A, Kirik V, Wada T, Okada K, Beermann A, Thumfahrt J, Jurgens G, Hülskamp M: **TRIPTYCHON and CAPRICE mediate lateral inhibition during trichome and root hair patterning in Arabidopsis**. *EMBO J* 2002, **21**:5036-5046.

26. Hülskamp M: **Plant trichomes: a model for cell differentiation**. *Nat Rev Mol Cell Biol* 2004, **5**:471-480.

27. • Grebe M: **The patterning of epidermal hairs in Arabidopsis — updated**. *Curr Opin in Plant Biol* 2012, **15**:31-37.
The author reviews the current literature in trichome and root hair patterning, highlighting newly discovered interactions among regulatory genes.

28. Payne CT, Zhang F, Lloyd AM: **GL3 encodes a bHLH protein that regulates trichome development in Arabidopsis through interaction with GL1 and TTG1**. *Genetics* 2000, **156**:1349-1362.

29. Zhao M, Morohashi K, Hatlestad G, Grotewold E, Lloyd A: **The TTG1-bHLH-MYB complex controls trichome cell fate and patterning through direct targeting of regulatory loci**. *Development* 2008, **135**:1991-1999.

30. • Khosla A, Paper JM, Boehler AP, Bradley AM, Neumann TR, Schrick K: **HD-zip proteins GL2 and HDG11 have redundant functions in arabidopsis trichomes, and GL2 activates a positive feedback loop via MYB23**. *Plant Cell* 2014, **26**:2184-2200.
The authors demonstrate that GL2 and HDG11 are functionally redundant, and that GL2 activates a positive feedback loop through MYB23. They also observe potential cross-talk between HD-Zip class IV transcription factors.

31. Morohashi K, Grotewold E: **A systems approach reveals regulatory circuitry for Arabidopsis trichome initiation by the GL3 and GL1 selectors**. *PLoS Genet* 2009, **5**:e1000396.

32. Morohashi K, Zhao M, Yang M, Read B, Lloyd A, Lamb R, Grotewold E: **Participation of the Arabidopsis bHLH Factor GL3 in trichome initiation regulatory events**. *Plant Phys* 2007, **145**:736-746.

33. Szymanski D, Lloyd AM, Marks MD: **Progress in the molecular genetic analysis of trichome initiation and morphogenesis in Arabidopsis**. *Trends Plant Sci* 2000, **5**:214-219.

34. Esch JJ, Chen M, Sanders M, Hillestad M, Ndkium S, Idelkope B, Neizer J, Marks MD: **A contradictory GLABRA3 allele helps define gene interactions controlling trichome development in Arabidopsis**. *Development* 2003, **130**:5885-5894.

35. Kim JY, Rim Y, Wang J, Jackson D: **A novel cell-to-cell trafficking assay indicates that the KNOX homeodomain is necessary and sufficient for intercellular protein and mRNA trafficking**. *Genes Dev* 2005, **19**:788-793.

36. Bouyer D, Geier F, Kragler F, Schnittger A, Pesch M, Wester K, Balkunde R, Timmer J, Fleck C, Hülskamp M: **Two-dimensional patterning by a trapping/depletion mechanism: the role of TTG1 and GL3 in Arabidopsis trichome formation**. *PLoS Biol* 2008, **6**:e141.

37. Balkunde R, Bouyer D, Hülskamp M: **Nuclear trapping by GL3 controls intercellular transport and redistribution of TTG1 protein in Arabidopsis**. *Development* 2011, **138**:5039-5048.

38. Failmezger H, Jaegle B, Schrader A, Hülskamp M, Tresch A: **Semi-automated 3D leaf reconstruction and analysis of trichome patterning from light microscopic images**. *PLoS Comput Biol* 2013, **9**:e1003029.

39. Pomeranz M, Campbell J, Siegal-Gaskins D, Engelmeier J, Wilson T, Fernandez V, Brkljacic J, Grotewold E: **High-resolution computational imaging of leaf hair patterning using polarized light microscopy**. *Plant J* 2013, **73**:701-708.

40. Walker JD, Oppenheimer DG, Concienne J, Larkin JC: **SIAMESE, a gene controlling the endoreduplication cell cycle in *Arabidopsis thaliana* trichomes**. *Development* 2000, **127**:3931-3940.

41. Churchman ML, Brown ML, Kato N, Kirik V, Hülskamp M, Inzé D, De Veylder L, Walker JD, Zheng Z, Oppenheimer DG *et al.*: **SIAMESE, a plant-specific cell cycle regulator, controls endoreplication onset in *Arabidopsis thaliana***. *Plant Cell* 2006, **18**:3145-3157.

42. Di Cristina M, Sessa G, Dolan L, Linstead P, Baima S, Ruberti I, Morelli G: **The Arabidopsis Athb-10 (GLABRA2) is an HD-Zip protein required for regulation of root hair development**. *Plant J* 1996, **10**:393-402.

43. Rerie WG, Feldmann KA, Marks MD: **The Glabra2 gene encodes a homeo domain protein required for normal trichome development in Arabidopsis**. *Genes Dev* 1994, **8**:1388-1399.

44. Bramsiepe J, Wester K, Weinl C, Roodbarkelari F, Kasili R, Larkin JC, Hülskamp M, Schnittger A: **Endoreplication controls cell fate maintenance**. *PLoS Genet* 2010, **6**:e1000996.

45. Schiefelbein J, Huang L, Zheng X: **Regulation of epidermal cell fate in Arabidopsis roots: the importance of multiple feedback loops**. *Front Plant Sci* 2014:5.

46. Galway ME, Masucci JD, Lloyd AM, Walbot V, Davis RW, Schiefelbein JW: **The TTG gene is required to specify epidermal cell fate and cell patterning in the arabidopsis root**. *Dev Biol* 1994, **166**:740-754.

47. Bernhardt C, Zhao M, Gonzalez A, Lloyd A, Schiefelbein J: **The bHLH genes GL3 and EGL3 participate in an intercellular regulatory circuit that controls cell patterning in the Arabidopsis root epidermis**. *Development* 2005, **132**:291-298.

48. Lee MM, Schiefelbein J: **WEREWOLF, a MYB-related protein in Arabidopsis, is a position-dependent regulator of epidermal cell patterning**. *Cell* 1999, **99**:473-483.

49. Ryu KH: **The WEREWOLF MYB protein directly regulates CAPRICE transcription during cell fate specification in the Arabidopsis root epidermis**. *Development* 2005, **132**:4765-4775.

50. Lee MM, Schiefelbein J: **Cell pattern in the Arabidopsis root epidermis determined by lateral inhibition with feedback**. *Plant Cell* 2002, **14**:611-618.

51. Simon M, Lee MM, Lin Y, Gish L, Schiefelbein J: **Distinct and overlapping roles of single-repeat MYB genes in root epidermal patterning**. *Dev Biol* 2007, **311**:566-578.

52. Wada T, Kurata T, Tominaga R, Koshino-Kimura Y, Tachibana T, Goto K, Marks MD, Shimura Y, Okada K: **Role of a positive regulator of root hair development, CAPRICE, in Arabidopsis root epidermal cell differentiation**. *Development* 2002, **129**:5409-5419.

53. Kurata T, Ishida T, Kawabata-Awai C, Noguchi M, Hattori S, Sano R, Nagasaka R, Tominaga R, Koshino-Kimura Y, Kato T *et al.*: **Cell-to-cell movement of the CAPRICE protein in Arabidopsis root epidermal cell differentiation**. *Development* 2005, **132**:5387-5398.

54. • Kang YH, Song SK, Schiefelbein J, Lee MM: **Nuclear trapping controls the position-dependent localization of CAPRICE in the root epidermis of Arabidopsis**. *Plant Phys* 2013, **163**:193-204.
The authors studied the intercellular movement of CAPRICE (CPC), the R3 MYB inhibitor of non-root hair cell fate. They found that CPC is able to travel long distances in the root and is retained preferentially in the nuclei of cells that will develop into root hair by binding to EGL3.

55. Berger F, Haseloff J, Schiefelbein J, Dolan L: **Positional information in root epidermis is defined during embryogenesis and acts in domains with strict boundaries**. *Curr Biol* 1998, **8**:421-430.

56. Kwak S-H, Shen R, Schiefelbein J: **Positional signaling mediated by a receptor-like kinase in Arabidopsis**. *Science* 2005, **307**:1111-1113.

57. Hassan H, Scheres B, Blilou I: **JACKDAW controls epidermal patterning in the Arabidopsis root meristem through a non-cell-autonomous mechanism**. *Development* 2010, **137**:1523-1529.

58. Song S-K, Ryu KH, Kang YH, Song JH, Cho Y-H, Yoo S-D, Schiefelbein J, Lee MM: **Cell fate in the Arabidopsis root epidermis is determined by competition between WEREWOLF and CAPRICE**. *Plant Phys* 2011, **157**:1196-1208.

59. Menand B, Yi K, Jouannic S, Hoffmann L, Ryan E, Linstead P, Schaefer DG, Dolan L: **An ancient mechanism controls the development of cells with a rooting function in land plants**. *Science* 2007, **316**:1477-1480.

60. Masucci JD, Schiefelbein JW: **The *rhd6* mutation of *Arabidopsis thaliana* alters root-hair initiation through an auxin- and ethylene-associated process**. *Plant Phys* 1994, **106**:1335-1346.

61. Bruex A, Kainkaryam RM, Wieckowski Y, Kang YH, Bernhardt C, Xia Y, Zheng X, Wang JY, Lee MM, Benfey P *et al.*: **A gene regulatory network for root epidermis cell differentiation in Arabidopsis**. *PLoS Genet* 2012, **8**:e1002446.

62. Berger F, Hung C-Y, Dolan L, Schiefelbein J: **Control of cell division in the root epidermis of *Arabidopsis thaliana***. *Dev Biol* 1998, **194**:235-245.

63. Sugimoto-Shirasu K, Roberts GR, Stacey NJ, McCann MC, Maxwell A, Roberts K: **RHL1 is an essential component of the plant DNA topoisomerase VI complex and is required for ploidy-dependent cell growth**. *Proc Natl Acad Sci USA* 2005, **102**:18736-18741.

64. Jaakola L: **New insights into the regulation of anthocyanin biosynthesis in fruits**. *Trends Plant Sci* 2013, **18**:477-483.

65. •• Davies KM, Albert NW, Schwinn KE: **From landing lights to mimicry: the molecular regulation of flower colouration and mechanisms for pigmentation patterning**. *Funct Plant Biol* 2012, **39**:619-638.
The authors review mechanisms of pigmentation patterning and hypothesize about the generation of several complex pigmentation patterns, including stripes, spots, and haloes.

66. Zhang Y, Butelli E, Martin C: **Engineering anthocyanin biosynthesis in plants**. *Curr Opin in Plant Biol* 2014, **19**:81-90.

67. Grotewold E: **The genetics and biochemistry of floral pigments**. *Annu Rev Plant Biol* 2006, **57**:761-780.

68. Zhang F, Gonzalez A, Zhao MZ, Payne CT, Lloyd A: **A network of redundant bHLH proteins functions in all TTG1-dependent pathways of Arabidopsis**. *Development* 2003, **130**:4859-4869.

69. •• Shang Y, Venail J, Mackay S, Bailey PC, Schwinn KE, Jameson PE, Martin CR, Davies KM: **The molecular basis for venation patterning of pigmentation and its effect on pollinator attraction in flowers of Antirrhinum**. *New Phytol* 2011, **189**:602-615.
The authors demonstrate that the pigment pattern 'venation' is controlled by vein-associated expression of the *Antirrhinum* gene *Venosa*, an R2R3 MYB. The results support that R2R3 MYBs control the positional specificity of the MBW complex in floral pigmentation patterns.

70. Albert NWN, Lewis DHD, Zhang HH, Schwinn KEK, Jameson PEP, Davies KMK: **Members of an R2R3-MYB transcription factor family in Petunia are developmentally and environmentally regulated to control complex floral and vegetative pigmentation patterning**. *Plant J* 2011, **65**:771-784.

71. •• Yuan Y-W, Sagawa JM, Frost L, Vela JP, Bradshaw HD: **Transcriptional control of floral anthocyanin pigmentation in monkeyflowers (Mimulus)**. *New Phytol* 2014, **204**:1013-1027.
The authors identify members of an MBW complex controlling anthocyanin production in *Mimulus*, an emerging model system. They identify two R2R3 MYB genes, *PELAN* and *NIGRAN*, controlling region-specific pigment expression. *Mimulus* contains many species with various flower colors and patterns, making it an attractive model system for future dissection of pigmentation patterning pathways.

72. Turing AM: **The chemical basis of morphogenesis**. *Philos Trans R Soc Lond B Biol Sci* 1952, **237**:37-72.

73. Zhu H-F, Fitzsimmons K, Khandelwal A, Kranz RG: **CPC, a single-repeat R3 MYB, is a negative regulator of anthocyanin biosynthesis in Arabidopsis**. *Mol Plant* 2009, **2**:790-802.

74. Kubo H, Peeters AJM, Aarts MGM, Pereira A, Koornneef M: **ANTHOCYANINLESS2, a homeobox gene affecting anthocyanin distribution and root development in Arabidopsis**. *Plant Cell* 1999, **11**:1217-1226.

75. Kubo H, Hayashi K: **Characterization of root cell of *anl2* mutant in *Arabidopsis thaliana***. *Plant Sci* 2011, **180**:679-685.

76. Melaragno JE, Mehrotra B, Coleman AW: **Relationship between endopolyploidy and cell size in epidermal tissue of Arabidopsis**. *Plant Cell* 1993, **5**:1661-1668.

77. Roeder AHK, Chickarmane V, Cunha A, Obara B, Manjunath BS, Meyerowitz EM: **Variability in the control of cell division underlies sepal epidermal patterning in *Arabidopsis thaliana***. *PLoS Biol* 2010, **8**:e1000367.

78. •• Roeder AHK, Cunha A, Ohno CK, Meyerowitz EM: **Cell cycle regulates cell type in the *Arabidopsis* sepal**. *Development* 2012, **139**:4416-4427.
The authors describe giant cells, a patterned cell type. They identify several genes necessary for giant cell patterning, including many genes with relevance to conserved patterning modules. They also indicate that cell cycle (endoreduplication) can regulate cell identity.

79. Meyer HM, Roeder AHK: **Stochasticity in plant cellular growth and patterning**. *Front Plant Sci* 2014, **5**:420.

80. Greese B, Hülskamp M, Fleck C: **Quantification of variability in trichome patterns**. *Front Plant Sci* 2014, **5**:596.

81. Tanaka H, Watanabe M, Watanabe D, Tanaka T, Machida C, Machida Y: **ACR4, a putative receptor kinase gene of *Arabidopsis thaliana*, that is expressed in the outer cell layers of embryos and plants, is involved in proper embryogenesis**. *Plant Cell Physiol* 2002, **43**:419-428.

82. Watanabe M, Tanaka H, Watanabe D, Machida C, Machida Y: **The ACR4 receptor-like kinase is required for surface formation of epidermis-related tissues in *Arabidopsis thaliana***. *Plant J* 2004, **39**:298-308.

83. Gifford ML, Dean S, Ingram GC: **The Arabidopsis ACR4 gene plays a role in cell layer organisation during ovule integument and sepal margin development**. *Development* 2003, **130**:4249-4258.

84. Takada S, Takada N, Yoshida A: **ATML1 promotes epidermal cell differentiation in Arabidopsis shoots**. *Development* 2013, **140**:1919-1923.

85. • Qu X, Chatty PR, Roeder AHK: **Endomembrane trafficking protein SEC24A regulates cell size patterning in *Arabidopsis thaliana***. *Plant Phys* 2014, **166**:1877-1890.
The authors show that loss of SEC24A, a COPII vesicle coat subunit, represses giant cell fate. They hypothesize that SEC24A transports an inhibitor of giant cell formation proteins.

86. Hernandez M, Passas H, Smith L: **Clonal analysis of epidermal patterning during maize leaf development**. *Dev Biol* 1999. [no volume].

87. Kadioglu A, Terzi R: **A dehydration avoidance mechanism: leaf rolling**. *Bot Rev* 2007, **73**:290-302.

88. O'Toole JC, Cruz RT, Singh TN: **Leaf rolling and transpiration**. *Plant Sci Lett* 1979, **16**:111-114.

89. Zou L-P, Sun X-H, Zhang Z-G, Liu P, Wu J-X, Tian C-J, Qiu J-L, Lu T-G: **Leaf rolling controlled by the homeodomain leucine zipper class IV gene Roc5 in rice**. *Plant Phys* 2011, **156**:1589-1602.

90. Becraft PWP, Li KK, Dey NN, Asuncion-Crabb YY: **The maize dek1 gene functions in embryonic pattern formation and cell fate specification**. *Development* 2002, **129**:5217-5225.

91. Hibara K-I, Obara M, Hayashida E, Abe M, Ishimaru T, Satoh H, Itoh J-I, Nagato Y: **The ADAXIALIZED LEAF1 gene functions in**

leaf and embryonic pattern formation in rice. *Dev Biol* 2009, **334**:345-354.

92. Cavallini A, Baroncelli S, Lercari B, Cionini G, Rocca M, D'Amato F: **Effect of light and gibberellic acid on chromosome endoreduplication in leaf epidermis of Triticum durum Desf**. *Protoplasma* 1995, **186**:57-62.

93. Perroud P-F, Demko V, Johansen W, Wilson RC, Olsen O-A, Quatrano RS: **Defective Kernel 1 (DEK1) is required for three-dimensional growth in Physcomitrella patens**. *New Phytol* 2014, **203**:794-804.

94. Ahn J-W, Kim M, Lim JH, Kim G-T, Pai H-S: **Phytocalpain controls the proliferation and differentiation fates of cells in plant organ development**. *Plant J* 2004, **38**:969-981.

95. Roeder AHK, Tarr PT, Tobin C, Zhang X, Chickarmane V, Cunha A, Meyerowitz EM: **Computational morphodynamics of plants: integrating development over space and time**. *Nat Rev Mol Cell Biol* 2011, **12**:265-273.

Ploidy and size in the *Arabidopsis* sepal

Dana O. Robinson[1,2], Jeremy E. Coate[3], Abhyudai Singh[4], Lilan Hong[1,2], Max Bush[5], Jeff Doyle[2,6], Adrienne H.K. Roeder[1,2].

1. Weill Institute for Cell and Molecular Biology, Cornell University, Ithaca, NY 14853, USA

2. School of Integrative Plant Science, Section of Plant Biology, Cornell University, Ithaca, NY 14853, USA

3. Reed College, Department of Biology, Portland, OR 97202, USA

4. Department of Electrical and Computer Engineering, Biomedical Engineering, University of Delaware, Newark, DE 19716, USA

5. Department of Cell and Developmental Biology, John Innes Centre, Norwich Research Park, Norwich NR4 7UH, UK

6. School of Integrative Plant Science, Section of Plant Breeding & Genetics, Cornell University, Ithaca, NY 14853, USA

Corresponding author: Adrienne H.K. Roeder (ahr75@cornell.edu).

The author responsible for distribution of materials integral to the findings presented in this article in accordance with the policy described in the Instructions for Authors (www.plantcell.org) is Adrienne H.K. Roeder (ahr75@cornell.edu).

Abstract

Ploidy and size phenomena have been correlated across several biological scales, from subcellular to organismal. Two kinds of ploidy change can affect plants. Whole-genome multiplication increases ploidy in whole plants and is broadly associated with increases in cell and organism size. Endoreduplication increases ploidy in individual cells and is strongly correlated with increased cell size and nuclear volume. Here, we investigate scaling relationships between ploidy and size by simultaneously quantifying nuclear size, cell size, and organ size in sepals from an isogenic series of diploid, tetraploid, and octoploid *Arabidopsis thaliana* plants, each of which contains an internal endopolyploidy series. We find that

pavement cell size (as well as transcriptome size) increases linearly with whole-organism ploidy, but organ area increases more modestly due to a compensatory decrease in cell number. We observe that cell size and nuclear size are maintained at a constant ratio; the value of this constant is similar in diploid and tetraploid plants, and slightly lower in octoploid plants. However, cell size is maintained in a mutant with reduced nuclear size, indicating that cell size is scaled to cell ploidy rather than to nuclear size. These results shed light on how size is regulated in plants and how cells and organisms of differing sizes are generated by ploidy change.

Introduction

Ploidy describes the number of genome copies (C) contained in a single nucleus. A diploid cell's nucleus contains two genome copies and is thus 2C; when C is greater than 2 (e.g. 3C, 4C, 8C), the cell and nucleus can be described as polyploid. A change in ploidy directly changes two parameters: 1. the bulk amount of chromatin in the nucleus and 2. the copy number of each gene. The indirect effects of ploidy increase are numerous and include changes in gene expression, nuclear size, cell size, and the size of organs and organisms [1-5] (Fig. 1A). The mechanisms by which ploidy change is translated into these indirect effects are poorly understood. Here, we study the scaling relationships between ploidy and size at multiple levels in a single tissue.

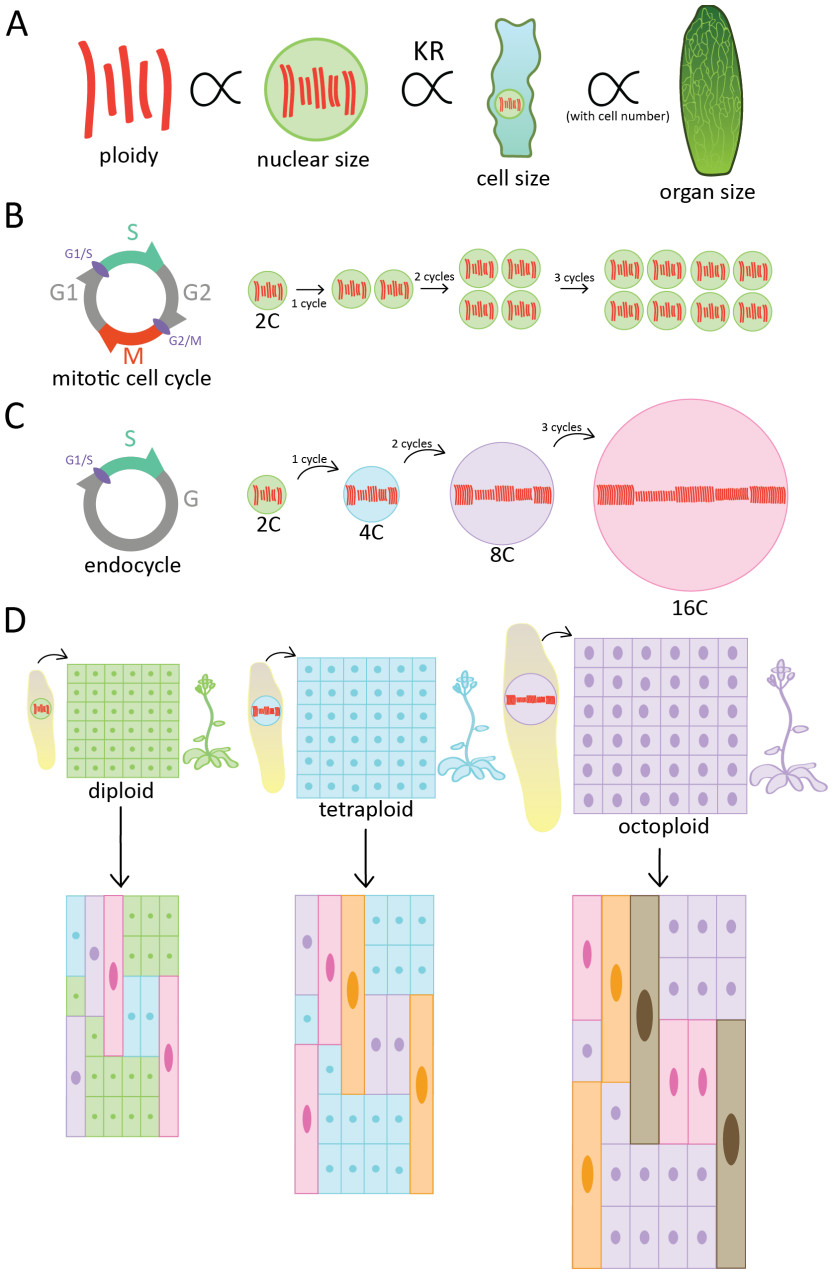

Figure 1. Whole-genome duplication and endoreduplication change ploidy.
A. Proposed proportional relationships among cell ploidy, nuclear size, and cell size. Cell ploidy is strongly correlated with both nuclear size and cell size. Nuclear size and cell size are related by a historically described scaling relationship, the karyoplasmic ratio (KR). The size of an organ is determined by the size and number of its constituent cells. **B**. The mitotic cell cycle. Cells duplicate the genome in S phase, then halve it in mitosis. Entry into S phase and M phase is gated by checkpoints (G1/S and G2/M). Three mitotic cell cycles generate eight diploid cells. **C.** The endocycle. Cells in the endocycle undergo S phase, but omit mitosis, retaining multiple genome copies in a single nucleus. Three endocycles generate one 16C cell. **D**. Whole-genome multiplication (WGM). A diploid zygote (green) gives rise to a plant with a base ploidy of 2C in all tissues. Zygotes with ploidy 4C (blue) or 8C (purple) give rise to

plants with base ploidy 4C or 8C in all tissues. Endoreduplication occurs in developing tissues, resulting in an interspersed pattern of cells at and above the base ploidy level.

Two kinds of ploidy change occur in plants

Two processes increase ploidy in plant cells. One of these, whole-genome multiplication (WGM; polyploidy), increases ploidy in every cell in the organism (Fig. 1D) [6-8]. WGM events are common in angiosperm evolution [9, 10] and are often associated with increases in plant size and cell size (the "Gigas" effect) and increased plant vigor [11-13]. In naturally occurring WGM lineages, these effects may also be partially attributable to hybridity (e.g., allopolyploidy) and to evolutionary processes affecting duplicated genes and genomes [12, 14]: here, we isolate the effects of ploidy change by considering only newly formed autopolyploid lineages.

Previous studies in *Arabidopsis* have demonstrated that increased ploidy increases cell size and organ size in the leaf [15-18]. In Col-0, abaxial leaf epidermal cells were shown to be 71% larger in autotetraploid plants than in the diploid [15]; leaf subepidermal cells were 1.76-fold larger in tetraploids [16]. Another study found that autotetraploid Col-0 cells were ca. 1.5-fold larger, but reduced in number about 1.5-fold [18]. This suggests that compensation for ploidy-based size increase may occur: a reduction in total cell number may lessen the effect of increased cell size change on organ size [19, 20]. Fewer studies have investigated size in *Arabidopsis* octoploid lines. Tsukaya notes a "high ploidy syndrome" in which octoploid body sizes are smaller than diploid or tetraploid despite increased cell size, and suggests that a total mass checkpoint may induce compensation at high ploidy levels [16, 20].

Transcription generally scales with cell size [21, 22]; in *Arabidopsis,* this scaling has been demonstrated for the gene FLOWERING LOCUS C (FLC) [23]. It is thus likely that transcriptome

size (transcript abundance per cell) is increased in newly formed *Arabidopsis* autopolyploids, for which cell size is increased [15, 16, 18, 24, 25], but this has not been measured to date. Aside from mechanisms to scale global transcriptional output to cell size, the effect of autopolyploidy on gene expression in a number of plant species, including *Arabidopsis*, tends to be modest relative to what is observed in allopolyploids [26, 27]. Nonetheless, as much as 10% of genes are differentially regulated in response to autopolyploidy, e.g. [18, 28-30]. The extent and nature of this response is genotype-specific [5], but some recurrent patterns have emerged. For example, genes involved in hormone signaling [4, 5] and stress response [5, 18, 30, 31] tend to be upregulated in diverse autopolyploids. Many transcriptional responses to autopolyploidy appear to represent adjustments to increased cell size; cell surface and cell wall proteins are differentially expressed in polyploid lineages in yeast and Arabidopsis [5, 32]. Thus, transcriptional responses to WGM may reflect a cell size-sensing mechanism [32], and may provide valuable insights into how such size sensing is achieved.

Endoreduplication, a second mechanism of ploidy change, occurs in individual cells during differentiation. It allows cells to increase their ploidy above the organism's "base" ploidy level, sometimes dramatically. Endoreduplication occurs via the endocycle (Figure 1C), an alternative to the mitotic cell cycle (Figure 1B): this cycle includes gap (G) and DNA synthesis (S) phases, but omits mitosis (M), causing multiple copies of the genome to be retained in a single nucleus. All diploid (2C) cells replicate their DNA to 4C during S phase of the cell cycle. Cells in the mitotic cycle divide into two 2C (diploid) daughter cells, whereas cells that endoreduplicate remain 4C and may enter consecutive endocycles to become 8C, 16C, 32C, and so on (Figure 1C). Endopolyploidy is present in most tissues in most angiosperms, including *Arabidopsis* [33,

34]. Endoreduplication is strongly associated with increased cell size, particularly in epidermal systems [3, 35, 36]. *Arabidopsis* sepal pavement cells in diploid plants have ploidy between 2C and 32C and vary ca. 40-fold in length [37], (Figure 1D). Live imaging of *Arabidopsis* sepal pavement cells has shown that endoreduplicating cells grow at the same relative rate, on average, as their dividing neighbors [38]; in essence, endoreduplicated cells are larger because they grow without being halved by division [37]. Endopolyploidy has also been linked to cell fate: nascent trichomes in which endoreduplication is blocked often lose their identity [39], and pavement cells differ in gene expression based on their level of endopolyploidy [40, 41].

The entry into endocycles is regulated by the activity of Cyclin-dependent Kinase Inhibitors (CKIs). The CKI LOSS OF GIANT CELLS FROM ORGANS (LGO), also called SIAMESE RELATED 1 (SMR1), is required for endoreduplication above 8C in leaf and sepal pavement cells. Its most closely related paralog SIAMESE (SIM) is required for endoreduplication in *Arabidopsis* trichomes [37, 42-45].

Distinctions between endopolyploidy and WGM ploidy change

Endoreduplication and whole-genome multiplication both create polyploid cells, but these cells are probably not identical in their cytology. Because WGM increases ploidy in the zygote and in all descendant somatic cells, WGM polyploid cells must undergo mitotic divisions with extra genome copies. In contrast, endoreduplicated cells arise during terminal differentiation and seldom divide [37, 46]. Because sister chromatids are not separated by the mitotic spindle, chromatin configuration may differ in these cells. In endoreduplicated *Drosophila* cells, sister chromatids remain tightly synapsed in polytene arrays [47]. Microscopic

observations of endoreduplicated chromosomes in plants have been more limited, but full or partial polyteny has been described in suspensor and tapetum cells, xylem cells, and trichomes [46, 48, 49]. Endoreduplicated plant chromosomes have been observed to be incompletely aligned or partially polytene, and the degree of chromatid synapsis tends to decrease as ploidy increases [50-52]. These differences in chromatin configuration between endopolyploid and WGM-polyploid nuclei might affect nuclear size, perhaps via chromatin volume: nuclei generated by endopolyploidy are slightly smaller than nuclei of equivalent ploidy generated by WGM [53].

Cells in WGM lineages also enter endocycles (Figure 1D): many cells in tetraploid and octoploid sepals thus have ploidy increased via both WGM and endoreduplication.

Relationships among nuclear size, cell size, and ploidy

Nuclear size can be intuitively linked to ploidy: because the nucleus is largely filled with chromatin, increasing chromatin amount might increase nuclear size. (However, note that DNA density is low in the *Arabidopsis* nucleus relative to other species [54]). Along these lines, the skeletal or nucleoskeletal theory posits that nuclear size is determined by chromatin bulk (amount and condensation) and by the amount of nuclear membrane synthesized [55]. DNA content might thus set a minimum nuclear size [56, 57]. In agreement with this theory, organisms with larger genomes tend to have larger nuclei [54, 58, 59], and nuclear size in the *Arabidopsis* endopolyploidy series scales linearly with ploidy [42, 60]. However, nuclear size may also be genetically regulated, and ploidy does not always affect nuclear volume in all organisms. Neumann and Nurse [56] found that a 2C-to-32C ploidy change in *Saccharomyces*

pombe did not change either nuclear volume or cell area, indicating that ploidy does not necessarily have a direct scaling effect on either parameter. In budding yeast, nuclear size expands with cell growth and does not directly depend on DNA content [61]. These studies conclude that, counter to the nucleoskeletal theory, nuclear size depends largely on cytoplasmic volume [62].

The mechanisms linking ploidy to cell size are more enigmatic. Because ploidy change occurs in the nucleus, many theories that aim to relate cell size to ploidy treat the nucleus as an intermediate step in transducing information. These theories are bolstered by the observation that nuclear size and cell size have been observed to maintain a constant ratio, the karyoplasmic (KR) or nuclear:cytoplasmic (N:C) ratio, in many species [2, 3, 36, 46, 60, 62-64]. The specific value of KR is generally distinct among different cell types, but robust within cell types. Given that nuclear volume generally scales with ploidy [37, 63], and that nuclear size and cell size maintain a constant ratio, it is tempting to hypothesize that cell size scales directly to nuclear size under ploidy change conditions. However, it is so far unknown whether nuclear size directly affects cell size, or by what mechanism this might occur [65]. Another possible model is that ploidy change, because it increases copy number of all loci, also increases biosynthesis and thereby increases cytoplasmic volume. Increased DNA content may also increase ribosome biogenesis, thus increasing translational capacity [36, 46].

<u>The sepal as a model system</u>

The *Arabidopsis* sepal has been developed as a model system for the study of endopolyploidy [37, 40]. The sepal's abaxial (outward-facing) surface has an interspersed pattern of non-endoreduplicated and endopolyploid pavement cells (Figure 1D, left; Figure 2A, WT) similar to that found in the leaf, but sepal cells are boxy rather than jigsaw-shaped [66]. Importantly, the sepal's small size makes it possible to image the organ *in toto*. This allows the quantification of every cell composing the abaxial epidermis, making possible the direct correlation of cell-level behaviors to organ size outcomes. Sepals are also produced in large numbers on a single plant and are consistent in their size [67], allowing for highly replicated measurements. Here, we use the sepal as a model for studying the interactions between ploidy and size.

Results

Altering endopolyploidy affects cell size, but not organ size

We first investigated the effect of endopolyploidy on cell size and organ size. Wild-type *Arabidopsis* sepals have a pattern of interspersed small, medium, and large (giant) cells with corresponding ploidy 2C-32C (Figure 2A,B, WT) [37]. The SIAMESE-related CDK inhibitor *LOSS OF GIANT CELLS FROM ORGANS* (LGO) has been shown to affect the proportion of cells entering endocycles: overexpression of LGO increases endoreduplication, and loss of function reduces it [37, 40, 41]. We have previously shown that the transcription factor *MERISTEM LAYER 1* (ATML1) affects the proportion of endoreduplicated cells in a dosage-dependent manner; *LGO* is genetically downstream of *ATML1* [42]. Here, we show that *LGO*'s effect on the entry into endocycles is also dosage-dependent (Figure 2). We generated plants with different levels of

LGO expression (Figure 2A). Plants homozygous for the overexpression construct *ML1::LGO* (*LGO OX*) had the highest *LGO* dosage—two copies of the overexpression transgene and two endogenous copies of *LGO*. Plants heterozygous for *LGO OX* had only one copy of the transgene and two endogenous copies of *LGO*, while WT had only endogenous *LGO* expression. Plants heterozygous for the loss-of-function allele *lgo-2* had one wild-type copy of *LGO*, and plants homozygous for *lgo-2* had none. We also made a double homozygous mutant of *lgo* and its most closely related paralog *siamese* (*sim*) (*sim-1 lgo-2*): SIM primarily controls endoreduplication in trichomes, but has also been shown to affect pavement cell endoreduplication (Figure 2A,B) [44, 68]. The proportion of cells with ploidy 8C-64C increased predictably with *LGO* dosage (Figure 2B). To quantify the observed differences in cell size (Figure 2A), we used a custom MatLab module [37, 69] to measure cell area for all pavement cells on the sepal's abaxial surface. In *sim-1 lgo-2* and *lgo*-2, where endoreduplication is dramatically decreased, average abaxial epidermal cell sizes were smaller and the distribution of sizes was relatively narrow (Figure 2C,D). Average cell size increased with the presence of one (het *lgo-2*) or two (WT) wild-type copies of *LGO*, and increased dramatically when *LGO* was

ectopically expressed (het *LGO OX*, *LGO OX*) (Figure 2C,D).

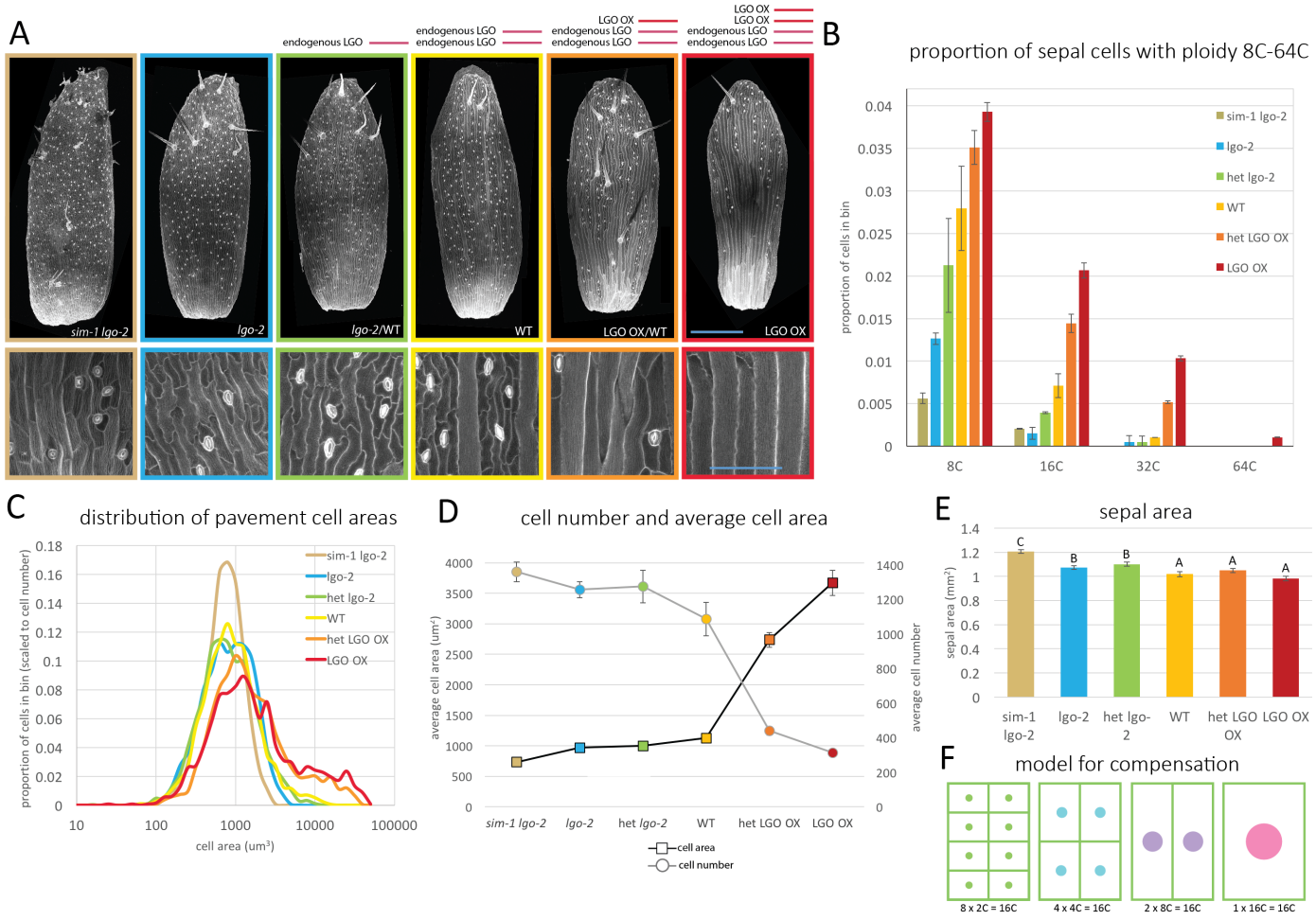

Figure 2. Level of endopolyploidy affects cell size, but does not strongly affect organ size.
A. Confocal images of mature abaxial sepals in *LGO* dosage series (abaxial surface, propidium iodide staining of cell walls (white)): L-R *sim-1 lgo-2, lgo-2, lgo-2/*WT heterozygote, WT (Col-0), LGO OX/WT heterozygote, LGO OX. White dots are stomata. Upper scale bar: 500 µm. Inset scale bar: 100 µm. **B.** Quantification of flow cytometry peaks 8C-64C in sepal nuclei stained with PI (includes both epidermal and internal tissues). Average of 2 replicates: bars represent standard deviation. **C.** Histogram representing pavement cell areas in segmented *LGO* dosage series (n=4 sepals per genotype, 17,658 cells). **D.** Mean pavement cell area (black line, left axis) and average cell number per segmented area (gray line, right axis). Bars represent standard error of the mean (SEM). **E.** Mean mature abaxial sepal area in LGO dosage series (n=50-60 sepals). Bars represent SEM. Letters indicate significantly different groups (unpaired t-test, $p<0.05$). **F.** Conceptual model for a compensation mechanism in endopolyploidy: varying levels of endoreduplication repackage a constant number of genome copies.

Notably, this dramatic increase in cell size did not increase the total size of the organ. Sepal size was fairly constant across the *LGO* dosage series, and sepals with reduced

endoreduplication and smaller cells (*sim-1 lgo-2*, *lgo-2*, and het *lgo-2*) were slightly, but significantly larger (Figure 2E). Because organ area is the product of cell area and cell number, we quantified the total number of abaxial epidermal cells in sepals from each genotype. We found that the number of pavement cells per sepal decreased dramatically as *LGO* dosage increased: *LGO OX* sepals had about 770 fewer cells than WT, while *sim-1 lgo-2* had ca. 270 more cells than WT (Figure 2D). These opposite trends in cell size and cell number generate relatively constant organ sizes across the LGO dosage series.

This compensatory effect is, at least in part, innate to endoreduplication. When a cell divides mitotically, it gives rise to two daughter cells that are usually of approximately equal (small) size (i.e. two 2C cells). When a cell endoreduplicates, its size increases, but cell number is not changed (one 4C cell) (Figure 1B,C). Thus four 2C cells, two 4C cells, and one 8C cell are equivalent in genome copy number, but have packaged the genome copies differently (Figure 2F). These data suggest a model in which the total area of a tissue is determined by the number of genome copies it contains: because this property is not affected by altering the level of endopolyploidy, all sepals in the LGO dosage series are roughly the same size.

Whole-genome multiplication increases cell size and organ size

We hypothesized that endopolyploidy does not affect organ size because it does not change the total number of genome copies in the organ. In contrast, WGM raises the base ploidy level in the zygote and thus increases the input number of genome copies. To investigate the relationship between whole-organism polyploidy and size, we generated isogenic WGM lines. Tetraploid and octoploid lines for WT Col-0 and several marker, mutant, and

overexpression lines (in the Col-0 background) were generated via colchicine treatment [24]. Colchicine-treated plants were allowed to grow and set seed, and neotetraploid and neo-octoploid individuals were identified in the next generation. Octoploids often arose from colchicine-treated diploids; some were generated from colchicine-treated tetraploids. Polyploid individuals were first identified by trichome branch screening on seedling leaves (Figure 3B) [24]. The leaf trichomes of diploid plants nearly always have three branches; a subset (25-50%) of tetraploid plants' trichomes have four branches, and octoploid plants' trichomes have three, four, or five branches. Phenotypic ploidy assessments were confirmed with flow cytometry on mature leaf tissue. The absence of a diploid peak indicated tetraploidy, and the absence of both diploid and tetraploid peaks indicated octoploidy.

Flower size increased markedly across the diploid-tetraploid-octoploid series. Organ shapes and allometric relationships among floral organs did not change dramatically (Figure 3A). Total sepal area increased with ploidy level: tetraploid sepals were (on average) 1.51-fold larger in area than diploid sepals, and octoploid sepals were 1.13-fold larger than tetraploid sepals (Figure 3C). Pavement cell area also increased across the ploidy series (Figure 3 D,E,F). Interestingly, the magnitude of this change was greater than for organ size: tetraploid sepal pavement cells are on average 1.76 times larger than diploid cells, and octoploid cells are 1.71 times larger than tetraploid cells (Figure 3F). A very similar fold change (1.76) has been reported for tetraploid vs. diploid leaf cells [16]; here, we show that ploidy-based size increase continues linearly in the octoploid.

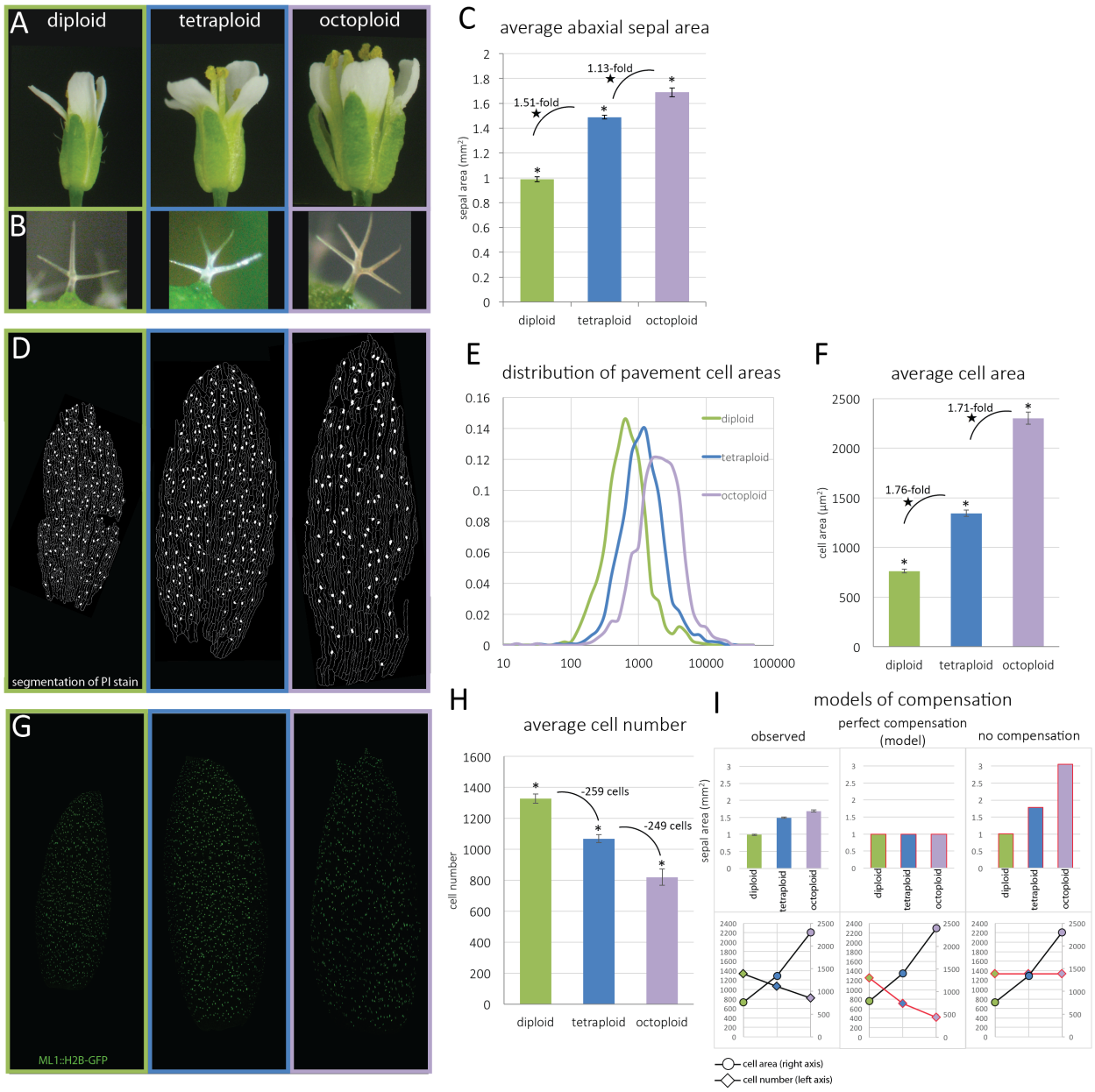

Figure 3. Whole-genome duplication increases cell size and organ size in the *Arabidopsis* sepal; cell number decreases.

A. Flowers from diploid, tetraploid, and octoploid plants in an isogenic ploidy series in Col generated by colchicine treatment. **B.** Representative trichome phenotypes on diploid, tetraploid, and octoploid leaves used for screening: trichome branch number increases with WGD ploidy level. **C.** Average mature abaxial sepal area in ploidy series (n=50-60). Bars indicate SEM. *: significant difference between samples, p< 0.001, unpaired t-test. ★: fold change differs significantly from doubling; one-sample t-test, p<0.001. **D.** Segmented abaxial surfaces of diploid, tetraploid, and octoploid mature sepals processed for cell area measurement. Marginal cells whose area could not be accurately measured have been erased. Guard cell pairs (filled in white) are excluded from measurement. **E.** Histogram representing pavement cell areas in ploidy series. n=2 sepals per genotype, total 4648 cells. **F.** Mean pavement cell area in ploidy series. Bars represent SEM. *: significant difference between samples, p< 0.05, unpaired t-

test. ★: fold change differs significantly from doubling; one-sample t-test, p<0.001.**G.** Abaxial surface of mature diploid, tetraploid, and octoploid abaxial sepals expressing *ML1::H2B-GFP*, an epidermis-specific nuclear marker. **H.** Average number of nuclei counted in abaxial sepal epidermis (n=9-20 sepals per ploidy level). Bars indicate SEM. *: p< 0.001, unpaired t-test. **I.** Measured vs. modeled compensation. Left: observed sepal area, cell number, and cell area. Cell number decreases slightly as cell area increases, moderating the increase in organ size. Center: model for perfect sepal size compensation. Cell size trends are presented as measured in F; cell number (red line) is calculated to yield constant sepal area. Right: model of a situation in which no compensation occurs. Cell size trends are presented as measured, and cell number is held constant at the measured diploid number (red line): sepal area increases more dramatically.

We hypothesized that changes in cell number underlie the difference in magnitudes of change between cell size and organ size. To accurately quantify cell number, we imaged the abaxial surface of sepals expressing *ML1::H2B-GFP*, an epidermis-specific nuclear marker (Figure 3G) and counted epidermal nuclei using image processing. Guard cell and trichome nuclei were excluded. These analyses revealed a linear decrease in cell number with increasing ploidy. Diploid sepals have an average of 1328 pavement cells; tetraploid sepals have on average 259 fewer cells than diploid sepals (-20%), and octoploid sepals have 249 fewer cells than tetraploid sepals (-23%) (Figure 3H).

Taken together, these results indicate that the organ size response to ploidy change is partially compensated. First, cell area increases linearly with base ploidy level (1.71-1.76-fold). Second, cell number decreases, also linearly. These opposing trends result in a moderately increased organ size (Figure 3I, observed). Organs are smaller than they would be if cell number were constant (Figure 3I, no compensation model), but cell number does not decrease sufficiently to maintain tetraploid and octoploid organs at a diploid size (Figure 3I, perfect compensation model). A similar compensatory phenomenon has been reported in diploid vs. tetraploid *Arabidopsis* leaves [18]. The mechanism controlling this change in cell number is

unknown, but it might arise via a reduction in the number of cells in sepal primordia or via changes in growth and cell division during development.

Other studies have indicated that scaling responses to ploidy are cell-type-specific [35]. To investigate this, we performed cell size and cell number assays for guard cells, a second epidermal cell type. Guard cells regulate the opening and closing of stomata, small pores that allow gas exchange. Guard cells do not endoreduplicate and are thus at the "base" or lowest ploidy level—2C in diploid plants, 4C in tetraploid plants, and 8C in octoploid plants. Because of the relative ease of measurement, stomatal size and density are often used as an indicator for ploidy: guard cell area or length have been shown to increase with ploidy, while the number of stomata per unit leaf area decreases [24, 25, 70-72]. We quantified guard cell pair area and guard cell number for whole sepals (Supplemental Figure 1). Our results were consistent with previous observations: guard cell area increased with ploidy and stomatal density decreased. Comparison to the pavement cell data reveals interesting differences in the response of these two cell types to ploidy. Whereas pavement cell area increased linearly with consecutive genome doubling (Figure 3F), guard cell area increased exponentially (Supplementary Figure 1A). This finding suggests that different size-control rules affect these two epidermal cell types.

We also observed that while guard cell number changes with increased ploidy, the trend differed from that observed in pavement cells. The average number of guard cell pairs did not significantly differ between diploid and tetraploid sepals (diploid: 157.3±18.6, tetraploid: 153.0±8.5 (SD)), but decreased by 25% in the octoploid (116.3±10.7 (SD)) (Supplementary Figure 1B). Stomatal density thus decreases as ploidy increases. However, because guard cell pair area increases exponentially with ploidy, the fraction of total area of the sepal epidermis

represented by guard cells remains fairly constant across ploidy levels (2.1-2.8%). Similar results were observed in a diploid vs. tetraploid comparison [25].

Entry into endocycles is affected by WGM ploidy level

Sepals in WGM plants have an increased base ploidy level, and endoreduplication further increases ploidy in developing cells (Figure 1D). Does an increase in base ploidy alter the proportion of endoreduplicating cells? To quantify this, we performed flow cytometry on epidermal cells of dissected mature sepals. We isolated the epidermis because our image processing data describe cells from this tissue; however, note that these data also include the adaxial epidermis, which was not analyzed by image processing. We found that endoreduplication decreased slightly as base ploidy level increased. In diploid sepals, the majority of epidermal cells are 2C (diploid); diminishing proportions of cells are 4C, 8C, 16C, and 32C (Figure 4A). In tetraploid sepals, the base ploidy is 4C. Endopolyploid peaks at 8C, 16C, and 32C are observed. The octoploid lines had base ploidy 8C and showed peaks at 8C, 16C, 32C, and 64C. These data can also be quantified as number of endocycles (Figure 4B): cells at the base ploidy level have undergone 0 endocycles, cells with double the base ploidy have undergone one endocycle or are in G2 of a mitotic cell cycle, and cells with four, eight, or sixteen times the base ploidy level have undergone two, three, or four endocycles. This analysis reveals that the frequency of endoreduplication is broadly similar across ploidy levels, but that endoreduplication is slightly reduced as ploidy increases. The number of cells undergoing 2-3 endocycles decreases ca. 18% between diploid and tetraploid sepals and 24% between tetraploid and octoploid sepals (Figure 4C). A similar overall pattern was observed in whole-

sepal tissue samples (including non-epidermal cells) (Figure 4C). This suggests a small negative interaction between high base ploidy level and the entry into endocycles. Previous observations of endopolyploidy in 2C vs. 4C leaf and flower tissue showed a similar trend, but did not report a significant difference [18].

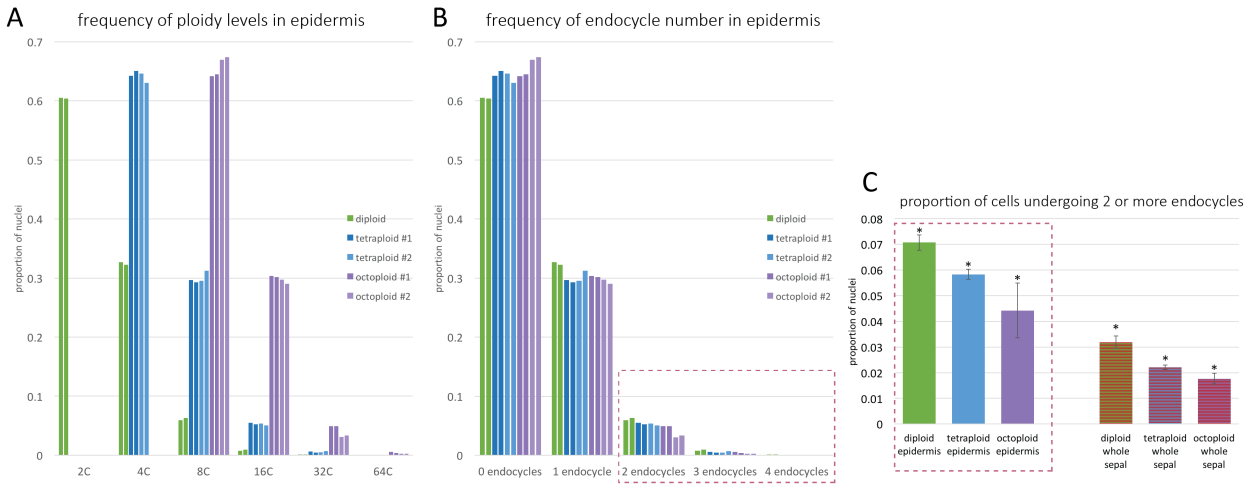

Figure 4. Whole-genome duplication has a minor effect on entry into the endocycle in sepal epidermal cells.
A. Quantification of flow cytometry peaks in diploid, tetraploid, and octoploid plants expressing the epidermal-localized marker *ML1::H2B-GFP*. All nuclei from the sepal were stained with PI; peaks were generated based on PI fluorescence, and then gated to include only GFP-positive (epidermal) nuclei. Two technical and two biological replicates are presented for each group. **B.** Data from A. presented as number of endocycles: cells at the base ploidy level (2C in diploid, 4C in tetraploid, and 8C in octoploid) have undergone 0 endocycles. **C.** Proportion of highly endopolyploid (2 or more endocycles; box in B.) cells in the sepal epidermis (left) and all sepal tissues (right). Average of 2 technical and 2 biological replicates. Bars indicate SEM. *: $p < 0.05$, unpaired t-test.

Whole-genome multiplication increases transcript abundance

We estimated total RNA transcriptome size by co-extracting total RNA and DNA from sepals and quantifying their ratios to obtain estimates of RNA mass per unit of DNA mass (µg RNA/µg DNA; [73]). Total RNA transcriptome size per cell was determined by multiplying this ratio by the average ploidy level relative to the diploid: 1, 1.8 and 3.5 for diploid, tetraploid and octoploid, respectively, as determined by the distribution of endopolyploidy in whole sepal flow

cytometry (Figure 4C). This estimates the abundance of all RNA species per cell (including mRNA, but predominantly rRNA and other non-coding transcripts). Similar to the observed increases in pavement cell area, total RNA transcriptome size per cell increased linearly with increasing ploidy (Figure 5A). On average, total transcriptome size per cell was 1.69-fold larger in tetraploid sepals than in diploid sepals and 1.85-fold larger in octoploid sepals than in tetraploid sepals.

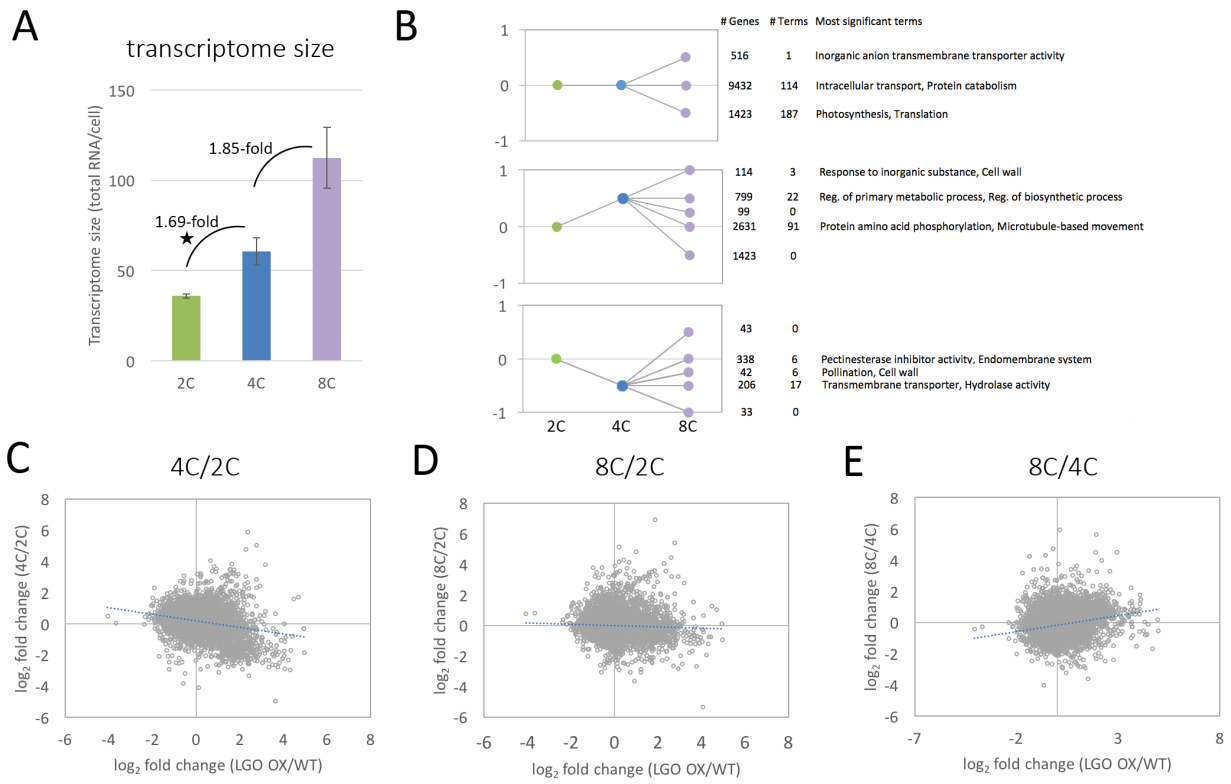

Figure 5. Whole-genome multiplication increases transcript abundance.
A. Estimates of total RNA per cell in diploid, tetraploid and octoploid *Arabidopsis* sepals (2C, 4C and 8C, respectively). Bars represent SD. ★: fold change differs significantly from doubling; one-sample t-test, $p<0.001$.**B.** Relative expression per genome (transcripts per µg of DNA) binned into 13 general responses classes. Numbers of genes and representative GO terms that are enriched in each class are shown next to each bin. **C.** Comparison of expression responses induced by changes in WGD (4C/2C; Y axis) vs. by changes in endopolyploidy (*LGO OX*/WT; X axis). **D.** Comparison of expression responses induced by changes in WGD (8C/2C; Y axis) vs. by changes in endopolyploidy (*LGOOX*/WT; X axis). **E.** Comparison of expression responses induced by changes in WGD (8C/4C; Y axis) vs. by changes in endopolyploidy (*LGO OX*/WT; X axis).

We also estimated mRNA transcriptome size by mRNA-Seq using ERCC spike-ins, as previously described ([73], Supplemental File 1). Briefly, we spiked sepal-derived total RNA with ERCC external control RNA in proportion to the ratio of DNA/RNA observed in the sepals (see Methods for further details), and performed mRNA-Seq (via poly(A) selection) on the spiked samples. *Arabidopsis*-derived read counts were then normalized to ERCC read counts to estimate expression per unit of DNA. These values were adjusted for average ploidy level as above to determine expression per cell. Expression per transcriptome was then estimated by standard TPM normalization. For each gene, we divided expression per cell by expression per transcriptome to obtain estimates of mRNA transcriptome size per cell. As with total RNA, the mRNA transcriptome increased with base ploidy level (data not shown). On average, mRNA transcriptome size per cell was 2.1-fold larger in tetraploid sepals than in diploid sepals, and was 1.6-fold larger in octoploid sepals than in tetraploid sepals. Thus, both total and mRNA transcriptomes scale with ploidy in a way that closely reflects the scaling of sepal pavement cell area with ploidy.

We grouped genes into 13 bins based on their expression response to increasing ploidy and examined each bin for gene ontology (GO) term enrichment (Figure 5B, Supplemental File 2). The largest bin consisted of genes showing no change in expression per genome copy and, therefore, a linear gene dosage dependency (N = 9432). These genes were enriched for core metabolic functions including intracellular transport and protein catabolism. This bin included GO terms related to mitochondria and the vacuole, both of which are known to scale in number or size with cell size [74]. A small group of genes showed an increase in expression per gene copy with increasing ploidy (N = 114). This bin was enriched for cell wall functions, consistent

with changes observed in yeast in response to both increasing ploidy and cell size [32]. A combined analysis of genes that were up- or down-regulated in response to polyploidy also yielded similar results to those observed in yeast [32], with enrichment for cell surface-related functions (cell wall and external encapsulating structure). Only 33 genes showed a linear decrease in expression per gene copy with increasing ploidy, and these were not enriched for any GO terms.

WGM generates expression profiles distinct from those associated with endopolyploidy

We next compared expression responses to WGM to expression responses to endopolyploidy as estimated by RNA-Seq data from a *LGO* dosage series [41]; *LGO* increases endopolyploidy in individual cells (see Figure 2). Cell types with high levels of endopolyploidy (e.g., trichomes and giant cells) have distinct gene expression profiles [40, 75]. Do polyploid cells generated by WGM express the same genes? We plotted expression fold change with increasing WGM (e.g., tetraploid vs. diploid) against expression fold change with increasing endopolyploidy (e.g., *LGO OX* vs. WT) (Figure 5C). The correlations between the two ploidy series were low ($R^2 < 0.1$), suggesting that transcriptional responses to WGM are generally distinct from transcriptional responses to endopolyploidy. Notably, however, expression responses to WGM at higher ploidy levels (8C vs 4C) were more similar to expression responses to endopolyploidy than were those involving lower WGM ploidy levels (4C vs 2C and 8C vs 2C). This observation is consistent with the fact that transcriptionally distinct endopolyploid cell types, such as trichomes [76] and giant cells [41] are at ploidy 16C-32C—more cells reach this level in octoploid than in tetraploid or diploid plants.

Relative growth rates are not affected by ploidy

In Figure 3, we found that sepal pavement cell number decreased significantly with increasing WGM ploidy. We were interested in understanding how this difference arose during development. We considered two mutually compatible hypotheses: 1. cell growth and proliferation occur more slowly at high ploidy, and/or 2. fewer founder cells are recruited from polyploid meristems into sepal primordia. There is some support for Hypothesis 1: mitotic cell cycle duration is strongly correlated with genome size, and polyploidy increases DNA content [59, 77, 78]. A genetically induced change in cell size in the meristem has been shown affect the meristem's "resolution", perturbing the formation of primordia and organ boundaries [78].

To test Hypothesis 1, we live-imaged growth of young sepals. Because size could not be used to accurately stage flowers across ploidy levels, we instead used differentiation of the stomatal lineage to roughly standardize the developmental stage. Guard cells differentiate in a tip-to-base wave in the sepal and the leaf [79-81]. The first image was taken when differentiated guard cells appeared at the sepal tip (t0); a second image was taken 24 hours later (t24) (Figure 6A). At these stages, cells were primarily expanding rather than dividing. We quantified average cell area at 0 and 24h in these images (Figure 6B). We see that series mostly cluster by ploidy, with some overlap between tetraploid and octoploid sepals—this is likely because images were taken at slightly different developmental stages. On average, tetraploid cells were about 1.90-fold larger than diploid cells, and octoploid cells were about 1.12-fold larger than tetraploid cells (Figure 6C). Tetraploid and octoploid sepals did not have fewer cells than diploid sepals at this stage, suggesting that cell number compensation phenomena have not yet occurred. We then tracked individual cells' growth across the sepal between t0 and t24

and created a heat map of cellular growth rates on the t24 image (Figure 6D). Cellular growth rate was roughly similar in all imaged flowers (Figure 6E). Average cellular growth rate does not differ significantly across ploidy levels (Figure 6F). These data indicate that, contrary to expectation, cellular growth rate is not affected by ploidy.

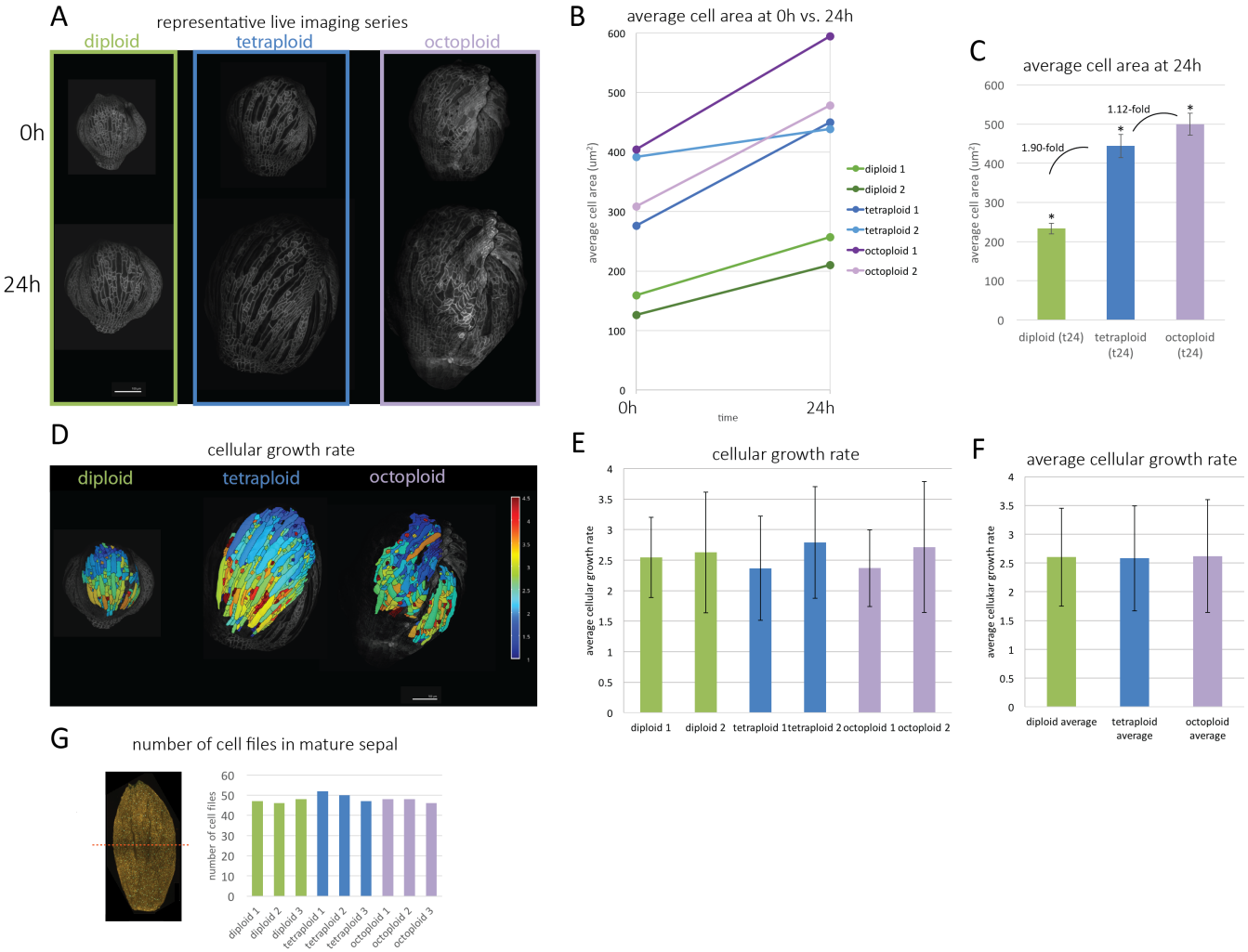

Figure 6. Whole-genome multiplication does not strongly affect cellular growth rate.
A. MorphoGraphX surface projection of developing flowers imaged at time point 0 (top) and 24h later (bottom). Flower stages were roughly synchronized by the appearance of the stomatal lineage, which differentiates in a tip-to-base wave. **B.** Average cell size of individual flowers in A. at 0h and 24h. **C.** Average size of cells from 2 diploid, 2 tetraploid, and 2 octoploid flowers at 24h. (747, 904, and 797 cells, respectively.) Bars indicate SEM. *: P<0.001, unpaired t-test. **D.** Heat map of cellular growth rate between t0 and t24. All images share the same scale. **E.** Average cellular growth rate for each of 2 diploid, 2 tetraploid, and 2 octoploid sepals. Bars represent SD. **F.** Average cellular growth rate for 2 flowers per ploidy level. Bars represent SD. *: p<0.001, unpaired t-test. **G.** Quantification of cell file

number in mature sepals. Left: line intersecting sepal midpoint. The number of cells intersecting this line was counted. Right: number of cell files in 3 diploid, 3 tetraploid, and 3 octoploid sepals.

We next tested Hypothesis 2, which proposes that fewer cells are recruited into polyploid primordia. We counted the number of cells intersecting a line drawn through the transverse midpoint of mature sepals (Figure 6G, left). Cell files arise by lateral division of an initial population of 8 cells on the lateral side of the floral meristem [37, 82]. We found that file number was remarkably invariant across ploidy levels: sepals at all ploidy levels had an average of 48±1.94 (SD) cell files (Figure 6G). This suggests that either the number of founding cells is constant across ploidy levels or that lateral divisions in polyploids rapidly recover a diploid-like file number; differences in cell number thus arise during growth after the primordium stage. Thus, neither of our hypotheses about young sepal development provide an explanation for the reduction in cell number observed in mature sepals. This discrepancy must arise relatively late in development—perhaps sepals at high ploidy terminate cell division sooner.

Scaling of nuclear size and cell size differs in the octoploid

The mechanism or mechanisms by which ploidy affects cell size are not known, but theories suggest that nuclear size plays a role. The phenomenon of a constant ratio between nuclear size and cell size (N:C ratio or karyoplasmic ratio (KR)) has been reported for many years, but direct measurements of this ratio have been limited. Here, we directly measure KR for all abaxial epidermal cells in diploid, tetraploid, and octoploid sepals to determine if KR is consistent or different across ploidy levels.

To quantify KR, we created a dual segmentation image processing pipeline (Figure 7A-D). We imaged mature sepals expressing two fluorescent markers in the epidermis: *ML1::RCI2A-mCitrine*, a plasma membrane marker, and *ML1::H2B-TFP*, a nuclear marker (Figure 7A). Sepals were imaged at 1:1:1 resolution on the X, Y, and Z axes to allow accurate three-dimensional quantification of nuclear volume. Channels were processed separately in MorphoGraphX: nuclei were segmented in 3D (Figure 7B), and pavement cells were segmented in two dimensions on a curved model of the sepal surface (Figure 7C). Pavement cell area is used as a proxy for cell surface area: because pavement cells are highly vacuolated, the volume of the cytoplasm may be better represented by surface area than by total cell volume [3, 83]. We are interested in cytoplasmic volume because past studies of KR (in non-vacuolated cells) have measured cytoplasmic volume. After processing, nuclei were manually paired with cells based on position (Figure 7D).

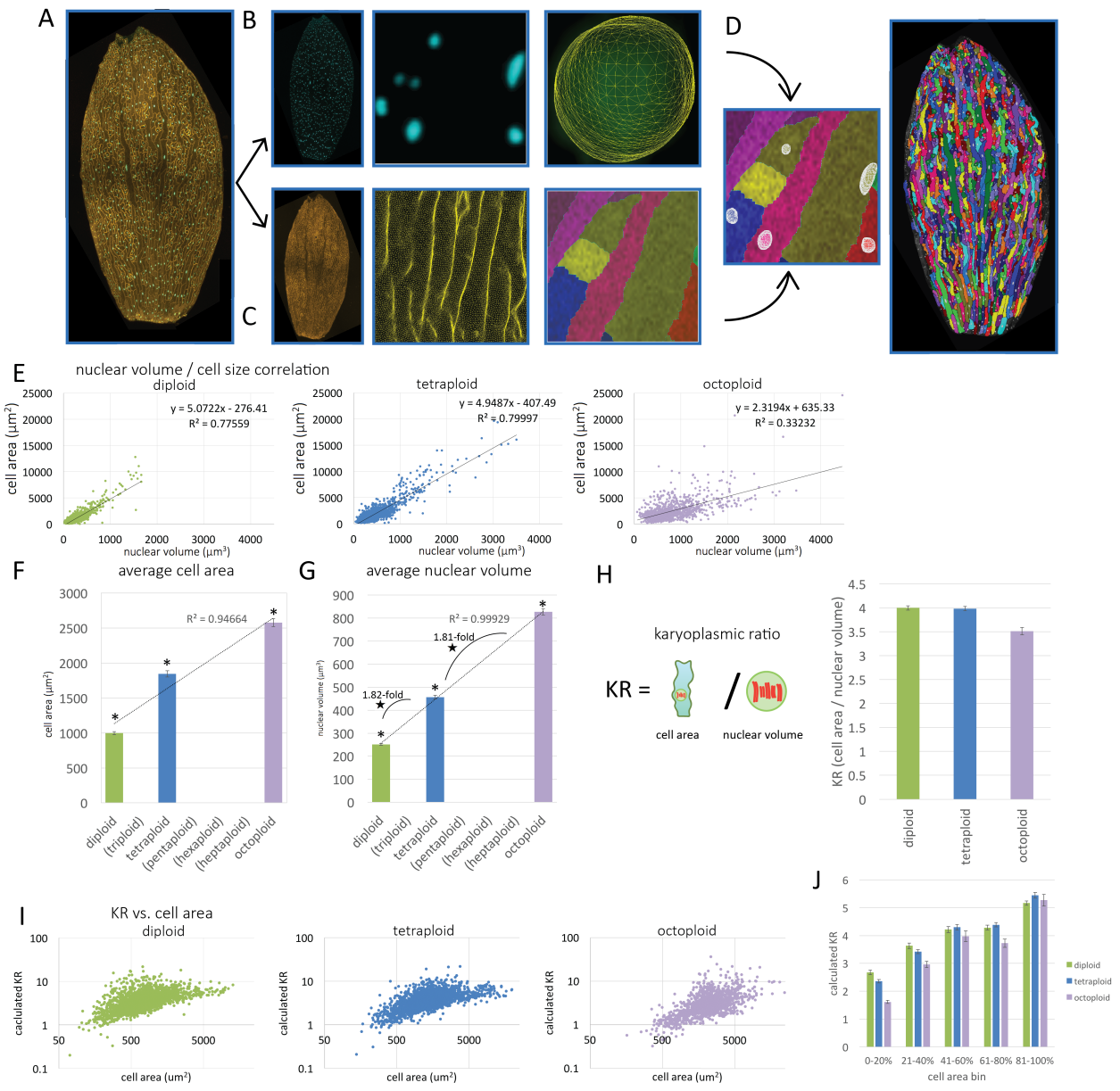

Figure 7. Cell size and nuclear size are strongly correlated across ploidy levels.
A-D: MorphoGraphX image processing pipeline for dual cell/nucleus segmentation. **A.** Maximum intensity projection of 1:1:1 confocal stack of a mature abaxial sepal expressing *ML1::mCitrine-RCI2A* (amber) and *ML1::H2B-TFP* (teal). **B.** Image processing pipeline for measurement of nuclear volume. **C.** Image processing pipeline for measurement of cell area. **D.** Manual pairing of nuclear volume and cell area. Sepal from A. with nuclei and cells segmented and paired. **E.** Correlation of nuclear volume and cell area for each ploidy level. 3 sepals per ploidy level: n=2126 cells for diploid, 1964 cells for tetraploid, 1228 cells for octoploid. Linear regression. **F.** Average cell area. Bars represent SEM. *: p<0.001, unpaired t-test. **G.** Average nuclear volume. Bars represent SEM. Linear regression**.** *: significant difference between samples, p<0.001, unpaired t-test. ★: fold change differs significantly from doubling; one-sample t-test, p<0.001. **H.** Average calculated karyoplasmic ratio for each ploidy level. *:

$p<0.001$, unpaired t-test. **I.** Cell area vs. calculated karyoplasmic ratio. **J.** Average karyoplasmic ratio in diploid, tetraploid, and octoploid for 5 bins as sorted by cell area. Bars indicate SEM.

Image processing confirmed our earlier finding that cell size increases with ploidy (Figure 7F). Nuclear volume also increases linearly with ploidy (Figure 7G). Nuclear volume and cell area correlate well in diploid and tetraploid sepals; the strength of correlation between nuclear volume and cell size is somewhat reduced in the octoploid (Figure 7E). The average calculated karyoplasmic ratio (nuclear volume divided by cell area) is nearly identical in diploid and tetraploid sepals (diploid: 4.00 ± 0.04; tetraploid: 3.98 ± 0.04 (SD)), and is significantly lower (3.51 ± 0.08 (SD)) in octoploid sepals, indicating a smaller ratio of cell area to nuclear size: this suggests that, although a characteristic average karyoplasmic ratio is maintained in these cells, its value can be changed by ploidy (Figure 7H). Although the average karyoplasmic ratio is about 4, we observe a range of values for KR in individual cells (Figure 7I). Nuclear size does not explain all variation in cell size (Figure 7E), suggesting that although the karyoplasmic ratio is maintained generally, there is some flexibility in size. Further, we find that smaller cells have lower KR (i.e. less cell area per unit area of nucleus) than larger cells (Figure 7J). Ploidy levels differ most strongly in average KR in the smallest 20% of cells: in this bin, tetraploid and octoploid sepals have progressively smaller KR.

Minimum nuclear volume increases with ploidy

The strong linear association between cell size and nuclear volume implies that smaller cells have a smaller nucleus. However, nuclei cannot reach a volume of zero: some space will always be occupied by chromatin. We hypothesized that DNA content sets a

minimum volume for the nucleus: minimum nuclear size should thus increase with ploidy in our ploidy series. We performed a linear regression of cell area vs. nuclear volume (data from Figure 7E, but with axes swapped) and used the y-axis intercept to represent the theoretical minimum nuclear volume (Supplemental Figure 2A). Note that this is a theoretical minimum based on a population of cells— we observe that some nuclei in the dataset are smaller than this average minimum value. Our analysis shows that theoretical minimum nuclear size increases linearly with ploidy (Supplemental Figure 2B).

Cell ploidy, not nuclear volume, controls cell size

Our data indicate that a precise ratio between nuclear volume and cell size is maintained, and that this ratio is ca. 4.0 in diploid sepals. These results do not, however, indicate how ploidy is transduced into size phenotypes: does increased nuclear size induce cell size scaling, as suggested by the nucleoskeletal theory [55], or does ploidy directly affect cell size? To investigate this, we observed a mutant with reduced nuclear volume, *crowded nuclei 1* (*crwn1*) (Figure 8). Mutation of the *CROWDED NUCLEI* (*CRWN*) genes reduces nuclear size, increases DNA density, and makes nuclear shape rounder (Figure 8B); the proportion of cells entering endocycles is not altered [84, 85]. We reasoned that if cell size is reduced concomitantly with nuclear size in *crwn1* (Figure 8A, 1.), then nuclear size might act as a determinant of cell size; if not, then another factor must link cell size to ploidy (Figure 8A, 2.).

We measured cell area and nuclear volume and calculated KR in *crwn1* sepals (Figure 8C). Average nuclear volume was reduced by about half relative to diploid Col-0, but cell area did not change significantly (Figure 8B,E). The correlation between nuclear and cell size

remained strong (Figure 8D), but the constant describing this relationship changed: average KR was 8.72±0.15 (SEM), indicating that there was substantially more cell area per unit area of nuclear volume (Figure 8E-G). These results indicate that nuclear size does not have a causal relationship in determining KR or cell size.

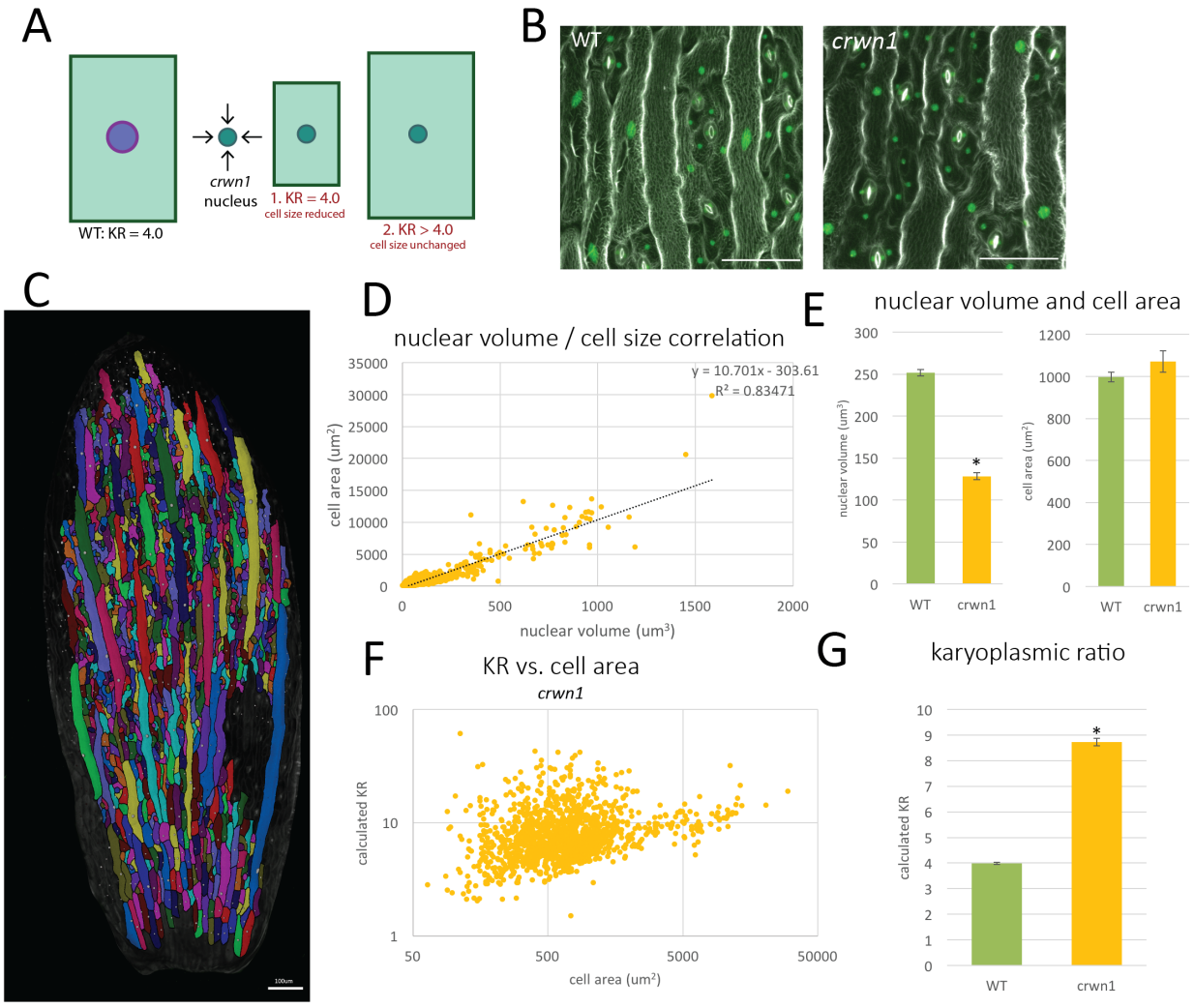

Figure 8. Nuclear size decreases in the *crwn1* mutant, but cell size is unchanged.
A. Model for hypotheses about the effect of a *crwn1* mutation, which reduces nuclear size relative to WT. If cell sizes are reduced in proportion, the average KR will resemble that of WT (ca. 4.0) (left); if cell sizes are constant or only somewhat reduced, KR will increase (right). **B.** Nuclear and cell size phenotypes in WT vs. *crwn1*. Green: *ML1::H2B-TFP*. White: propidium iodide staining of cell walls. **C.** Dual segmentation of a sepal homozygous for *crwn1.* Nuclei (white) were segmented using *ML1::H2B-TFP* signal. Cells were segmented using propidium iodide stain. **D.** Correlation of nuclear volume and cell area. Linear regression. 2 sepals: n=1351 cells. **E.** Average *crwn1* nuclear volume and cell area data relative to WT (diploid) presented in Figure 7. Bars represent SEM. *: p<0.001, unpaired t-test. **F.** Cell

area vs. calculated karyoplasmic ratio. **G.** Average karyoplasmic ratio for *crwn1* vs. WT (diploid) presented in Figure 7. Bars represent SEM. *: $p<0.001$, unpaired t-test.

Discussion

Compensation mechanisms reduce the size effects of ploidy

We and many others have observed that cell area increases with ploidy. In our analyses, we observed a ca. 1.75-fold increase in cell area with genome doubling; this is somewhat less than the doubling in size that might naively be expected (Figure 3E,F). We measure only 2-dimensional cell area as an indication of sepal pavement cell size. This parameter is a reasonable approximation of functional (cytoplasmic) volume in sepal pavement cells, as the majority of these cells' volume is occupied by the vacuole—cytoplasmic volume is roughly proportional to the surface area of the cell [3]. Other geometric measurements likely also scale with ploidy: we are not able to directly measure cell volume, but because volume increases disproportionately to surface area, the fold change in cell volume is likely to be greater than that in area.

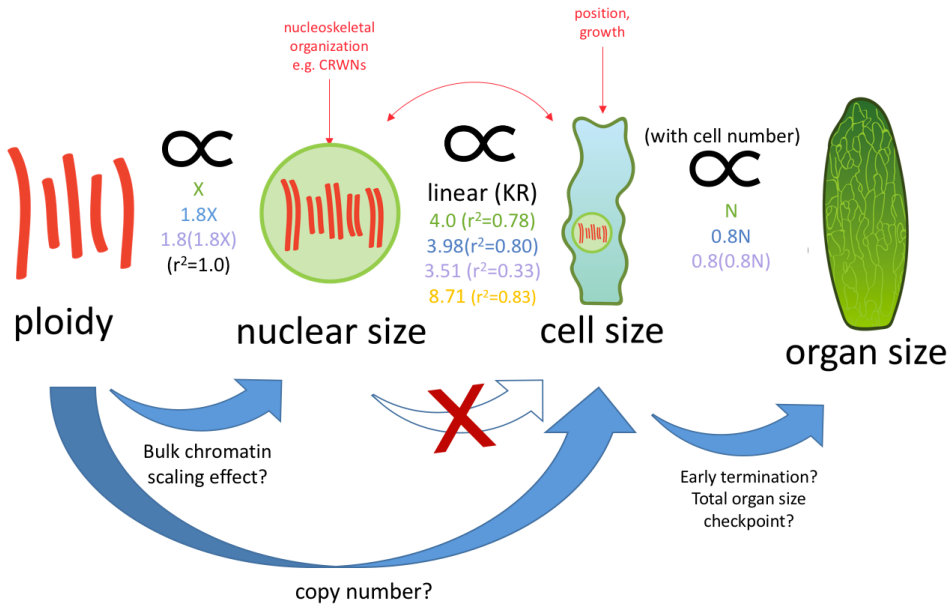

Figure 9. Summary of findings. Nuclear size, cell size, and organ size increase with ploidy. Nuclear size and cell size are correlated by a relatively constant karyoplasmic ratio (KR; ca. 4.0 in diploid (green) and tetraploid (blue) sepal pavement cells, 3.5 in octoploid (purple) cells); however, reduction of nuclear size does not change cell size (more than doubling KR; *crwn1* (yellow)), suggesting that nuclear size does not have a direct scaling effect on cell size. We instead hypothesize that ploidy directly affects both nuclear size (with chromatin bulk a likely factor) and cell size (possibly via a ploidy-sensing mechanism). Sepal area increases as a result of increased cell size, but this change is partially compensated by a decrease in cell number that occurs late in development.

We also observed that sepal area increased with ploidy, but that the magnitude of this change (ca. 1.35-fold) was smaller than the magnitude of size change in sepals' constituent cells (Figure 3C). These results are summarized in Figure 9. We discovered a ca. 20% decrease in total cell number that explains this discrepancy. We identify this as a compensation phenomenon. Compensation is an interplay between cell size and cell number: it occurs when a change in one of these mitigates a change in the other [19, 20, 86, 87]. This tradeoff is demonstrated clearly in our LGO dosage series: cell size increases, but is balanced by decreased cell number to result in consistent organ size (Figure 2). However, sepals do not compensate completely for WGM ploidy change: polyploid sepals are smaller than they would be if cell

number remained constant, but are not diploid-sized (Figure 3I). Our live imaging data indicate that this cell number change arises late in development: actively growing sepals of all ploidy levels have the same number of cell files and grow at roughly the same rate (Figure 6). A relatively late-acting mechanism must affect proliferation to enact compensation. One possibility consistent with our results would be that maturation and termination of cell division and growth occur earlier in higher ploidy sepals. The cause of this cell number reduction is so far unknown—is this intrinsic to the growth of polyploid cells, or might it be a response to a total organ size checkpoint [20, 46, 88-90]?

Similarly, the increase in transcriptome size due to whole genome duplication appears to be partially compensated (i.e. less than doubled). We estimate that the total RNA transcriptome increases 1.7-1.9-fold, and the mRNA transcriptome increases 1.6 to 2.1-fold, for each whole genome duplication. Transcriptome size compensation was also observed in a natural allopolyploid of *Glycine* [91] as well as in leaf tissue of synthetic *Arabidopsis* autotetraploids (Coate et al. in preparation), suggesting that this is a conserved response to genome duplication in plants. Mammalian embryonic stem cells showed a larger increase in cell size with WGM (2.2-fold) than we observe here, but they exhibited a similar coordination of transcript abundance with cell size [92]. The fact that cell size and transcriptome size show similar increases is consistent with previous observations that transcription scales with cell size [21-23, 93, 94].

Cell size scales with ploidy, not nuclear size

Previous studies have described a strong scaling relationship between cell size and nuclear size (KR). We confirmed this correlation by directly measuring nuclear volume, cell area,

and KR for nearly every cell in the sepal epidermis. We found that the average KR for diploid and tetraploid WGM lines was remarkably similar (ca. 4.0), and that octoploid plants had slightly less cell area per unit of nuclear volume (Figure 7H). We also found that KR is somewhat higher in larger cells (Figure 7J) and that individual cells vary somewhat in their karyoplasmic ratio. This variability is consistent with our previous findings that cell size and ploidy do not perfectly correlate in the sepal epidermis—rather, cell size varies around a mean set by ploidy level [37]. Bourdon et al. similarly found that tomato pericarp cell size is controlled both by ploidy and by the cell's position in the pericarp [95].

One simple model of cell size control is that ploidy change directly affects the volume of the nucleus, which indirectly affects the volume of the cell. Our data do not support this model. We find that although cells maintain a fairly constant ratio between nuclear size and cell size (KR; ca. 4.0 in sepal pavement cells), cell size is not dependent on nuclear size. When nuclear size was decreased in *crwn1,* cell size did not decrease correspondingly. The correlation between nuclear size and cell size remained strong, but the constant describing this relationship (KR) increased to ca. 8.7—cells had substantially more area per unit area of nuclear volume (Figure 8). This suggests that ploidy and cell size are related directly rather than via nuclear volume. Nuclear volume itself is likely controlled both by ploidy and by cell size: measured nuclear volumes have a continuous distribution (Figure 7E) rather than the discrete, stepwise distribution that would be expected if ploidy were the sole control on nuclear volume. Also, *crwn1* nuclei are smaller than wild-type nuclei with the same amount of DNA: this indicates that wild-type nuclei are larger than the minimum required to fit the DNA, and suggests additional regulation of nuclear size. This conclusion is consistent with our finding that

minimum nuclear size is smaller in *crwn1* and scales with ploidy in wild-type cells (Supplemental Figure 2).

Interaction of ploidy with other cell size control mechanisms

We have shown that ploidy is an important contributor to cell size; however, ploidy is not the only size control mechanism acting in cells. The majority of size-related studies address mechanisms of cell size homeostasis. Many cell types maintain a consistent average size: to achieve this, cells must constrain variance introduced by fluctuations in growth rate and asymmetric division [96]. Single-cellular organisms like yeast and bacteria maintain a consistent cell size in populations, and many studies have investigated size control mechanisms that buffer stochasticity in these systems [97, 98]. Plant cells maintain a consistent size during divisions in the meristem and primordium [78, 99, 100]. However, mature *Arabidopsis* epidermal cells are notably non-homogeneous in size, varying more than 100-fold in area with level of endopolyploidy. It seems likely that at least two groups of size control mechanisms exist: one group that promotes size homeostasis, and another, linked to ploidy, that facilitates the generation of cells of vastly different sizes.

If homeostasis mechanisms are at work in polyploid cells, they must be recalibrated to an increased baseline cell size: 16C cells are as much as 100 times larger than 2C cells. One hint that size control mechanisms are active in such cells is that adherence to the karyoplasmic ratio does not appear to change much with increasing cell area (and increasing endopolyploidy): cell sizes are still relatively constrained (Figure 7I). Further, cells in WGM tetraploid and octoploid lines do not show substantially greater variance in size than WT cells (Figure 3F). It is unclear whether this consistent sizing could arise directly from growth. Sepal pavement cells' growth

rates are highly variable at the cellular level, but undergo spatiotemporal averaging to yield consistent growth [67]. Most known size control mechanisms modulate the timing of division by regulating START, the transition from G1 to S [101, 102]. Endoreduplicating cells also go through START, so these size control mechanisms could potentially act on endoreduplicating as well as mitotic cells; the challenge is "setting" regulation to a size that is appropriate for the cell's ploidy.

Do cells sense their ploidy?

We speculate that the mechanism linking ploidy to cell size is based on active sensing of ploidy rather than passive scaling. Several pieces of evidence support this hypothesis. First, the magnitude of size change in response to ploidy is cell-type-specific: the size of sepal pavement cells increases linearly with ploidy level (Figure 3F), but that of guard cells scales to ploidy exponentially, resulting in a much greater magnitude of change in octoploid guard cells (Supplemental Figure 1). Meanwhile, mesophyll cells have little or no size response to endopolyploidy [35]. These differences argue against a single, intrinsic effect of ploidy on cell size, and instead suggest that cell types can enact different ploidy-based scaling rules as they differentiate [35]. Also, we observed that endocycling is slightly downregulated as base ploidy level increases, which may indicate that cells target a specific ploidy level to some extent. Finally, ploidy sensing might offer a mechanism by which cell size homeostasis mechanisms are "set" to a new point to accommodate ploidy-based variation in cell size.

There are several means by which a cell might sense its ploidy. The direct effects of ploidy change are 1. an increased bulk of DNA its associated proteins and 2. increased copy number at every locus: a hypothetical mechanism should offer a readout of one or both of

these parameters. One hypothesis is that DNA bulk increases nuclear size, which then affects cell size; our *crwn1* data (Figure 8) lead us to reject this hypothesis. DNA bulk might be sensed in another way, or the ploidy-sensing mechanism might sense copy number. Mechanisms that count chromosome number do exist: in *Drosophila*, sex is determined by counting the number of X chromosomes in comparison to the number of autosomes. X-linked genes like *scute, sisterless-a*, and *runt* act as "numerators", while autosomal loci act as "denominators" against which the number of X-linked genes is titrated [103]. X chromosomes are also counted in *C. elegans* [104]; a mechanism that senses ploidy might similarly sense copy number of a specific gene locus or gene product. Loci that might act as a numerator are abundant: all loci increase in copy number when ploidy increases. If sensed/counted loci exist, they might be identified in a screen for plants in which cell size does not respond to ploidy change. Conversely, increasing copy number of these loci might give a cell a false report of its ploidy, causing cell size to increase without WGM. Loci or factors that act as denominators are harder to envision; the denominator would ideally remain at a constant level as ploidy increases, but all chromosomal loci are amplified equally. Cell components whose number does not scale with ploidy, such as the nucleolus, might offer a "constant" against which locus number could be compared. Determining whether ploidy is sensed, and if so how it is sensed, will be the next step in unraveling the relationship between ploidy and size.

Materials and Methods

Generation and identification of polyploid lineages

Polyploid lineages of all genotypes were generated and identified by a protocol modified from [24]. A drop (ca. 2 µL) of 0.25% colchicine solution was placed on the vegetative meristem of seedlings with three young leaves. Treated plants were covered with a lid and left to sit for 24h before being returned to the growth chamber. Each treated pot contained approx. 15 plants; all

plants from a pot were pooled for seed collection, and independent events of tetraploidy and octoploidy were defined as originating from different pooled pots.
Probable neopolyploid individuals were identified by screening for trichome phenotype in seedling leaves. Trichomes on diploid leaves generally have 3 branches. Tetraploid plants' leaves have approx. 25% 4-branched trichomes. Octoploid plants have >50% 4-branched trichomes and ~10% 5-branched trichomes. Ploidy was confirmed with flow cytometry.

Flow cytometry

To determine whole-plant ploidy level, we harvested a young rosette leaf. Leaf tissue was chopped with a new razor blade in 600 µL Aru buffer [105]. Suspended nuclei were filtered through a 40 µm Fisherbrand cell strainer, treated with RNAse (0.001 µg/100 µL sample), and stained with propidium iodide (0.001 µg /100 µL sample). Samples were run on an Accuri C6 flow cytometer, and base ploidy level was diagnosed by presence or absence of 2C and 4C peaks.
For flow cytometry on sepals expressing pAR180 (*ML1::H2B-GFP*), 100 mature sepals from all four sepal positions (abaxial, adaxial, and lateral) were dissected into 800 µL Aru buffer and processed as above. Events were gated to separate epidermal (GFP-positive) nuclei from non-epidermal (GFP-negative) nuclei [37].
Average ploidy level for whole sepals was determined by multiplying the fraction of events at a given ploidy level by the value of that ploidy level (i.e. 2, 4, 8, 16, 32, or 64), and summing the values for all ploidy levels.

Sepal area measurement

Mature abaxial sepals (n=50-64) were dissected with a needle, aligned on a microscope slide, flattened with a second slide, and photographed at 20x (5x on microscope, 4x on camera) against a black background with a Canon Powershot A640 camera mounted on a Zeiss Stemi 2000C dissecting microscope. Sepal area was measured using a custom Python contour extraction pipeline reported in [67].

MATLAB 2D cell area measurement

Sepals were stained with 2% PI in H_2O for 15 min and imaged at 10x on a Zeiss 710 laser scanning confocal microscope. Samples were excited with a 514 nm laser. PI emission was collected at 566-649 nm. Pavement cell areas for all clearly visible epidermal cells were measured using a custom MATLAB module reported in [37] and [69]. Guard cell pair areas were measured manually in FIJI by tracing as freehand selections in 10x or 20x confocal images.

MorphoGraphX cell size and nuclear volume measurement

For diploid and tetraploid plants, sepals expressing pAR169 (*ML1::mCitrine-RCI2A*) and pAR229 (*ML1::H2B-TFP*) were imaged using a 20x water objective (NA = 1.0) on a Zeiss 710 confocal microscope. mCitrine was excited with a 514 nm laser and emission was collected from 519-649 nm. TFP was excited with a 458 nm laser and emission was collected from 463-509 nm. 3-9 tiles were used to capture whole sepals. Stacks were optimized to 1:1:1 X:Y:Z resolution. Channels were split in FIJI.

The TFP channel (marking nuclei) was processed in MorphoGraphX as follows: 1. Brighten Darken (2.0). 2. Gaussian Blur (x,y,z sigma=0.7). 3. Binarize stack (threshold 10,000) 4. Hand correct stack: use Pixel Editor tool to remove noise and any misrepresented nuclei. 5. Generate Marching Cubes 3D mesh (cube size=1). 6. Clear segmentation from mesh; seed each nucleus individually; run Watershed Segmentation. These processes generate three-dimensional representations of individual nuclei.

The mCitrine channel (marking plasma membranes) was processed in MorphoGraphX as follows: 1. Gaussian Blur 2x (x,y,z sigma=1). 2. Edge Detect (Threshold=8000). 3. Fill Holes 1-3x. 4. Generate Marching Cubes Surface (cube size=15). 5. Delete adaxial (flat) face of mesh. 6. Alternately smooth and subdivide mesh until at least 500,000 vertices exist. Delete bad normals. 7. Project plasma membrane signal onto surface (Min Dist 8, Max Dist 12; adjust for best signal). 8. Smooth mesh signal (Passes: 3). 9. Run auto-segmentation. 10. Hand-correct original segmentation to match plasma membrane signal; overlay nuclear channel for additional positional information. These processes generate two-dimensional representations of cell area that take into account the sepal's curvature.
Nuclei and cells were manually paired using the Lineage Tracking tool. Nuclear volumes were generated using Heat Map (Heat Map Type: Volume; Signal Average; Global Coordinates). 2D cell areas were generated using Heat Map (Heat Map Type: Area; Signal Average; Global Coordinates). Nuclear and cell size measurements were paired using the Parents spreadsheet generated by Lineage Tracking.
Octoploid sepal images were processed in the same way, but nuclei were marked by pAR180 (*ML1::H2B-mGFP*) and cell walls were stained with propidium iodide. Samples were excited with a 488 nm laser. GFP emission was collected from 493-556 nm. PI emission was collected from 566-649 nm.
For *crwn1* plants, propidium iodide (PI) was used to stain cell walls. TFP was excited with a 458 nm laser and emission was collected from 463-523 nm. PI was excited with a 561 nm laser and emission was collected from 566-649 nm.

<u>Nuclear number counting</u>
Sepals expressing the construct pAR180 (*ML1::H2B-GFP*) were imaged using a 10x objective on a Zeiss 710 confocal microscope. Sepals were stained with propidium iodide (PI) to ensure that all cells were visible for imaging and that no cells were dead (PI stains dead cells' nuclei). Samples were excited with a 488 nm laser. GFP emission was collected from 493-556 nm. PI emission was collected from 566-649 nm. Channels were split in FIJI and the GFP channel was processed in MorphoGraphX [106] as follows: 1. Brighten Darken (2.0). 2. Gaussian Blur 2x (x,y,z sigma=1). 3. Binarize stack (threshold 5000) to exclude guard cell nuclei (relatively dim). 4. Gaussian Blur 2x (x,y,z sigma=1). 5. Hand correct stack: import PI channel and use Pixel Editor tool to remove trichome nuclei and any remaining guard cell nuclei. Nuclei were counted using the Costanza plugin in FIJI with the following custom settings: Peak Remover=10.0, Background Extraction=40.0, use Extended Neighborhood, Mean Filter=2.0, Peak Merger= 10.0. Misidentified nuclei (usually a single nucleus split in two) were identified by comparison to the original image and corrected for in the cell number report.

Cell file counting

A horizontal line passing through the midpoint was drawn across the sepal. The number of cells intersecting this line was counted. Three replicates were performed for each ploidy level.

Live imaging

Inflorescences of plants expressing the plasma membrane markers pLH13 (35S::*mCitrine-RC12A*) or *PM d35s::mCherry* [107] were dissected with a needle to expose developing flowers. Dissected inflorescences were severed and taped to a coverslip. Cut stems were embedded in 0.8% agarose containing 0.5X Murashige & Skoog media, 1% sucrose, 0.25X vitamin mix, and 1 µL/mL Plant Preservative Mixture (PPM) in small petri dishes [108]. Dissected inflorescences in plates were placed upright in a Percival growth chamber (24h light) between time points. Flowers were imaged at 24h intervals on a Zeiss 710 confocal microscope, 20X water immersion objective (numerical aperture = 1.0). mCitrine was excited with a 514 nm laser and emission was collected from 519-632 nm. mCherry was excited with a 561 nm laser and emission was collected from 578-649 nm. Flowers were immersed in water for 30 minutes before the first time point and for 5 minutes before each subsequent time point.

RNA-Seq

Diploid, tetraploid and octoploid sepals were dissected from flowers in the final bud stage (stage 12; [109]), and immediately frozen in liquid nitrogen. Three biological replicates were collected per ploidy level, with 100-200 sepals from 2-4 individuals pooled per replicate. All samples were collected between 1pm and 4pm to minimize the effects of diurnal variation in gene expression.

Total nucleic acids were extracted using a custom protocol as follows: sepals were pulverized in 200 µL GTC Lysis buffer (Omega Bio-Tek) containing 4 µL of β-mercaptoethanol, then passed through a homogenizer column (Omega Bio-Tek) by centrifugation at 15,000 x g. The flowthrough was mixed with one volume of 100% EtOH, and nucleic acids were recovered following the Clean & Concentrator-5 protocol (Zymo Research) beginning at step 3. Nucleic acids were eluted with 50 µL of nuclease-free water. The resulting total nucleic acids were split into two fractions, and one was treated with Turbo DNase (Invitrogen) to yield purified RNA following the manufacturer's instructions. The other fraction was treated with RNase cocktail enzyme mix (Invitrogen) at room temperature for 10 minutes to recover purified DNA. RNA and DNA concentrations and yields were measured using Qubit RNA Broad Range and DNA High Sensitivity assays (Life Technologies).

Purified RNA was spiked with External RNA Controls Consortium (ERCC) Spike-in Mix 1 (Ambion) in proportion to the DNA to RNA ratio obtained from Qubit assays as follows. The ERCC recommends adding 2 µL of a 1:100 dilution of ERCC Mix 1 per 1 µg of total RNA. We adjusted this volume based on the amount of DNA associated with 1 µg of total RNA in a given sample. The ratio of DNA to total RNA was 0.0278 in diploids, 0.0294 in tetraploids, and 0.0315 in octoploids, and the average of all three ploidies was 0.0296. The relative amounts of DNA per unit of RNA, therefore, were 0.941 (0.0278/0.0296), 0.995, and 1.064 for diploids, tetraploids and octoploids, respectively. Consequently, we spiked in the following volumes of a 1:100

dilution of ERCC Mix 1 per 1 µg of total RNA: 1.88 µL (2 µL x 0.941), 1.99 µL (2 µL x 0.995), and 2.13 µL (2 µL x 1.064) for diploids, tetraploids and octoploids, respectively. Strand specific RNA-Seq libraries were made from spiked RNA using the NEBNextµLtra Directional RNA library kit for Illumina (New England Biolabs) at the RNA Sequencing Core in the College of Veterinary Medicine at Cornell University. All nine libraries (three ploidy levels x three biological replicates) were multiplexed and sequenced on an Illumina NextSeq 500 (75 nt read lengths).

Raw FASTQ files were filtered and trimmed to removed low quality and adapter sequences using Trimmomatic [110] with settings: ILLUMINACLIP:TruSeq3-SE.fa:2:30:10 LEADING:3 TRAILING:3 SLIDINGWINDOW:4:15 MINLEN:36., Filtered reads were aligned to the *Arabidopsis* reference sequence (TAIR10) or to the ERCC reference using HISAT2 [111]. Read counts per gene were tallied using HTSeq [112]. Fold changes in expression between ploidy levels and differentially expressed genes were identified using DESeq2 [113]. In order to estimate fold-change in expression per genome between ploidy levels, ERCC specific size factors estimated by DESeq2 were used to normalize DESeq2-based analysis of *Arabidopsis* read counts.

Plant growth conditions

All plants were grown under 24h light conditions at 22^{o}C in Percival growth chambers. All seeds except those used for RNA-seq were sown on Lambert Mix LM-111 soil and cold-stratified at 4^{o}C for 3-5 days. Seeds used for RNAseq (grown at Reed College) were sown on Sunshine Mix #4. All seeds were cold-stratified at 4^{o}C for 3-5 days.

Accessions and transgenes

Columbia (Col-0) was used as wild type.

lgo-2 (SALK_033905) is a loss-of-function allele of *LOSS OF GIANT CELLS FROM ORGANS* (*LGO*: AT3G10525) containing a T-DNA insertion. Homozygous ABRC accession CS69160.

sim-1 lgo-2 was obtained by crossing *lgo-2* to *sim-1* (CS23884), a recessive EMS allele of *SIAMESE* (*SIM*: AT5G04470). Plants were self-fertilized twice to yield a double homozygous mutant in the F3 generation.

LGO OX is *ML1::LGO* (pAR178) [40, 41].

Heterozygous lines in the *LGO* dosage series were generated by crossing *LGO OX* or *lgo-2* [40] to WT Col. Heterozygous plants were identified in the F1 generation.

pAR180 is *ML1::H2B-mGFP* [37]. It was transformed into Col-0 by *Agrobacterium*-mediated floral dipping.

pAR169/pAR229 was created by crossing Col-0 lines containing pAR169 (*ML1::mCitrine-RCI2A*) [37] and pAR229 (*ML1::H2B-mTFP*).

pLH13 is *35S::mCitrine-RCI2a*.

crwn1 was recovered in a forward genetic screen (unpublished).

PM d35s::mCherry (pm-rk *CD3-1007*) is localized to the plasma membrane by the coding region of *AtPIP2A* [107].

Sequence data (FASTQ files from RNA-Seq experiments) from this article can be found in the National Center for Biotechnology Information Sequence Read Archive as BioProject: PRJNA448456.

List of Supplementary Materials

Supplemental Figure 1. Sepal guard cells follow an alternative scaling rule.
Supplemental Figure 2. Minimum nuclear size increases with ploidy.
Supplemental File 1. RNA-Seq data.
Supplemental File 2. Gene ontology enrichment by expression response bin.

Author Contributions

DOR, AHKR, JEC, and JJD designed the research; DOR and JEC performed research; LH and MB contributed marker and polyploid lines; DOR, JEC, and AS analyzed data; DOR made figures and wrote the paper; AHKR, JEC, JJD, AS, LH, and MB contributed text and/or suggestions.

Acknowledgements

Erika Hughes and Eric Richards shared *crwn1* mutant seeds and genotyping information. Mingyuan Zhu shared live imaging techniques. Heather Meyer shared MorphoGraphX image processing techniques. Joe Cammarata and Eric Richards gave valuable comments on the manuscript. We thank Robert Sablowski for interesting discussions.

Funding

D.O.R. was supported by a Deans McNair Graduate Diversity Fellowship.
Work on LGO was supported by NSF IOS-1553030.
RNA-Seq work was supported by NSF DEB-1257522.
A.S. was supported by National Institutes of Health Grant 1R01GM126557-01.

Supplementary Figures

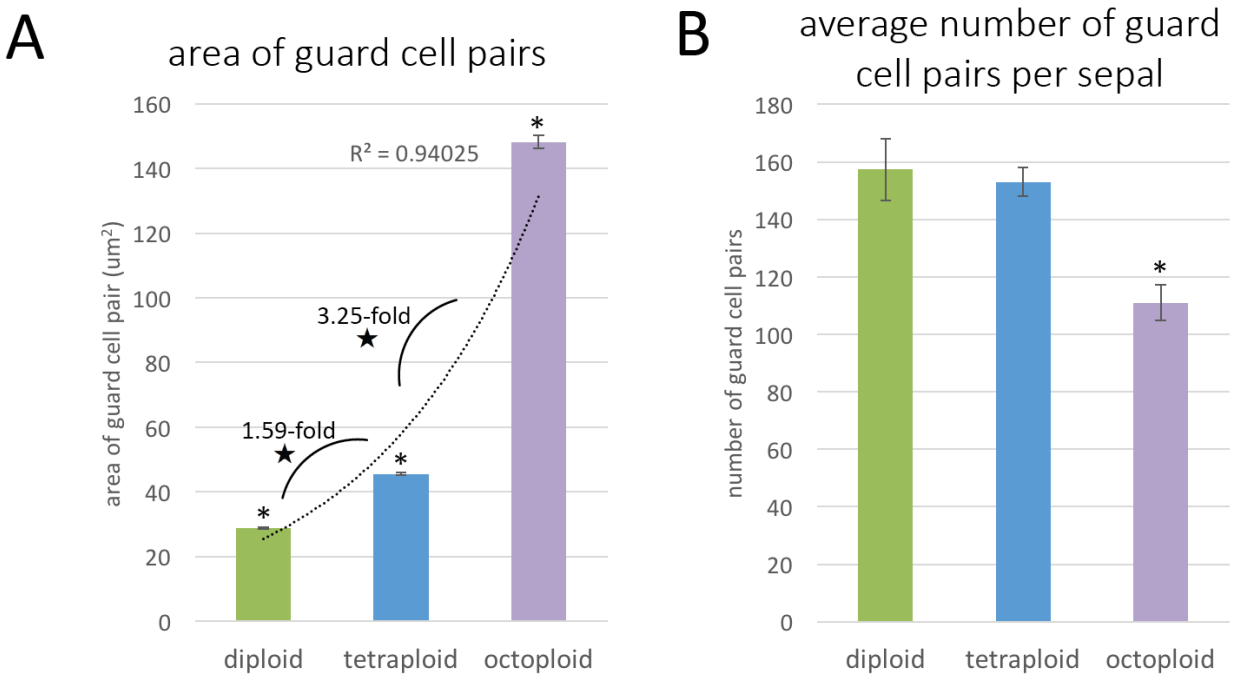

Supplemental Figure 1. Sepal guard cells follow an alternative scaling rule.

A. Measured area of guard cell pairs for 3 diploid, 3 tetraploid, and 3 octoploid sepals. N= 472 cell pairs (diploid), 459 cell pairs (tetraploid), 333 cell pairs (octoploid). Bars represent SEM. *, significant difference between samples, p<0.001, unpaired t-test. ★: fold change differs significantly from doubling; one-sample t-test, p<0.001. **B.** Average number of guard cell pairs per sepal. N=3 sepals. Bars represent SEM. * p<0.05, unpaired t-test.

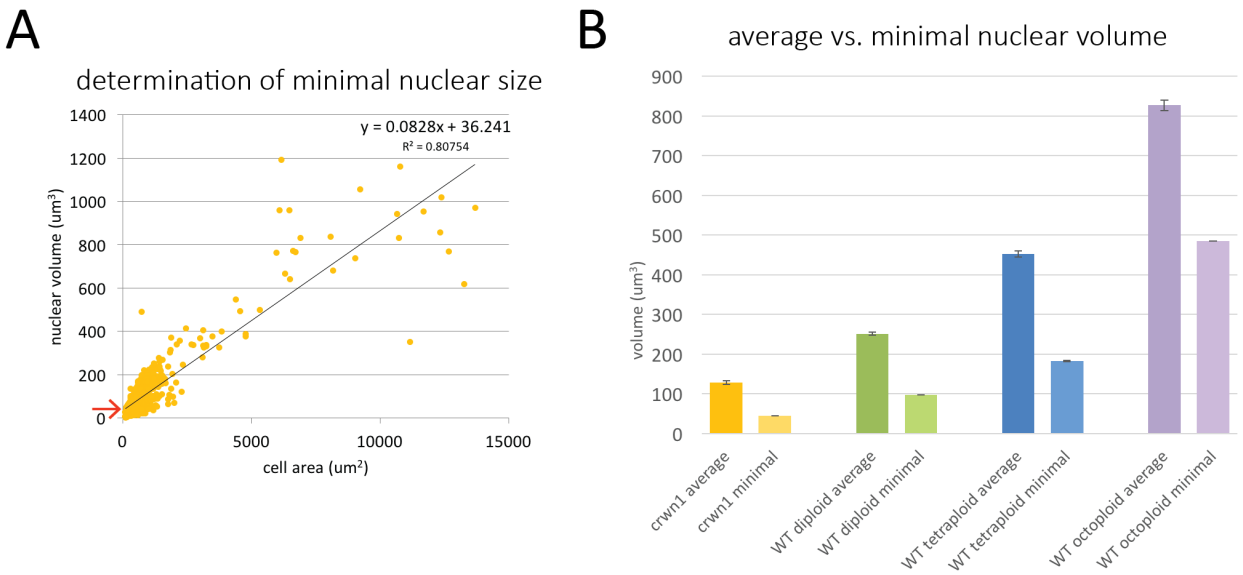

Supplemental Figure 2. Minimum nuclear size increases with ploidy. A. Example of derivation of minimum nuclear size for one *crwn1* replicate. A linear regression was performed for cell area vs. nuclear volume. Minimum nuclear volume is the Y-intercept of this line (red arrow). **B.** Average nuclear volume (left) vs. minimum nuclear volume (right) for diploid *crwn1* mutant and diploid, tetraploid, and octoploid wild-type sepal pavement cells. Bars indicate SEM. Data are averages for 2 *crwn1* sepals and 3 diploid, tetraploid, and octoploid sepals. Number of cells = 1351 (*crwn1*), 2126 (diploid), 1967 (tetraploid), 1228 (octoploid).

Works Cited

1. Slabodnick, M.M., et al., *The Macronuclear Genome of Stentor coeruleus Reveals Tiny Introns in a Giant Cell.* Curr Biol, 2017. **27**(4): p. 569-575.
2. Fankhauser, G., *The Effects of Changes in Chromosome Number on Amphibian Development.* The Quarterly Review of Biology, 1945. **20**(1): p. 20-78.
3. Melaragno, J.E., Mehrotra, B., and Coleman, A.W., *Relationship between endopolyploidy and cell size in epidermal tissue of Arabidopsis.* The Plant Cell, 1993. **5**: p. 1661-1668.
4. Zhao, Z., et al., *Genome-wide expression analysis of salt-stressed diploid and autotetraploid Paulownia tomentosa.* PLoS One, 2017. **12**(10): p. e0185455.
5. Yu, Z., et al., *Impact of natural genetic variation on the transcriptome of autotetraploid Arabidopsis thaliana.* PNAS, 2010. **107**(41): p. 17809-17814.
6. Bomblies, K. and A. Madlung, *Polyploidy in the Arabidopsis genus.* Chromosome Res, 2014. **22**(2): p. 117-34.
7. Ramsey, J.a. and D.W. Schemske, *Pathways, mechanisms, and rates of polyploid formation in flowering plants.* Annual Review of Ecology and Systematics, 1998. **29**: p. 467-501.

8. Mason, A.S. and J.C. Pires, *Unreduced gametes: meiotic mishap or evolutionary mechanism?* Trends Genet, 2015. **31**(1): p. 5-10.
9. Jiao, Y., et al., *Ancestral polyploidy in seed plants and angiosperms.* Nature, 2011. **473**(7345): p. 97-100.
10. Ruprecht, C., et al., *Revisiting ancestral polyploidy in plants.* Science Advances, 2017. **3**(7): p. 1-6.
11. Otto, S.P., *The evolutionary consequences of polyploidy.* Cell, 2007. **131**(3): p. 452-62.
12. Ramsey, J. and D.W. Schemske, *Neopolyploidy in flowering plants.* Annual Review of Ecology and Systematics, 2002. **33**: p. 589-639.
13. Snodgrass, S.J., J. Jareczek, and J.F. Wendel, *An examination of nucleotypic effects in diploid and polyploid cotton.* AoB Plants, 2017. **9**.
14. Comai, L., *The advantages and disadvantages of being polyploid.* Nat Rev Genet, 2005. **6**(11): p. 836-46.
15. Li, X., et al., *Developmental, cytological and transcriptional analysis of autotetraploid Arabidopsis.* Planta, 2012. **236**(2): p. 579-596.
16. Tsukaya, H., *Does ploidy level directly control cell size? Counterevidence from Arabidopsis genetics.* PLoS One, 2013. **8**(12): p. e83729.
17. Jagna, K., H. Weiss-Schneeweiss, and J. Maluszynska, *Structural and embryological studies of diploid and tetraploid Arabidopsis thaliana (L.) Heynh.* Acta biologica Cracoviensia. Series botanica, 2000. **42**(2): p. 113-124.
18. del Pozo, J.C. and E. Ramirez-Parra, *Deciphering the molecular bases for drought tolerance in Arabidopsis autotetraploids.* Plant Cell Environ, 2014. **37**(12): p. 2722-37.
19. Czesnick, H. and M. Lenhard, *Size control in plants--lessons from leaves and flowers.* Cold Spring Harb Perspect Biol, 2015. **7**(8): p. a019190.
20. Tsukaya, H., *Controlling size in multicellular organs: focus on the leaf.* PLoS Biol, 2008. **6**(7): p. e174.
21. Zhurinsky, J., et al., *A coordinated global control over cellular transcription.* Curr Biol, 2010. **20**(22): p. 2010-5.
22. Marguerat, S. and J. Bahler, *Coordinating genome expression with cell size.* Trends Genet, 2012. **28**(11): p. 560-5.
23. Ietswaart, R., et al., *Cell-Size-Dependent Transcription of FLC and Its Antisense Long Non-coding RNA COOLAIR Explain Cell-to-Cell Expression Variation.* Cell Syst, 2017. **4**(6): p. 622-635 e9.
24. Yu, Z., et al., *A large number of Arabidopsis thaliana lines, generated by a rapid strategy, reveal high stability of neo-tetraploids during consecutive generations.* Theoretical and Applied Genetics, 2009. **118**: p. 1107-1119.
25. Monda, K., et al., *Enhanced Stomatal Conductance by a Spontaneous Arabidopsis Tetraploid, Me-0, Results from Increased Stomatal Size and Greater Stomatal Aperture.* Plant Physiol, 2016. **170**(3): p. 1435-44.
26. del Pozo, J.C. and E. Ramirez-Parra, *Whole genome duplications in plants: an overview from Arabidopsis.* J Exp Bot, 2015. **66**(22): p. 6991-7003.
27. Spoelhof, J.P., P.S. Soltis, and D.E. Soltis, *Pure polyploidy: Closing the gaps in autopolyploid research.* Journal of Systematics and Evolution, 2017. **55**(4): p. 340-352.

28. Allario, T., et al., *Tetraploid Rangpur lime rootstock increases drought tolerance via enhanced constitutive root abscisic acid production.* Plant Cell Environ, 2013. **36**(4): p. 856-68.
29. Stupar, R.M., P.J. Hermanson, and N.M. Springer, *Nonadditive expression and parent-of-origin effects identified by microarray and allele-specific expression profiling of maize endosperm.* Plant Physiol, 2007. **145**(2): p. 411-25.
30. Lu, B., et al., *A genome-wide comparison of genes responsive to autopolyploidy in Isatis indigotica using Arabidopsis thaliana Affymetrix genechips.* Plant Molecular Biology Reporter, 2006. **24**(2): p. 197-204.
31. Kim, E.D. and Z.J. Chen, *Unstable transcripts in Arabidopsis allotetraploids are associated with nonadditive gene expression in response to abiotic and biotic stresses.* PLoS One, 2011. **6**(8): p. e24251.
32. Wu, C.Y., et al., *Control of transcription by cell size.* PLoS Biol, 2010. **8**(11): p. e1000523.
33. Barow, M., *Endopolyploidy in seed plants.* Bioessays, 2006. **28**(3): p. 271-81.
34. Galbraith, D.W., Harkins, K.R., and Knapp, S., *Systemic endopolyplody in Arabidopsis thaliana.* Plant Physiology, 1991. **96**: p. 985-989.
35. Katagiri, Y., et al., *The coordination of ploidy and cell size differs between cell layers in leaves.* Development, 2016. **143**(7): p. 1120-5.
36. Chevalier, C., et al., *Endoreduplication and fruit growth in tomato: evidence in favour of the karyoplasmic ratio theory.* J Exp Bot, 2014. **65**(10): p. 2731-46.
37. Roeder, A.H., et al., *Variability in the control of cell division underlies sepal epidermal patterning in Arabidopsis thaliana.* PLoS Biol, 2010. **8**(5): p. e1000367.
38. Tauriello, G., et al., *Variability and Constancy in Cellular Growth of Arabidopsis Sepals.* Plant Physiol, 2015. **169**(4): p. 2342-58.
39. Bramsiepe, J., et al., *Endoreplication controls cell fate maintenance.* PLoS Genet, 2010. **6**(6): p. e1000996.
40. Roeder, A.H., et al., *Cell cycle regulates cell type in the Arabidopsis sepal.* Development, 2012. **139**(23): p. 4416-27.
41. Schwarz, E.M. and A.H. Roeder, *Transcriptomic Effects of the Cell Cycle Regulator LGO in Arabidopsis Sepals.* Front Plant Sci, 2016. **7**: p. 1744.
42. Meyer, H.M., et al., *Fluctuations of the transcription factor ATML1 generate the pattern of giant cells in the Arabidopsis sepal.* Elife, 2017. **6**.
43. Churchman, M.L., et al., *SIAMESE, a plant-specific cell cycle regulator, controls endoreplication onset in Arabidopsis thaliana.* Plant Cell, 2006. **18**(11): p. 3145-57.
44. Kumar, N., et al., *Functional Conservation in the SIAMESE-RELATED Family of Cyclin-Dependent Kinase Inhibitors in Land Plants.* Plant Cell, 2015. **27**(11): p. 3065-80.
45. Walker, J.D., et al., *SIAMESE, a gene controlling the endoreduplication cell cycle in Arabidopsis thaliana trichomes.* Development, 2000. **127**: p. 3931-3940.
46. Sugimoto-Shirasu, K. and K. Roberts, *"Big it up": endoreduplication and cell-size control in plants.* Current Opinion in Plant Biology, 2003. **6**(6): p. 544-553.
47. Smith, A.V. and T.L. Orr-Weaver, *The regulation of the cell cycle during Drosophila embryogenesis: the transition to polyteny.* Development, 1991. **112**: p. 997-1008.
48. Carvalheira, G.M.G., *Plant polytene chromosomes.* Genetics and Molecular Biology, 2000. **23**(4): p. 1043-1050.

49. Nagl, W., *Banded polytene chromosomes in the legume Phaseolus vulgaris.* Nature, 1969. **221**: p. 70-71.
50. Schubert, V., et al., *Sister chromatids are often incompletely aligned in meristematic and endopolyploid interphase nuclei of Arabidopsis thaliana.* Genetics, 2006. **172**(1): p. 467-75.
51. Schubert, V., A. Berr, and A. Meister, *Interphase chromatin organisation in Arabidopsis nuclei: constraints versus randomness.* Chromosoma, 2012. **121**(4): p. 369-87.
52. Matzke, A.J., et al., *Use of two-color fluorescence-tagged transgenes to study interphase chromosomes in living plants.* Plant Physiol, 2005. **139**(4): p. 1586-96.
53. Sas-Nowosielska, H. and T. Bernas, *Spatial relationship between chromosomal domains in diploid and autotetraploid Arabidopsis thaliana nuclei.* Nucleus, 2016. **7**(2): p. 216-31.
54. Fujimoto, S., et al., *An upper limit of the ratio of DNA volume to nuclear volume exists in plants.* Genes and Genetic Systems, 2005. **80**(5): p. 345-350.
55. Cavalier-Smith, T., *Economy, speed and size matter: evolutionary forces driving nuclear genome miniaturization and expansion.* Ann Bot, 2005. **95**(1): p. 147-75.
56. Neumann, F.R. and P. Nurse, *Nuclear size control in fission yeast.* J Cell Biol, 2007. **179**(4): p. 593-600.
57. Cavalier-Smith, T., *Skeletal DNA and the Evolution of Genome Size.* Annual Review of Biophysics and Bioengineering, 1982. **11**: p. 273-302.
58. Beaulieu, J.M., et al., *Genome size is a strong predictor of cell size and stomatal density in angiosperms.* New Phytol, 2008. **179**(4): p. 975-86.
59. Simova, I. and T. Herben, *Geometrical constraints in the scaling relationships between genome size, cell size and cell cycle length in herbaceous plants.* Proc Biol Sci, 2012. **279**(1730): p. 867-75.
60. Jovtchev, G., et al., *Nuclear DNA content and nuclear and cell volume are positively correlated in angiosperms.* Cytogenet Genome Res, 2006. **114**(1): p. 77-82.
61. Jorgensen, P., et al., *The Size of the Nucleus Increases as Yeast Cells Grow.* Molecular Biology of the Cell, 2007. **18**: p. 3523-3552.
62. Kume, K., et al., *A systematic genomic screen implicates nucleocytoplasmic transport and membrane growth in nuclear size control.* PLoS Genet, 2017. **13**(5): p. e1006767.
63. Bourdon, M., et al., *Evidence for karyoplasmic homeostasis during endoreduplication and a ploidy-dependent increase in gene transcription during tomato fruit growth.* Development, 2012. **139**(20): p. 3817-26.
64. Henery, C.C. and M.H. Kaufman, *Relationship between cell size and nuclear volume in nucleated red blood cells of developmentally matched diploid and tetraploid mouse embryos.* The Journal of Experimental Zoology, 1992. **261**: p. 472-478.
65. Edens, L.J., et al., *Nuclear size regulation: from single cells to development and disease.* Trends Cell Biol, 2013. **23**(4): p. 151-9.
66. Sapala, A., et al., *Why plants make puzzle cells, and how their shape emerges.* Elife, 2018. **7**.
67. Hong, L., et al., *Variable Cell Growth Yields Reproducible OrganDevelopment through Spatiotemporal Averaging.* Dev Cell, 2016. **38**(1): p. 15-32.

68. Hamdoun, S., et al., *Differential Roles of Two Homologous Cyclin-Dependent Kinase Inhibitor Genes in Regulating Cell Cycle and Innate Immunity in Arabidopsis.* Plant Physiol, 2016. **170**(1): p. 515-27.
69. Cunha, A.L., A.H.K. Roeder, and E.M. Meyerowitz, *Segmenting the sepal and shoot apical meristem of Arabidopsis thaliana.* Conf Proc IEEE Eng Med Biol Soc, 2010(2010): p. 5338-5342.
70. Sax, K. and H.J. Sax, *Stomata size and distribution in diploid and polyploid plants.* Journal of the Arnold Arboretum, 1937. **18**(2): p. 164-172.
71. Tan, G.Y. and G.M. Dunn, *Relationship of Stomatal Length and Frequency and Pollen-Grain Diameter to Ploidy Level in Bromus inermis Leyss.* Crop Science, 1973. **13**: p. 332-334.
72. Beck, S.L., R.W. Dunlop, and A. Fossey, *Stomatal length and frequency as a measure of ploidy level in black wattle, Acacia mearnsii (de Wild).* Botanical Journal of the Linnean Society, 2003. **141**(2): p. 177-181.
73. Coate, J.E. and J.J. Doyle, *Variation in transcriptome size: are we getting the message?* Chromosoma, 2015. **124**(1): p. 27-43.
74. Cole, L.W., *The Evolution of Per-cell Organelle Number.* Front Cell Dev Biol, 2016. **4**: p. 85.
75. Marks, M.D., et al., *Transcriptome analysis of Arabidopsis wild-type and gl3-sst sim trichomes identifies four additional genes required for trichome development.* Mol Plant, 2009. **2**(4): p. 803-22.
76. Jakoby, M.J., et al., *Transcriptional profiling of mature Arabidopsis trichomes reveals that NOECK encodes the MIXTA-like transcriptional regulator MYB106.* Plant Physiol, 2008. **148**(3): p. 1583-602.
77. Francis, D., M.S. Davies, and P.W. Barlow, *A strong nucleotypic effect on the cell cycle regardless of ploidy level.* Ann Bot, 2008. **101**(6): p. 747-57.
78. Serrano-Mislata, A., K. Schiessl, and R. Sablowski, *Active Control of Cell Size Generates Spatial Detail during Plant Organogenesis.* Curr Biol, 2015. **25**(22): p. 2991-6.
79. Larkin, J.C., Young, N., Prigge, M., and Marks, M.D., *The control of trichome spacing and number in Arabidopsis.* Development, 1996. **122**: p. 997-1005.
80. Serna, L., J. Torres-Contreras, and C. Fenoll, *Clonal analysis of stomatal development and patterning in Arabidopsis leaves.* Dev Biol, 2002. **241**(1): p. 24-33.
81. Larkin, J.C., et al., *The control of trichome spacing and number in Arabidopsis.* Development, 1996. **122**: p. 997-1005.
82. Bossinger, G., Smyth, D.R., *Initiation patterns of flower and floral organ development in Arabidopsis thaliana.* Development, 1996. **122**(4): p. 1093-1102.
83. Sliwinska, E., J. Mathur, and J.D. Bewley, *On the relationship between endoreduplication and collet hair initiation and tip growth, as determined using six Arabidopsis thaliana root-hair mutants.* J Exp Bot, 2015. **66**(11): p. 3285-95.
84. Wang, H., T.A. Dittmer, and E.J. Richards, *Arabidopsis CROWDED NUCLEI (CRWN) proteins are required for nuclear size control and heterochromatin organization.* BMC Plant Biology, 2013. **13**(200): p. 1-13.
85. Sakamoto, Y. and S. Takagi, *LITTLE NUCLEI 1 and 4 regulate nuclear morphology in Arabidopsis thaliana.* Plant Cell Physiol, 2013. **54**(4): p. 622-33.

86. Hisanaga, T., K. Kawade, and H. Tsukaya, *Compensation: a key to clarifying the organ-level regulation of lateral organ size in plants.* J Exp Bot, 2015. **66**(4): p. 1055-63.
87. Horiguchi, G., G.T. Kim, and H. Tsukaya, *The transcription factor AtGRF5 and the transcription coactivator AN3 regulate cell proliferation in leaf primordia of Arabidopsis thaliana.* Plant J, 2005. **43**(1): p. 68-78.
88. Potter, C.J. and T. Xu, *Mechanisms of size control.* Current Opinion in Genetics & Development, 2001. **11**(3): p. 279-286.
89. Krizek, B.A., *Making bigger plants: key regulators of final organ size.* Curr Opin Plant Biol, 2009. **12**(1): p. 17-22.
90. Powell, A.E. and M. Lenhard, *Control of organ size in plants.* Curr Biol, 2012. **22**(9): p. R360-7.
91. Coate, J.E. and J.J. Doyle, *Quantifying whole transcriptome size, a prerequisite for understanding transcriptome evolution across species: an example from a plant allopolyploid.* Genome Biol Evol, 2010. **2**: p. 534-46.
92. Imai, H., Fujii, W., Kusakabe, K.T., Kiso, Y., Kano, K., *Effects of whole genome duplication on cell size and gene expression in mouse embryonic stem cells.* Journal of Reproduction and Development, 2016. **62**(6): p. 571-576.
93. Padovan-Merhar, O., et al., *Single mammalian cells compensate for differences in cellular volume and DNA copy number through independent global transcriptional mechanisms.* Mol Cell, 2015. **58**(2): p. 339-52.
94. Kempe, H., et al., *The volumes and transcript counts of single cells reveal concentration homeostasis and capture biological noise.* Molecular Biology of the Cell, 2015. **26**(4): p. 797-804.
95. Bourdon, M., et al., *In planta quantification of endoreduplication using fluorescent in situ hybridization (FISH).* Plant J, 2011. **66**(6): p. 1089-99.
96. Ginzberg, M.B., R. Kafri, and M. Kirschner, *Cell biology. On being the right (cell) size.* Science, 2015. **348**(6236): p. 1245075.
97. Turner, J.J., J.C. Ewald, and J.M. Skotheim, *Cell size control in yeast.* Curr Biol, 2012. **22**(9): p. R350-9.
98. Chien, A.C., N.S. Hill, and P.A. Levin, *Cell size control in bacteria.* Curr Biol, 2012. **22**(9): p. R340-9.
99. Willis, L., et al., *Cell size and growth regulation in the Arabidopsis thaliana apical stem cell niche.* Proc Natl Acad Sci U S A, 2016. **113**(51): p. E8238-E8246.
100. Schiessl, K., et al., *JAGGED controls growth anisotropyand coordination between cell sizeand cell cycle during plant organogenesis.* Curr Biol, 2012. **22**(19): p. 1739-46.
101. Schmoller, K.M., et al., *Dilution of the cell cycle inhibitor Whi5 controls budding-yeast cell size.* Nature, 2015. **526**(7572): p. 268-72.
102. Talarek, N., E. Gueydon, and E. Schwob, *Homeostatic control of START through negative feedback between Cln3-Cdk1 and Rim15/Greatwall kinase in budding yeast.* Elife, 2017. **6**.
103. Sánchez, L., B. Granadino, and M. Torres, *Sex determination in Drosophila melanogaster: X-linked genes involved in the initial step of sex-lethal activation.* Developmental Genetics, 1994. **15**(3): p. 251-264.

104. Nicoll, M., C.C. Akerib, and B.J. Meyer, *X-chromosome-counting mechanisms that determine nematode sex.* Nature, 1997. **10**(388): p. 200-204.
105. Arumuganathan, K. and E.D. Earle, *Estimation of nuclear DNA content of plants by flow cytometry.* Plant Molecular Biology Reporter, 1991. **9**(3).
106. Barbier de Reuille, P., et al., *MorphoGraphX: A platform for quantifying morphogenesis in 4D.* eLife, 2015. **4**: p. 05864.
107. Nelson, B.K., X. Cai, and A. Nebenfuhr, *A multicolored set of in vivo organelle markers for co-localization studies in Arabidopsis and other plants.* Plant J, 2007. **51**(6): p. 1126-36.
108. Hamant, O., Das, P., Burian, A., *Time-Lapse Imaging of Developing Meristems Using Confocal Laser Scanning Microscope*, in *Plant Cell Morphogenesis*, C.F. Žárský V., Editor. 2013, Humana Press: Totowa, NJ.
109. Smyth, D.R., Bowman, J.L., and Meyerowitz, E.M., *Early flower development in Arabidopsis.* The Plant Cell, 1990. **2**: p. 755-767.
110. Bolger, A.M., M. Lohse, and B. Usadel, *Trimmomatic: a flexible trimmer for Illumina sequence data.* Bioinformatics, 2014. **30**(15): p. 2114-20.
111. Pertea, M., et al., *Transcript-level expression analysis of RNA-seq experiments with HISAT, StringTie and Ballgown.* Nat Protoc, 2016. **11**(9): p. 1650-67.
112. Anders, S., P.T. Pyl, and W. Huber, *HTSeq--a Python framework to work with high-throughput sequencing data.* Bioinformatics, 2015. **31**(2): p. 166-9.
113. Love, M.I., W. Huber, and S. Anders, *Moderated estimation of fold change and dispersion for RNA-seq data with DESeq2.* Genome Biol, 2014. **15**(12): p. 550.

3. Expression pattern of LOSS OF GIANT CELLS FROM ORGANS (LGO) in the sepal

Abstract

Previous work in the Roeder lab has shown that the SIAMESE-related CDK inhibitor LGO (LOSS OF GIANT CELLS FROM ORGANS*)* is required for giant cell formation in the sepal epidermis [1]. In the sepal abaxial epidermis, endoreduplicating cells with ploidy 8C-32C are scattered among non-endoreduplicated cells [1,2] [Robinson et al. in preparation]. In the *lgo-2* loss-of-function mutant, the proportion of cells with ploidy 8C-32C decreases dramatically-- fewer cells enter endocycles [1,2][Robinson et al. in preparation]. As a CDK inhibitor, LGO likely acts directly in enacting the switch from the mitotic cell cycle to the endocycle in select cells; however, the regulatory mechanisms that localize *LGO* to specific cells are not yet known. Here, we report preliminary imaging of two reporters: a translational reporter (*pLGO::3X Venus-LGO*), which reports protein localization, and a transcriptional reporter (*pLGO::3X Venus N7*), which reports activity of the *LGO* promoter. We combine observations of these reporters with prior knowledge about *LGO* to create a tentative model of *LGO* regulation.

Introduction

We recently showed that *LGO*'s effect on endocycles is dosage-dependent [Robinson et al. in preparation]. We compared sepals that were heterozygous vs. homozygous for the *LGO* overexpression construct *ML1::LGO*. The *ML1* promoter drives *LGO* expression in all epidermal cells, and thus both the heterozygous and homozygous lines likely have LGO expressed in every epidermal cell: however, we found that significantly more cells had ploidy ≥8C in the homozygous lines. Cells in these sepals presumably receive a higher dosage of LGO because they have two copies of the overexpression construct, and this dosage increase means that more cells exceed a LGO threshold and enter endocycles. LGO's induction of endocycles is thus not based on binary presence or absence, but is instead affected by concentration: this suggests a threshold-based mechanism for regulation of endoreduplication by LGO [Robinson et al. in preparation].

These observations mirror reports regarding the transcription factor *MERISTEM LAYER 1* (*AtML1*). *AtML1* also affects the entry into endocycles in a dosage-dependent manner [3]. *AtML1* expression patterns the entry into endocycles via a threshold-based mechanism: the protein is expressed in all cells in the developing sepal, but endocycles occur only in cells that surpass a threshold level of AtML1 in G2 phase of the cell cycle. Fluctuations in AtML1 expression, which appear to be stochastic, create the scattered pattern of endopolyploid cells [3]. *LGO* is genetically downstream of *AtML1* [2,3]. Meyer et al. [3] speculate that expression of ATML1, a transcription factor, directly or indirectly controls *LGO* expression to enact the entry into endocycles.

Here, we visualize patterns of *LGO* promoter expression and protein localization in developing sepals. We predict that LGO protein should be expressed in cells prior to their entry into endocycles and should be absent or at lower concentration in cells that do not enter endocycles. We hope that comparing the patterns of LGO transcription and translation gives insight into whether regulation occurs primarily at the transcriptional or the translational level.

A *LGO* protein reporter has dim, scattered expression

The *LGO* translational reporter pAR270 (*pLGO::3X Venus-LGO*) was transformed into the *lgo-2* mutant background. We selected F3 lines with "rescue" phenotypes; sepals in these lines had a number of giant cells similar to that in wild type. Careful selection was necessary because LGO's effect is dosage-dependent [Robinson et al. in preparation]: different transgene insertion events have slightly different levels of *LGO* expression, so some lines have more or fewer giant cells than WT.

We identified two discrete expression patterns for *LGO* in the developing sepal-- early and late. Both are exclusively nuclear. Early expression (in young sepals) occurs in scattered cells, consistent with variable entry into endocycles in the sepal epidermis (Figure 1A-C). This signal appears primarily in larger cells, consistent with LGO's role in promoting endoreduplication. This signal is very dim. LGO expression was not detected in mature sepals (Figure 1D). A late expression pattern, observed in older (but not

mature) sepals and mature petals, is much brighter and is present in every nucleus (Figure 1E-G). These tissues have ceased cell division, so LGO expression is unlikely to relate to endocycling at this stage. Expression includes the smallest nuclei, which are likely non-endoreduplicated (Figure 1F,G). This late expression pattern suggests that *LGO* might play a second role later in development—it first induces scattered cells to enter endocycles, and later performs a second function that might relate to *SIAMESE*-related genes' previously reported roles in defense or in drought response [4,5,6,7].

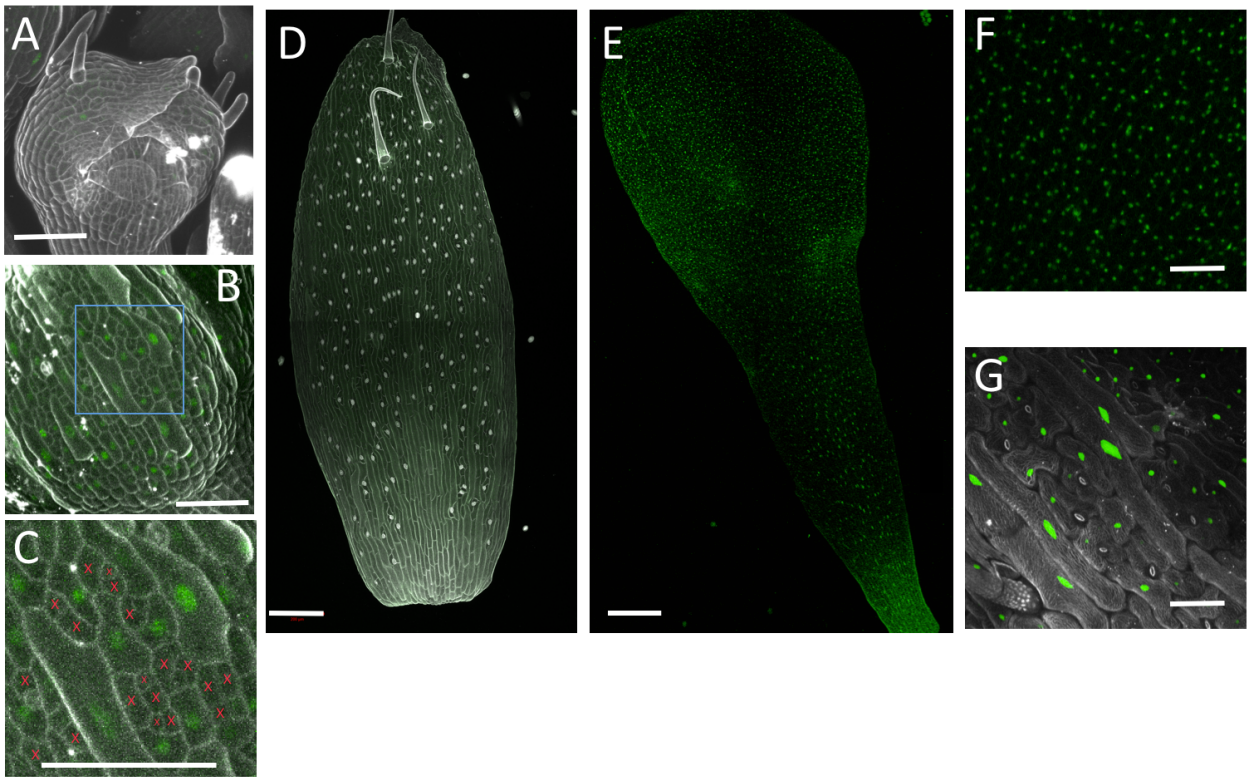

Figure 1. Expression of pAR270 (LGO::3X Venus-LGO; green), a translational reporter for LGO, in sepals stained with PI (gray) and in unstained petals. **A.**,**B.** Scattered, dim expression in young sepals. **C.** Magnified view of B. (blue box). Cells without clear LGO expression in the nucleus are marked with a red X. **D.** Absence of expression in a mature sepal. Laser intensity was 10-14% for panels A-D. **E.** Broad, bright LGO expression in a mature petal. **F.** Magnified view of E. showing LGO expression in small (likely 2C) cells. **G.** Broad, bright LGO expression in an older sepal. Laser intensity was 2-3% for panels E-G. Scale bar 50um on A, B, C, F and G, 200um on D and E.

<u>A reporter for LGO promoter activity is broadly expressed</u>

A reporter for LGO promoter expression (pDR67; *pLGO-3X Venus N7*) is broadly expressed in all epidermal cells in young sepal pavement cells (Figure 2A-C) and in trichomes (Figure 2C, arrows). Expression is maintained in mature sepals (Figure 2D), and expression in underlying cell layers is apparent from the appearance of multiple nuclei underlying a single epidermal cell (Figure 2E, arrows). This contrasts with the dim and scattered expression of the protein reporter, suggesting that regulation of LGO expression is primarily post-transcriptional: *LGO* is transcribed in all cells, but the protein may not be translated in all cells or may be rapidly degraded after translation.

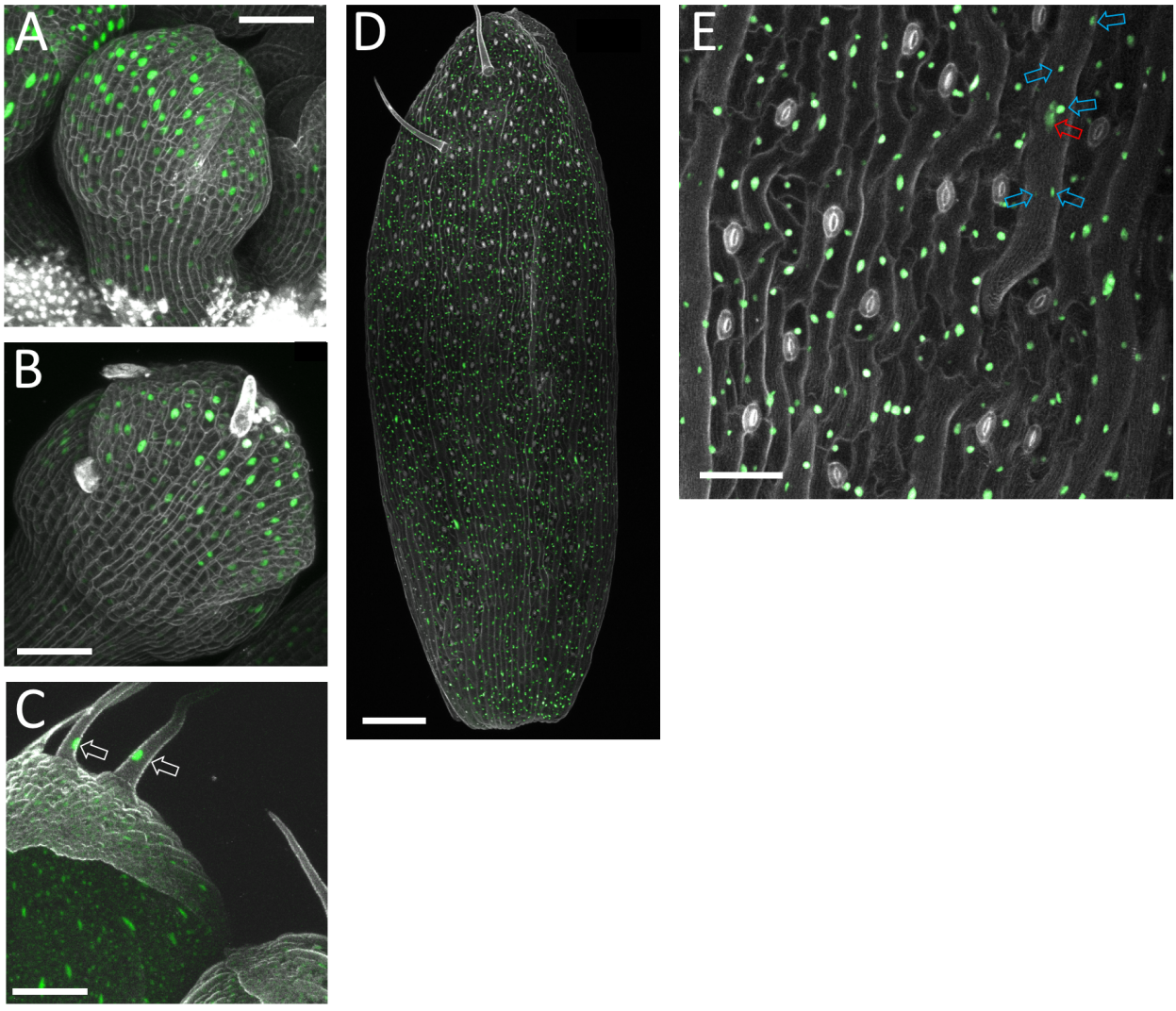

Figure 2. Expression of pDR67 (*LGO::3X Venus N7*; green), a nuclear-localized reporter for LGO promoter activity, in sepals stained with PI (gray). **A.** and **B.** Broad, bright expression in young sepals. **C.**: Expression in trichomes (arrows). **D.** Broad expression in a mature sepal. **E.** Magnified view D. showing construct expression in all

epidermal cells and in underlying cell layers (red arrow indicates probable nucleus of epidermal cell; blue arrows indicate probable underlying mesophyll nuclei). Scale bar 50um on A, B, C, and E, 200um on D.

Model for regulation of *LGO* expression

The above data suggest a model for the regulation of *LGO* expression (Figure 3). *LGO* is transcribed in every epidermal cell in the young sepal (Figure 3A). An unknown mechanism, likely downstream of stochastic *ATML1* fluctuations, then directs post-transcriptional regulation of LGO such that LGO is present only in scattered cells (Figure 3B). LGO has been shown to be degraded by the 26S proteasome [6]. Cells with LGO dosage above a threshold endoreduplicate, whereas cells with LGO dosage below this threshold divide mitotically (Figure 3C).

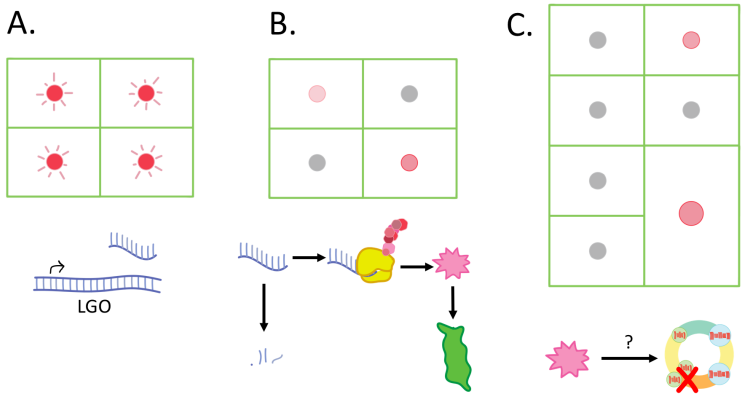

Figure 3. Theoretical model for regulation of LGO expression. **A.** LGO is transcribed in every cell (pink: LGO transcription). **B.** Post-transcriptional regulation limits protein expression to a subset of cells (pink: relatively high *LGO* abundance; gray: absence or low level of *LGO*). Below: degradation of *LGO* by the proteasome (one possible method of post-transcriptional regulation). **C.** cells divide or endoreduplicate based on *LGO* dosage.

Suggestions for future work

Our data indicate that post-transcriptional regulation of *LGO* limits *LGO* to a subset of cells: transcription is broad in the epidermis, whereas the protein is present only in scattered cells at low abundance. This correlates well with the interspersed pattern of ploidy levels observed in the epidermis. LGO is genetically downstream of the transcription factor ATML1, and stochastic fluctuations of *ATML1* in the young sepal predict cells' entry into endocycles [3]: it thus seems reasonable that *ATML1*

fluctuations should pattern *LGO* expression. Our data suggest that this control may not be at the level of *LGO* transcription, as this pattern is broad rather than scattered. *ATML1*'s control of *LGO* may be indirect-- *ATML1* might control transcription of a factor that directs post-transcriptional regulation of *LGO*. The mechanism by which LGO is post-transcriptionally regulated in developing sepals is also unknown. If LGO is degraded by the proteasome in young sepals, this could be confirmed by treatment with a proteasome inhibitor such as MG132: MG132 treatment should cause LGO to accumulate in cells.

Live imaging of the LGO translational reporter (pAR270) might help to reveal whether and how LGO expression correlates to individual cells' entry into endocycles. Do cells that express *LGO* always enter endocycles, or must a threshold be reached, as with ATML1 [3]? Do cells without LGO ever endoreduplicate? Imaging of this reporter, however, is complicated by the dimness of the LGO signal: the laser intensity currently used to image the construct is likely to photodamage plant tissues and negatively affect growth. These investigations might be complemented by imaging a tagged LGO overexpression construct (*pML1::3X Venus-LGO*): because this construct is overexpressed, its signal is brighter and is present in more cells.

Materials and methods

Plant materials:

pDR67 is *LGO::3X Venus-N7*. It was created by LR recombination of pAR334 (3X Venus N7 in the pENTR D TOPO vector) into pAR242 (pMLBART vector with LGO promoter and terminator flanking the gateway site). It was transformed into WT Col by Agrobacterium-mediated floral dipping, and successful transformants were selected with BASTA.

pAR270 is *LGO::3X Venus-LGO*. It was transformed into *lgo-2* by Agrobacterium-mediated floral dipping. F3 plants were selected for rescue phenotype (WT-like number of giant cells) by PI staining and epifluorescence imaging (Zeiss 710 confocal microscope, mCherry setting).

lgo-2 (SALK_033905) is a loss-of-function allele of *LOSS OF GIANT CELLS FROM ORGANS* (*LGO*:AT3G10525) containing a T-DNA insertion. Homozygous ABRC accession CS69160.

Imaging:

Sepals were stained with 2% PI in H_2O for 15 min and imaged at 10x or 20X (water dipping lens; NA = 1.0) on a Zeiss 710 confocal laser scanning microscope. Samples were excited with a 514 nm laser. Venus emission was collected at 519-564 nm and PI emission was collected at 599-649 nm.

Funding

Work on LGO was supported by NSF IOS-1553030.

References

1. Roeder, A.H. K., et al., *Variability in the control of cell division underlies sepal epidermal patterning in Arabidopsis thaliana.* PLoS Biol, 2010. **8**(5): p. e1000367.
2. Roeder, A.H. K., et al., *Cell cycle regulates cell type in the Arabidopsis sepal.* Development, 2012. **139**(23): p. 4416-27.
3. Meyer, H.M., et al., *Fluctuations of the transcription factor ATML1 generate the pattern of giant cells in the Arabidopsis sepal.* Elife, 2017. **6**.
4. Hamdoun, S., et al., *Differential Roles of Two Homologous Cyclin-Dependent Kinase Inhibitor Genes in Regulating Cell Cycle and Innate Immunity in Arabidopsis.* Plant Physiol, 2016. **170**(1): p. 515-27.
5. Peres, A., et al., *Novel plant-specific cyclin-dependent kinase inhibitors induced by biotic and abiotic stresses.* J Biol Chem, 2007. **282**(35): p. 25588-96.
6. Dubois, M., et al., *SIAMESE-RELATED1 is regulated post-translationally and participates in repression of leaf growth under moderate drought.* Plant Physiol, 2018.
7. Wang, S. et al., *A noncanonical role for the CKI-RB-E2F cell-cycle signaling pathway in plant effector-triggered immunity.* Cell Host Microbe, 2014.

4. Survey of diversity in sepal endopolyploidy in Brassicaceae

Abstract

Arabidopsis sepal pavement cells vary in ploidy from 2C to 32C [1],[Robinson et al. in preparation]. An individual cell's entry into endocycles is stochastic, and the position of the largest cells varies from sepal to sepal; however, the proportion of cells at each ploidy level remains relatively constant across sepals [1-3]. This proportion is important in controlling sepal curvature: sepals with too many giant cells curve outward, whereas sepals with too few giant cells curve inward [2]. Here, we survey several species in Brassicaceae to investigate whether cell size is patterned similarly and thus whether this mechanism of curvature control is likely to be conserved. We also investigate the presence or absence of *LGO*, a gene involved in the entry into endocycles in *Arabidopsis*, in diverse Brassicaceae genomes.

Introduction

Cell size has previously been shown to play a mechanical role in organ curvature control. In many monocots, large, endoreduplicated bulliform cells control leaf curvature [4]. These cells are found on the adaxial (upper) leaf surface and deflate under water stress, causing leaves to roll up [5,6,7]. There is no evidence that *Arabidopsis* pavement cells change turgor during development, but they may nevertheless play a similar mechanical role in controlling sepal shape. Changes to curvature during anthesis may arise from subtle differences in growth: anthesis (flower opening) is often regulated by cell expansion, and curvature changes can result from differential growth of the abaxial vs. adaxial organ

faces [8]. In *A. thaliana,* more endopolyploid cells occur on the abaxial face, creating an asymmetry that might impact growth.

Results: Cell size patterning differs among species in *Brassicaceae*

The abaxial epidermis of wild-type *Arabidopsis* sepals has an interspersed pattern of small and larger cells (Figure 1B). Sepals overexpressing LGO (pATML1::LGO) have an increased proportion of large cells (Figure 1A), while sepals mutant for LGO (*lgo-2*) have only small cells (Figure 1C). We imaged mature sepals from four other species in Brassicaceae: *Cardamine hirsuta*, *Schrenkiella parvula*, *Sisymbrium irio*, and *Brassica rapa*. We found considerable diversity in sepal cell size patterning among these four species. In *Cardamine hirsuta*, the sepal epidermis is composed mainly of large cells (Figure 1D) and resembles the LGO overexpression phenotype in *Arabidopsis*. Cells in *Schrenkiella parvula* vary from small to large, like WT *Arabidopsis,* but cell borders are crenated rather than straight (Figure 1E). *Sisymbrium irio* also shows a range of cell sizes with moderately crenated cell borders. Large cells are concentrated near the sepal midrib (Figure 1F). *Brassica rapa* has only small cells of homogeneous size (Figure 1G), much like the *Arabidopsis lgo-2* mutant. Two other species in the genus *Brassica, B. rapa* and *B. napus*, showed a similar phenotype (data not shown).

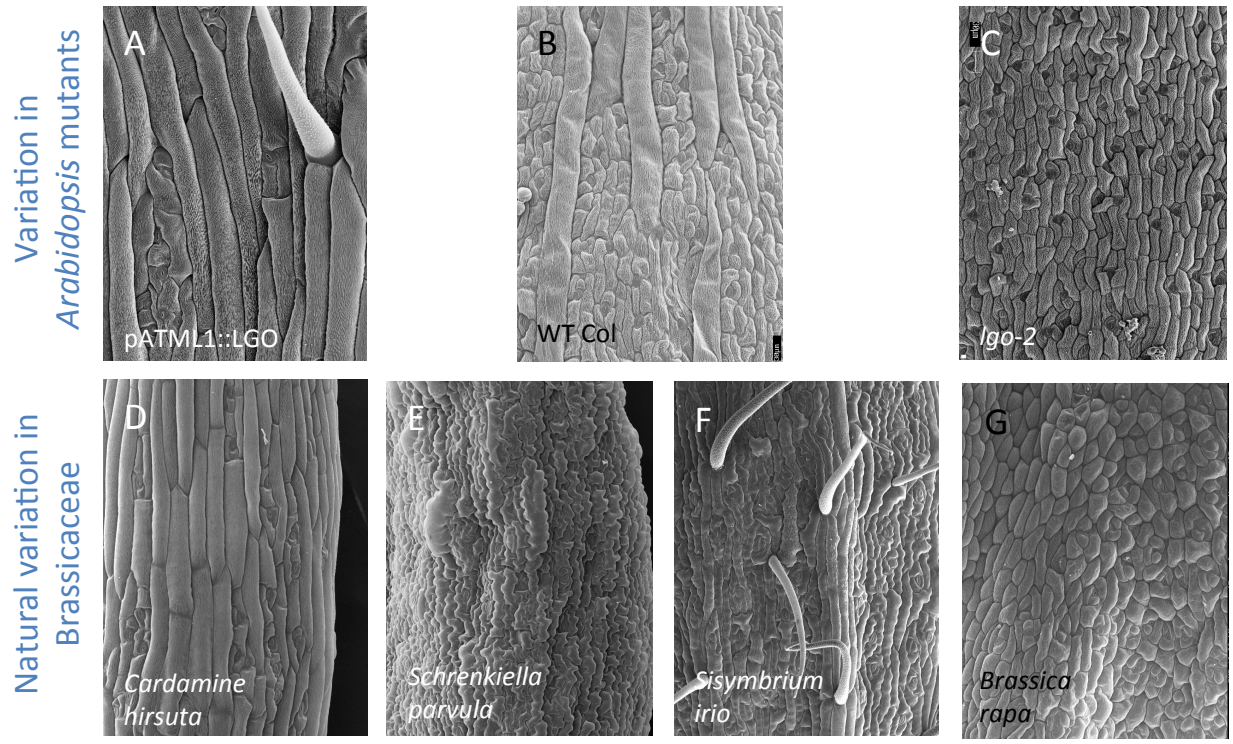

Figure 1. SEM images of pavement cells in the abaxial sepal epidermis of species in *Brassicaceae*. **A.** Epidermis-specific overexpression of LGO in *A. thaliana* (*pATML1::LGO*) increases the proportion of large cells. **B.** Wild-type *A. thaliana* has scattered large and small cells **C.** The *A. thaliana lgo-2* mutant has only small cells. **D.** *Cardamine hirsuta* has many large, elongated cells. **E.** *Schrenkiella parvula* has scattered large and small cells with crenated borders. **F.** *Sisymbrium irio* has scattered large and small cells. **G.** *Brassica rapa* has small cells with little variation in size.

Species in *Brassicaceae* differ in sepal curvature at anthesis

In *Arabidopsis,* mutants that alter the relative proportion of small and large cells (*lgo-2,* pATML1::LGO) cause changes in sepal curvature. We found that cell size distributions in Brassicaceae species resembled these *Arabidopsis* mutant phenotypes: we were therefore interested in determining whether these differences correlated with differences in sepal curvature. To assess curvature, we photographed flowers at consecutive stages of anthesis (Figure 2). We observed that species with large pavement cells appear to flatten along the longitudinal axis as the petals emerge (Figure 2A, B). In contrast, species lacking giant cells did not modulate curvature along the longitudinal axis during anthesis. Additionally, we observed a difference in final sepal position in species lacking giant cells: in *Brassica* species, the sepal bends backward from the base to become nearly perpendicular to the stem. This may represent an alternative strategy to prevent sepal interaction with petals after anthesis.

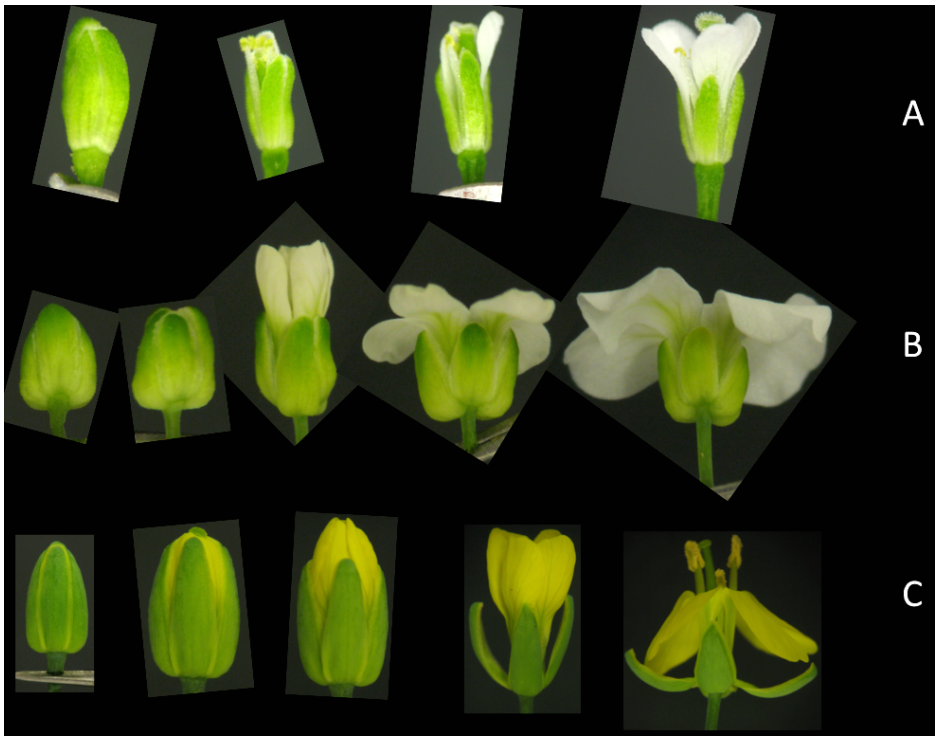

Figure 2. Representative anthesis series from three species. **A.** *Cardamine hirsuta* (many large cells). **B.** *Arabidopsis lyrata* (some large cells). **C.** *Brassica napus* (only small cells).

To better understand the "final sepal position" parameter, I quantified sepal angle for several species at full anthesis: sepal angle was defined as the angle made by a line passing through the tip and base of the sepal to a line through the pedicel. I found that a range of angles from 2.5^{o} (*Matthiola longipetala*) to 81.1^{o} (*Brassica rapa*) occurs (Figure 3): these measurements are preliminary (only single flowers), but they indicate that substantial variation in this parameter exists across species.

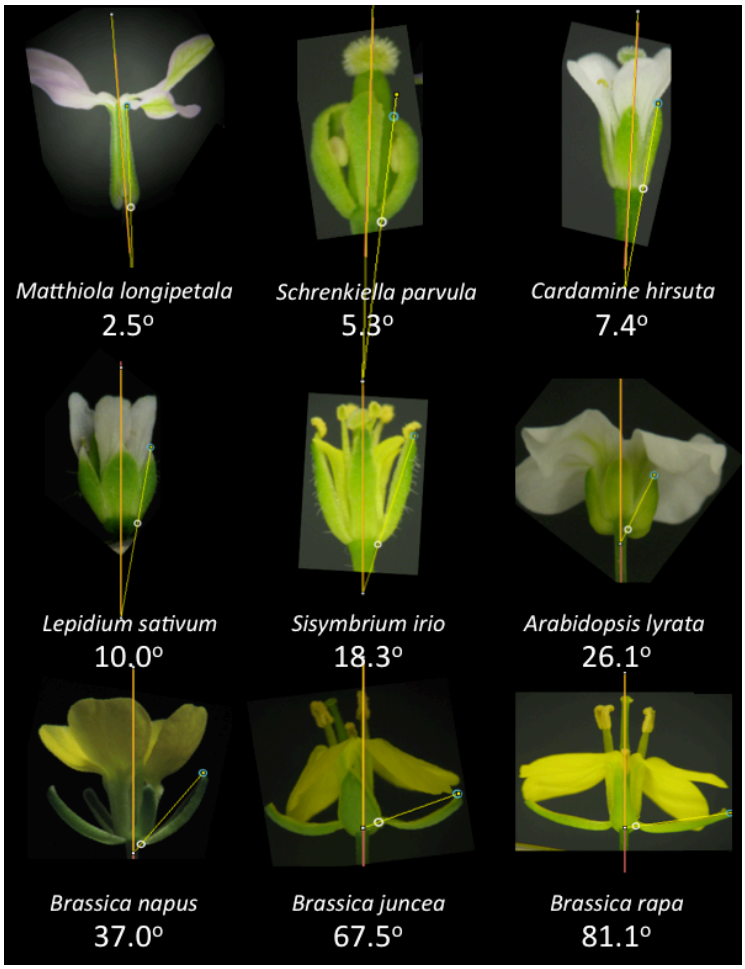

Figure 3. Sepal angle to pedicel at full anthesis in nine species in Brassicaceae. Sepal angle was measured as the angle between a line intersecting the tip and base of the sepal and a line drawn along the pedicel.

LGO and giant cell specification

The *SIAMESE*-related CDK inhibitor *LGO* is required for giant cell differentiation in *Arabidopsis* sepal pavement cells [1, 2]. If pavement cell endoreduplication in other species is patterned by a common mechanism, then LGO may also play a role in these tissues. We confirmed that LGO homologs are present in the species of interest: the *Arabidopsis LGO* genomic sequence was BLASTed against the genome sequences of *Arabidopsis lyrata*, *Boechera stricta, Brassica rapa, Capsella rubella,* and *Eutrema salsugineum* in Phytozome, and in each case a region with strong identity (82-95%) to the sequence was

identified. Two such regions were identified in *Brassica rapa*, which underwent an ancient genome triplication event [9]. The nearest upstream gene of *LGO* and all putative homologs is a WD40 repeat-like superfamily protein; all homologs except for one of the *B. rapa* paralogs are upstream of a gene annotated as "leghemoglobin-related". This synteny is evidence that these genes are homologous to *LGO* and not another protein in the *SIAMESE*-related (SMR) family. Alignment of the protein sequence of homologs revealed especially strong conservation in SMR family motifs identified by Churchman et al., including a potential cyclin-binding (zRxL) motif [10] (Figure 4).

Figure 4. Clustal-W alignment of protein sequences from *A. thaliana, A. lyrata, B. stricta, C. rubella, E. salsugineum,* and *B. rapa* (two paralogs). Sequence conservation is especially strong in putative SMR family motifs (blue boxes) identified by Churchman et al. [10].

Conclusions and suggestions for future work

We observed that sepal cell size patterning and sepal curvature at anthesis differ among species in Brassicaceae, and we tentatively describe two models for sepal behavior at anthesis: sepals with diverse pavement cell sizes modulate their curvature during anthesis (e.g. *Arabidopsis thaliana*, *Arabidopsis lyrata*, *Cardamine hirsuta*), whereas sepals with homogenous cell size bend away from the petals (e.g. *Brassica rapa*). This correlation could be strengthened with SEM observation of cell size and

careful analysis of sepal curvature in a wider range of species; however, a true test of the role of cell size in sepal curvature in these species would require a genetic approach. If large cells in other species are endoreduplicated, it's likely that at least one CDK inhibitor acts in their differentiation, and all genomes surveyed contain a region homologous to *LGO*. Misexpression of this locus, either by mutation or overexpression, is likely to alter the proportion of endopolyploid cells in the sepal. We could then test whether these changes in cell size correlate with changes to sepal curvature. This depends on the development of transgenic tools for several species.

Materials and methods

Plant materials:

lgo-2 (SALK_033905) is a loss-of-function allele of *LOSS OF GIANT CELLS FROM ORGANS* (*LGO*:AT3G10525) containing a T-DNA insertion. Homozygous ABRC accession CS69160.

LGO OX is *pATML1::LGO* (pAR178) [2, 11].

Lepidium sativum (PI 633257) and *Matthiola longipetala* subsp. *bicornis* (PI 650274) were obtained from the USDA National Plant Germplasm System (NPGS).

The following lines were obtained from the ABRC stock center:

Schrenkiella parvula (*Thellungiella parvula*) (CS22663).

Sisymbrium irio (CS22563).

Brassica rapa (CS29001).

Arabidopsis lyrata subsp. *lyrata* (CS22696).

Brassica napus and *Brassica juncea* seeds were obtained from Martin Yanofsky and Sherry Kempin.

Cardamine hirsuta seeds were obtained from Miltos Tsiantis.

Photography

Flowers were photographed against a black background with a Canon Powershot A640 camera mounted on a Stemi 2000 dissecting microscope. Sepal angle was measured using the "angle" tool in ImageJ to measure the angle formed by a line passing through the base and tip of the sepal to the pedicel.

Scanning electron microscopy

SEM was performed as described in [1, 3]. Mature sepals were dissected, fixed in FAA overnight, and dehydrated using an ethanol series. Sepals were then infiltrated with liquid CO_2, critical point dried, and sputter-coated with platinum palladium. Sepals were imaged on a LEICA 440 scanning electron microscope.

Acknowledgements

This work made use of the Cornell Center for Materials Research Facilities supported by the National Science Foundation under Award Number DMR-1719875.

References

1. Roeder, A.H.K., et al., *Variability in the control of cell division underlies sepal epidermal patterning in Arabidopsis thaliana.* PLoS Biol, 2010. **8**(5): p. e1000367.
2. Roeder, A.H.K., et al., *Cell cycle regulates cell type in the Arabidopsis sepal.* Development, 2012. **139**(23): p. 4416-27.
3. Meyer, H.M., et al., *Fluctuations of the transcription factor ATML1 generate the pattern of giant cells in the Arabidopsis sepal.* Elife, 2017. **6**.
4. Cavallini, A., Baroncelli, S., Lercari, B., Cionini, G., Rocca, M., D'Amato, F. , *Effect of light and gibberellic acid on chromosome endoreduplication in leaf epidermis of Triticum durum Desf.* Protoplasma, 1995. **186**(1-2): p. 57-62.
5. Kadioglu, A., Terzi, R. , *A Dehydration Avoidance Mechanism: Leaf Rolling.* Botanical Review, 2007. **73**(4): p. 290-302.
6. O'Toole, J.T., Cruz, R.T., *Leaf rolling and transpiration.* Plant Science Letters, 1979. **16**: p. 111-114.

7. Zou, L.P., et al., *Leaf rolling controlled by the homeodomain leucine zipper class IV gene Roc5 in rice.* Plant Physiol, 2011. **156**(3): p. 1589-602.

8. van Doorn, W.G. and U. Van Meeteren, *Flower opening and closure: a review.* J Exp Bot, 2003. **54**(389): p. 1801-12.

9. Cheng, F., J. Wu, and X. Wang, *Genome triplication drove the diversification of Brassica plants.* Hortic Res, 2014. **1**: p. 14024.

10. Churchman, M.L., et al., *SIAMESE, a plant-specific cell cycle regulator, controls endoreplication onset in Arabidopsis thaliana.* Plant Cell, 2006. **18**(11): p. 3145-57.

11. Schwarz, E.M. and A.H. Roeder, *Transcriptomic Effects of the Cell Cycle Regulator LGO in Arabidopsis Sepals.* Front Plant Sci, 2016. **7**: p. 1744.

5. Concluding remarks

Size is an important property at all scales of biology. J.B.S. Haldane remarks on the importance of size at the organ and organism level: organ size is precisely calibrated to serve a particular biological function [1]. This is the case in the *Arabidopsis* flower: all four sepals must have correct and similar sizes to effectively enclose and protect the developing floral organs. At the cell level, size is equally important: morphogenesis requires the generation of cells of multiple types (e.g. guard cells), each of which have a characteristic size and shape. Homeostasis mechanisms are known to robustly constrain variation at set cell sizes [2], however, the mechanisms that regulate cell size and organ size are not yet fully understood. Here, we investigate a property that increases size at the subcellular, cellular, organ, and organism levels: ploidy.

Ploidy refers to the number of sets of chromosomes contained in an individual nucleus. The archetypal plant cell is diploid (2C, or two copies of the genome); however, ploidy in plant cells is remarkably labile, and cells of many different ploidy levels are observed in nature. In individual cells, endoreduplication amplifies ploidy, and this increase in ploidy has a strong positive correlation with cell size [3]. Endoreduplication can thus be considered a tool to increase cell size in development: it supports the generation of large cells. In *Arabidopsis*, characteristically endopolyploid cells include trichomes (large, hairlike cells that protect the leaf surface) [4] and giant cells (elongated pavement cells that control curvature in the sepal) [5, 6]. Our first study describes the mechanisms by which these cell types are patterned, and our fourth study further develops our understanding of how endopolyploid sepal cells are patterned.

In whole plants and plant lineages, ploidy can be increased by whole-genome multiplication (WGM). Unlike endopolyploidy, WGM is not developmentally programmed; it occurs when gametes with more than one copy of the genome, often the result of a meiotic error, fuse to form a zygote [7].

This zygote undergoes all cell divisions with additional copies of the genome, creating an organism that is polyploid in every cell. In our second study, we investigate WGM *Arabidopsis* lineages that are diploid, tetraploid, and octoploid in every cell.

That ploidy change affects size has long been known [8]; however, it is not well understood how a change in genome copy number is propagated to nuclear size, cell size, and organ size. Scaling relationships have been described at each step in this series—most notably, the relationship between nuclear size and cell size (KR) has been measured in many species and cell types [9-12]. However, few studies have directly integrated cell-level with organ-level behavior, either because they deal with single-celled organisms or because organ sizes are prohibitively large. Here, we take advantage of the small size of the *Arabidopsis* sepal to directly measure nuclear size, cell size, cell number, and organ size for all cells in a tissue. This allows us to track the effects of ploidy across biological scales, giving a clearer picture of how higher-order size changes arise.

We observed that both nuclear volume and cell size increase with ploidy; however, we demonstrated that cell size is not scaled to nuclear size. This leaves open the question of how, mechanistically, ploidy change affects cell size. We also observed that organ size shows a partially compensated response to WGM ploidy change: average cell area increases, but total cell number decreases late in development and moderates the effect of ploidy on organ size change. This may indicate the presence of an organ-level mechanism of size control [13, 14]. Our results lead us to speculate that ploidy is an element of size homeostasis in plant cells: cells must both be consistent in their size and generate the wide range of sizes observed in development. We further postulate the existence of a mechanism for sensing cell ploidy, perhaps analogous to sex chromosome-counting mechanisms in insects and nematodes [15, 16]: this ploidy perception could elicit appropriate cell size scaling responses in cells at different ploidy levels, and would also allow cells of different types to calibrate size and gene expression responses to ploidy [17].

References

1. Haldane, J.B.S., *On Being the Right Size.* Harper's Magazine, 1926.
2. Ginzberg, M.B., R. Kafri, and M. Kirschner, *Cell biology. On being the right (cell) size.* Science, 2015. **348**(6236): p. 1245075.
3. Melaragno, J.E., Mehrotra, B., and Coleman, A.W., *Relationship between endopolyploidy and cell size in epidermal tissue of Arabidopsis.* The Plant Cell, 1993. **5**: p. 1661-1668.
4. J.D. Walker, D.G.O., J. Concienne, J.C. Larkin, *SIAMESE, a gene controlling the endoreduplication cell cycle in Arabidopsis thaliana trichomes.* Development, 2000. **127**: p. 3931-3940.
5. Roeder, A.H., et al., *Cell cycle regulates cell type in the Arabidopsis sepal.* Development, 2012. **139**(23): p. 4416-27.
6. Roeder, A.H., et al., *Variability in the control of cell division underlies sepal epidermal patterning in Arabidopsis thaliana.* PLoS Biol, 2010. **8**(5): p. e1000367.
7. Schemske, J.R.a.D.W., *Pathways, mechanisms, and rates of polyploid formation in flowering plants.* Annual Review of Ecology and Systematics, 1998. **29**: p. 467-501.
8. Otto, S.P., *The evolutionary consequences of polyploidy.* Cell, 2007. **131**(3): p. 452-62.
9. Bourdon, M., et al., *Evidence for karyoplasmic homeostasis during endoreduplication and a ploidy-dependent increase in gene transcription during tomato fruit growth.* Development, 2012. **139**(20): p. 3817-26.
10. Fankhauser, G., *The Effects of Changes in Chromosome Number on Amphibian Development.* The Quarterly Review of Biology, 1945. **20**(1): p. 20-78.
11. Jovtchev, G., et al., *Nuclear DNA content and nuclear and cell volume are positively correlated in angiosperms.* Cytogenet Genome Res, 2006. **114**(1): p. 77-82.
12. Henery, C.C., Kaufman, M.H., *Relationship between cell size and nuclear volume in nucleated red blood cells of developmentally matched diploid and tetraploid mouse embryos.* The Journal of Experimental Zoology, 1992. **261**: p. 472-478.
13. Sugimoto-Shirasu, K. and K. Roberts, *"Big it up": endoreduplication and cell-size control in plants.* Current Opinion in Plant Biology, 2003. **6**(6): p. 544-553.
14. Tsukaya, H., *Controlling size in multicellular organs: focus on the leaf.* PLoS Biol, 2008. **6**(7): p. e174.
15. Sánchez, L., Granadino, B., Torres, M., *Sex determination in Drosophila melanogaster: X-linked genes involved in the initial step of sex-lethal activation.* Developmental Genetics, 1994. **15**(3): p. 251-264.
16. Nicoll, M., Akerib, C.C., Meyer, B.J., *X-chromosome-counting mechanisms that determine nematode sex.* Nature, 1997. **10**(388): p. 200-204.
17. Katagiri, Y., et al., *The coordination of ploidy and cell size differs between cell layers in leaves.* Development, 2016. **143**(7): p. 1120-5.